Wave attenuation in coastal mangroves

Mangrove squeeze in the mekong delta

Phan Khanh, Linh

DOI
10.4233/uuid:9397d964-1674-4838-a13a-504742dba55e

Publication date
2019

Document Version
Final published version

Citation (APA)
Phan Khanh, L. (2019). *Wave attenuation in coastal mangroves: Mangrove squeeze in the mekong delta*. [Dissertation (TU Delft), Delft University of Technology]. https://doi.org/10.4233/uuid:9397d964-1674-4838-a13a-504742dba55e

WAVE ATTENUATION IN COASTAL MANGROVES

MANGROVE SQUEEZE IN THE MEKONG DELTA

WAVE ATTENUATION IN COASTAL MANGROVES

MANGROVE SQUEEZE IN THE MEKONG DELTA

Proefschrift

ter verkrijging van de graad van doctor
aan de Technische Universiteit Delft,
op gezag van de Rector Magnificus prof. dr. ir. T. H. J. J. van der Hagen,
voorzitter van het College voor Promoties,
in het openbaar te verdedigen op
Vrijdag 14 Juni 2019 om 12:30 uur

door

Linh KHANH PHAN

Master of Science in Civil Engineering,
Delft University of Technology,
geboren op 18 October 1986 te Ha Noi, Vietnam.

Dit proefschrift is goedgekeurd door de promotoren.

Samenstelling promotiecommissie bestaat uit:

Rector Magnificus,	voorzitter
prof. dr. ir. M. J. F Stive	Technische Universiteit Delft, promotor
prof. dr. ir. S. G. J Aarninkhof	Technische Universiteit Delft, promotor
dr. ir. M. Zijlema	Technische Universiteit Delft, copromotor

Onafhankelijke leden:

prof. dr. Trinh Minh Thu	Thuy Loi University
dr. Tomohiro Suzuki	Flanders Hydraulics Research
prof. dr. W. S.J Uijttewaal	Technische Universiteit Delft
prof. dr. ir. A. J.H.M. Reniers	Technische Universiteit Delft

The work presented in this thesis was performed at the Department of Hydraulic Engineering of the Faculty of Civil Engineering and Geosciences of Delft University of Technology. This research was fund by the Dutch organisation for internationalisation in education (Nuffic).

Keywords: Coastal mangroves, Coastal squeeze, Wave attenuation, Erosion, Laboratory experiment, Numerical modeling.

Printed by: Linh K. Phan

Front & Back: mangrove degradation and coastal erosion along the Mekong Delta, Vietnam

ISBN 978-94-6384-045-3

An electronic version of this dissertation is available at
http://repository.tudelft.nl/.

For Sumi and Sumo.

Contents

Summary

This study explores the influence of the wave characteristics on the attenuation process of waves through coastal mangroves, which are threatened by the coastal mangrove squeeze phenomenon.

Coastal mangrove squeeze is the phenomenon where coastal regions, even when sediment availability is sufficient, are eroding due to a lack of accommodation space caused by the land use on the landside and by sea level rise on the waterside. Along the Mekong Delta Coast, only a narrow strip of mangroves of less than 140 m is left at the locations where a strong erosion of up to 100 m$\,$yr^{-1} is observed. Furthermore, observations at the southeastern and the eastern coasts of the Mekong Delta are, that a mangrove width ranging from approximately 30 m to260 m and 140 m on average, appears to be stable. Therefore, a hypothesis regarding coastal mangrove squeeze is proposed based on the empirical relationship between mangrove forest width and coastline evolution. The hypothesis is proposed, that a minimum space of coastal mangroves is required for a sustainable development of the mangrove forest.

To start, a schematized model mimicking the wave attenuation processes in the Soc Trang province was built using the XBeach model. The simulation results showed that there was a large difference between the attenuation process of long waves and short waves. While the short-wave height was substantially reduced to almost zero after passing through 100 m of mangrove width, the long waves (low frequency wave height) were able to penetrate much further, to about 10 % of the wave height at the seaward edge of the mangroves after 300 m, and to almost zero after 1000 m into the mangrove forest. In this context, within the mangrove forest the long waves appear to play a more important role in creating a favorable environment for seedlings and sedimentation than short waves.

In order to obtain more insight, a unique laboratory experiment of wave attenuation through mangroves was set up and conducted at Delft University of Technology. The experiment, comprising different scenarios covering a wide range of wave characteristics, included different wave heights and periods, as well as regular, irregular, broken and non-broken waves. The experimental results confirmed the role of vegetation in damping the wave energy. Furthermore, it was shown that, in certain scenarios, the wave height damping processes were significantly affected by the non-linearity of the waves. In other words, waves with a different wave height, wave period and wavelength attenuated differently inside the vegetation region. In this context, evaluating the wave height damping processes in terms of the length of mangrove width seemed no longer

appropriate, as a dependence of wave height reduction within mangroves on their characteristic could not be seen. Therefore, a new and more effective wave transmission coefficient was proposed, where the wave height reduction was evaluated according to a relative length, i.e. the number of wavelengths.

Furthermore, in order to clarify the dependence of wave height reduction on the characteristics of waves, the Ursell number was introduced. The results illustrate that the wave attenuation processes are significantly affected by the wave characteristics when the Ursell number is within a range of 0 to 250. Nevertheless, when the Ursell number is larger than 250, the wave attenuation processes appeared to be independent of the wave characteristics. Moreover, the laboratory experimental data were used to validated the SWASH model, including different types of waves, such as long waves and short waves. The model with default parameters can well reproduce the transformation and attenuation processes of incoming waves through mangroves. In this context, the numerical model can be used to broaden the experiment, i.e. to increase the length of the mangrove in the experiment. Consequently, the wave attenuation rate of over up to ten wavelengths could be predicted. In this way, the wave attenuation rate for a specific mangrove density can be presented as a function of the number of wave lengths and the Ursell number, using experimental data and extended numerical results.

As wave characteristics were shown to play a role in the attenuation process of waves through vegetation, it is essential to investigate the attenuation process of different types of waves, including long waves, short waves, bound long waves, free long waves, and mixed bound and free long waves. The experimental results suggest that long waves require a further distance, depending on their corresponding lengths to dampen at the same attenuation rate achieved by short waves. Although long waves appear to penetrate further inside the mangrove than short waves, the damping rate per number of wavelengths of the long waves is larger than that of short waves for conditions tested. It is suggested that free long waves have the larger attenuation rate and bound long waves have the smaller attenuation rate. It is also seen that bound long waves and mixed bound and free long waves strongly depend on the wave characteristics, while free long waves are more independent on the wave non-linearity.

Last but not least, in order to understand the knowledge as obtained from field information, a real scale schematized numerical model mimicking natural mangrove bathymetries was built in SWASH. The outcome of the numerical model showed that the bathymetry within mangroves does have an influence on the wave characteristics around and within the mangrove forest. The steeper the slope inside the mangrove forest, the larger the wave height propagating at the edge of mangroves and the faster the normalized wave energy is dissipated inside the mangrove forest. The larger the slopes in front of the mangrove forest, the larger the wave heights in front of the mangrove forest and the slower the wave height energy absorption inside the mangrove forest. To conclude, the smaller the mangrove width, the larger the significant wave height inside the mangroves and the slower the attenuation processes.

Despite the increased understanding reported in the various chapters, many knowledge gaps still exist. This dissertation concludes that the most challenging efforts to improve our further understanding are real scale validations and simulations of bed and suspended sediment processes.

Samenvatting

In deze studie wordt de invloed onderzocht van specifieke golf kenmerken op het dempingsproces van golven binnen mangroven onder druk van het zgn. vernauwingsfenomeen in de mangrovebossen aan de kust (in deze tekst: “coastal mangrove squeeze phenomenon”).

“Coastal mangrove squeeze” is het fenomeen van erosie in kustgebiedn, zelfs wanneer voldoende sediment beschikbaar is, als gevolg van het ontbreken aan accommodatieruimte en veroorzaakt door de druk aan beide kanten, zowel aan de landkant door landgebruik en aan de waterkant door zeespiegelstijging. Langs de kust van de Mekong Delta bevindt zich slechts nog een smalle strook mangroven van minder dan 140 m, daar waar een sterke erosie van tot 100 myr^{-1} wordt waargenomen. Bovendien tonen observaties aan de zuidoostelijke en de oostelijke kusten van de Mekong Delta dat een mangrovebreedte variërend van ongeveer 30 m tot 260 m, en gemiddeld 140 m, stabiel lijkt te zijn. Daarom wordt een hypothese over de “coastal mangrove squeeze” voorgesteld op basis van de empirische relatie tussen de breedte van een mangrove bos en de evolutie van de kustlijn. De hypothese stelt, dat een minimale ruimte van mangroven aan de kust is vereist voor een duurzame ontwikkeling van het mangrove bos.

Om te beginnen werd een geschematiseerd model gebouwd met het XBeach model, de golf dempingsprocessen in de provincie Soc Trang nabootsend. De simulatieresultaten toonden aan dat er een groot verschil was tussen het dempingsproces van lange golven en dat van korte golven. Terwijl de korte golfhoogte aanzienlijk gereduceerd werd tot bijna nul na het passeren van 100 m brede mangroven, waren de lange golven (lage frequentiegolf hoogte) in staat om verder door te dringen, nl. tot ongeveer 10% van de golfhoogte aan de zeewaartse rand van de mangroves na 300 m, en tot bijna nul na 1000 m binnen het mangrove bos. In deze context, lijken de lange golven een belangrijkere rol te spelen in het creëren van een gunstige omgeving voor zaailingen en sedimentatie binnen het mangrove bos dan korte golven.

Om meer inzicht te krijgen werd een uniek experiment van golfdemping in mangroven opgezet en uitgevoerd in een laboratorium van de TU Delft. Het experiment, bestaande uit verschillende scenario’s met een breed scala aan golfkenmerken, omvatte ook verschillende golfhoogten en periodes, evenals regelmatige, onregelmatige, ongebroken en gebroken golven. De experimentele resultaten bevestigden de rol van vegetatie in het dempen van de golfenergie. Bovendien werd aangetoond dat in bepaalde scenario’s de golfhoogte dempingsprocessen significant beïnvloed werden door de nietlineariteit van de golven. Met andere woorden, golven met een verschillende golfhoogte,

golfperiode en golflengte zwakten op verschillende wijzen binnen het vegetatiegebied af. In deze context is de evaluatie van de golfhoogte-dempingsprocessen in termen van de lengte van de mangrove breedte niet meer relevant; namelijk, afhankelijkheid van golfhoogtevermindering binnen mangroves op hun kenmerken kon niet worden vastgesteld. Daarom werd een nieuwe en meer effectieve golf transmissiecoëfficiënt voorgesteld, waar de golfhoogte-reductie werd geëvalueerd volgens een relatieve lengte, d.w.z. het aantal golflengten.

Tevens werd het Ursell getal ingevoerd om de afhankelijkheid van golfhoogtevermindering op de kenmerken van golven te verduidelijken. De resultaten illustreren dat de golfdempingsprocessen aanzienlijk worden beïnvloed door de golfkenmerken wanneer het Ursell getal binnen 0 tot 250 ligt. Niettemin, wanneer het Ursell getal groter is dan 250 bleken de golfdempingsprocessen niet gerelateerd te zijn aan de golfkenmerken. Tevens werden de experimentele gegevens van het laboratorium gebruikt om het SWASH model te valideren, met inbegrip van verschillende soorten golven, zoals lange golven en korte golven. Het model met standaardparameters is in staat om de transformatie- en dempingsprocessen van inkomende golven door mangroven goed te reproduceren. In deze context kan het numerieke model worden gebruikt om het experiment uit te breiden, i.e. toename van de lengte van de mangroven in het experiment. Derhalve kan de golfdempingssnelheid van meer dan maximaal tien golflengten worden voorspeld. Op deze manier kan met behulp van de experimentele gegevens en de uitgebreide numerieke resultaten de golfdempingsratio voor een specifieke mangrovedichtheid worden gepresenteerd als een functie van het aantal golflengtes en het Ursell getal.

Daar aangetoond werd dat golfkenmerken een rol spelen in het verzwakkingsproces van golven door vegetatie, is het essentieel om het verzwakkingsproces van verschillende types van golven, met inbegrip van lange golven, korte golven, gebonden lange golven, vrije lange golven en gemengde gebonden en vrije lange golven te onderzoeken. De experimentele resultaten suggereren dat lange golven een langere afstand vereisen, afhankelijk van hun overeenkomstige lengtes om dezelfde dempingssnelheid te bereiken als korte golven. Hoewel lange golven verder lijken door te dringen in de mangrove dan korte golven, is de dempingratio per aantal golflengtes van de lange golven groter dan die van korte golven voor de geteste omstandigheden. Er wordt gesuggereerd dat vrije, lange golven een groter dempingratio hebben en gebonden lange golven een lagere dempingssnelheid. Opgemerkt kan worden dat gebonden lange golven en gemengde, gebonden en vrije, lange golven sterk afhankelijk zijn van de golfkenmerken, terwijl de vrije lange golven onafhankelijker zijn van de niet-lineariteit van golven.

Ten slotte, om de kennis en informatie verkregen uit het veld te begrijpen, werd een geschematiseerd numeriek model op schaal, met de natuurlijke mangrove dieptemetingen nagebootst, gebouwd in SWASH. De uitkomst van het numerieke model toont aan dat de bathymetry binnen de mangroven invloed uitoefent op de golfkenmerken rond en binnen het mangrovebos. Hoe steiler de helling in het mangrove bos, hoe hoger de golfhoogte stijging aan de rand van de mangroven en hoe sneller de genormaliseerde golfenergie wordt gereduceerd in het mangrove bos. Hoe steiler de hellingen aan de voorkant van het mangrovebos, hoe groter de golfhoogten aan de voorkant van de mangrovebos en hoe langzamer de energieabsorptie van de golfhoogte in het mangrovebos. Tot slot, hoe smaller de breedte van de mangrove, hoe groter de significante golfhoogte

in de mangroven en hoe langzamer de dempings- processen.

Ondanks de toegenomen kennis en besef van het belang van de processen beschreven in de verschillende hoofdstukken, bestaan er nog steeds lacunes. Dit proefschrift concludeert dat de grootste uitdaging de verdieping van ons begrip ligt in de validaties op werkelijke schaal en in de simulaties van bedding en zwevend sedimentprocessen.

Chapter 1

Introduction

The Earth is 4.6 billion years old. Let's scale that to 46 years. We have been here for 4 hours. Our industrial revolution began 1 minute ago.
In that time, we have destroyed more than half of the world forests.

sciencealert.com.au

1

1.1 Scope and context of the research

THe attenuation of waves through mangrove forest, *i.e.* the reduction of the wave height inside the mangroves, will be investigated in this thesis; in specific the related "squeeze phenomenon", *i.e.* where the mangrove forest width is restricted, will be focus of the research.

Mangroves are species of trees to be recognized by their complex system of roots and stems (Chapman, 1976) developing mostly in the tropical and sub-tropical regions (Alongi, 2009), and living at the intertidal area of the sea water and the land (Duke and Schmitt, 2016). Mangrove roots, stems and canopies (see Figure 1.1) provide an effective tool to inhibit and damp the incoming waves and flows, enhancing fine sediment to be deposited (Kathiresan, 2003). Therefore, it is assumed that the presence of mangrove forests fosters coastal stability reduces erosion induced by flows and waves (Furukawa et al., 1997; Mazda et al., 1995; Wolanski et al., 1990). Mangroves are very sensitive and important ecosystem in the prevention of coastal erosion.

Figure 1.1: Typical mangroves and its complex roots, stems and canopy in the Mekong Delta coast, Vietnam. Photo taken by Marcel Stive, 2015.

However despite the importance role of mangroves in the protection of the shoreline, mangrove forests are one of the most vulnerable ecosystems of the world (Gilman et al., 2008). Mangroves are usually cleared for fish-farming, agriculture (Larson, 2004; Polidoro et al., 2010) and other human activity, and more than 30% of mangroves have disappeared worldwide (Makowski and Finkl, 2018). Consequently, a severe degradation of mangroves has been usually observed along with the erosion of the coastal regions (Phan et al., 2015; Truong et al., 2017).

It should be noted that changes and influences induced by humans are the first to affect the hydrodynamics of the ecosystem, *i.e.* the incoming waves and the attenuation processes of waves in front of and inside the coastal mangrove forest (Yu and Zhang, 2011). Furthermore, the motion of water, caused by waves and tides is of primary importance for the biochemical, trophodynamic and morphodynamic processes inside the mangrove forest and in particular, long waves are the dominant factor controlling the movement of water and sedimentation within a mangrove forest (Massel et al., 1999). Human interventions can directly or indirectly affect incoming waves, reflecting waves

and the attenuation processes of waves inside the mangrove forest, and thereby may also have a considerable influence on the growing conditions of the mangroves. However, knowledge about this topic is still quite limited. The attenuation of surface waves by mangrove trees as well as the mutual interactions between the attenuation process and the changes in hydraulic boundary conditions caused by human intervention is unknown, especially in the context of the presence of long waves, which has only been recognized in recent decades (Masselink, 1995).

Wind-generated waves, or so called wind waves, are surface waves that are generated on the open surface of oceans, seas or rivers when the wind is blown over a large fluid surface area (Kinsman, 2002). Wind waves can travel thousands of kilometers before reaching and entering a mangrove forest. Since the 1980s, the presence of long waves has been recognized (Masselink, 1995). Long waves, or so called low frequency waves, also known as infra-gravity waves, are waves created offshore as bound long waves or at the surf zone as free long waves (Hamm et al., 1993). When high frequency waves (short waves) propagate toward the foreshore, they change their amplitude due to the changes in the water depth and thereby lose their energy and break over the location of depth changes (Agnon, 1993; Longuet-Higgins and Stewart, 1964). In this way, bound low frequency waves may be released to propagate freely becoming free long waves. Furthermore, wave energy can also be transferred from high frequency waves to low frequency waves through the fluctuation of wave set-up in response to fluctuations in incident wave amplitude (List, 1991) or the movement of break points (Schäffer, 1993; Symonds et al., 1982). These mechanisms can occur simultaneously depending on the boundary conditions. Therefore, in reality, long waves can include bound long waves, free long waves and a mixture between the two of them. The presence of these types of waves and their propagation and penetration into the mangrove forest definitely play an important role for the mangrove system from the environmental engineering aspects.

This thesis is a story about coastal mangroves and waves. A range of disciplines, from environmental aspects to specific topics of wave attenuation inside mangroves, are explored. Therefore, different approaches are required during the study, comprising physical, analytical and numerical model. The most fundamental focus of this study is to understand the penetration process of surface waves through mangroves and to relate this process to a study of the “squeeze” phenomenon in the Mekong Delta, Vietnam.

1.2 Coastal mangroves: a delicate balance

Coastal ecological system in general and mangroves in particular are being damaged by changes brought by people on the coastal land as well as in the coastal waters surrounding them. It should be note that more than a billion people live in coastal regions in the world (Neumann et al., 2015). As a consequence, increasing human construction in coastal regions results in an increasing amount of toxic waste, garbage being dumped into the coastal environment, and thus damaging the coastal ecological systems. Additionally, sea level rise caused by the warming climate has also put more pressure on the coastal wetland system which are already suffering from intensive human interventions.

As a result, there are more and more regions of inundation, salt intrusion, mangrove degradation and shoreline erosion (Erlandson, 2008; Zhang et al., 2004). Along

the Mekong Delta coast, coastal mangroves have degraded and the coasts are suffering from erosion at a rapid rate of 50 to 100 m yr^{-1} (SIWRR, 2010). The increase of local fish-farms is considered to be the main reason for the consequential degradation of coastal mangroves (Renaud and Kuenzer, 2012). Many attempts to recover the coastal mangrove system and to protect the coastal region from erosion as for example, by planting thousands of mangrove trees and hard solutions, *i.e.* the defensive concrete structures, are taking place along the Mekong Delta Coast. However, these solutions do not have the wished for effect. The mangrove trees that were planted do not survive after few seasons (Seto and Fragkias, 2007); the concrete structures are considered controversial regarding the long-term and environmental perspective (Nordstrom, 2014).

Figure 1.2: Examples of mangrove restoration project including soft solutions (left panel) and hard solution (righ panel) along the Mekong Delta coast, Vietnam.

Coastal mangroves can retreat landward to deal with the sea-level rise, however, human interventions usually disturb this process, and thereby sometimes making the situation even worse (Doody, 2004; Torio and Chmura, 2013). An accurate understanding of the interactions between a sea dike or fish-farm and the wave attenuation by coastal mangroves is still lacking. Consequently, the achievement and success of restoration projects is quite restricted.

In the literature, wave attenuation studies through coastal mangroves have mostly been conducted for a healthy mangrove forest and where the mangrove width is not restricted. In the Mekong Delta, however, in most locations only a narrow strip of mangroves of about 100-600 m is left (Phan et al., 2015; Truong et al., 2017). In the case study of the mangroves in Mekong Delta, the attenuation of waves, especially long waves, has not been taken into account. The sediment and nutrient exchange through the wave attenuation processes are considered an important factor for a sustainable development of the mangrove system and in our case, of the Mekong Delta mangrove forest.

In summary, insufficient knowledge about the coastal mangroves and its corresponding dominant hydrodynamic processes make it difficult to (1) understand how and why coastal mangroves keep degrading, (2) explain why regions with degraded mangrove usually suffer from more erosion, and (3) propose long term management strategies. These initial issues are the fundamental inspirations of this study.

1.3 Key research questions

As described in the previous section, there are scientific knowledge gaps in (1) understanding the possible relationship between the coastal mangrove forest width and the erosion of the coastal region; (2) the attenuation of waves, short waves as well a long waves, through a coastal mangrove system; and (3) the mutual interaction between different types of waves (long waves, short waves and the mixture of them) within a mangrove forest. In order to find appropriate answers for these knowledge gaps, the gaps are formulated into research questions.

The main question of the research can be stated as follows: ***"How do the wave attenuation processes respond to forces and changes in squeezed coastal mangroves?"***. The term wave attenuation processes refers to the reduction of the wave height induced by the presence of vegetation, the term squeeze is related to the restricted width of the mangrove forest due to the construction of sea dikes land ward. Based on the main research question, several key and sub-key questions can be formulated.

1: "What are the characteristics of coastal mangroves?" (Chapter 2)
2: "Why and how do coastal mangrove forests degrade ?" (Chapter 2)
3: "How does wave non-linearity affects the wave attenuation?" (Chapter 3)
4: "How does the infragravity wave attenuation by vegetation? "(Chapter 4)
5 : "To what extent can the knowledge obtained be applied to a real situation, *i.e.* how is the wave attenuation manifested through a coastal mangrove squeeze in the Mekong Delta ?" (Chapter 5)

1.4 Research methodology and outline

To begin with, mangrove settings in the Mekong Delta coast have been studied through the current literature. The coastal evolution data were collected along with the data of the mangrove forest in all its aspects, but most important for this research, especially the aspect of width. Then, a hypothesis of the coastal mangrove squeeze phenomenon was proposed using an empirical relationship between the mangrove forest width and the coastal evolution data. The explanations were given based on the results of a numerical model, constructed with the state-of-the-art XBeach vegetation model.(Chapter 3)

Subsequently, in order to study the propagation and attenuation processes of waves by vegetation in more detail, a unique laboratory experiment mimicking the coastal mangrove in the Mekong Delta was conducted. The experimental data (the wave height) was collected and analysed.(Chapter 4).

A numerical model mimicking the experiment was constructed in Swash and Swan (Chapter 4). The numerical results were validated using the experimental data, showing the capability of the model in the simulation of wave attenuation processes. The numerical model was then used to expand to the reality scale schematised model mimicking the coastal region of the Mekong Delta. The attenuation of long and short waves was approached at a real scale (Chapter 5). In chapter 6 a synthesis of the conclusions and recommendations for a healthy Mekong Delta mangrove are presented.

References

Agnon, Y. (1993). On a uniformly valid model for surface wave interaction. *Journal of Fluid Mechanics*, 247:589–601.

Alongi, D. (2009). *The Energetics of Mangrove Forests*. SpringerLink: Springer e-Books. Springer Netherlands.

Chapman, V. J. (1976). *Mangrove vegetation*. J. Cramer , California, 447 pp.

Doody, J. P. (2004). ?coastal squeeze?–an historical perspective. *Journal of Coastal Conservation*, 10(1):129–138.

Duke, N. C. and Schmitt, K. (2016). Mangroves: Unusual forests at the seas' edge. In *Tropical Forestry Handbook, Second Edition*, volume 2, pages 1693–1724.

Erlandson, J. M. (2008). Racing a rising tide: Global warming, rising seas, and the erosion of human history.

Furukawa, K., Wolanski, E., and Muellerc, H. (1997). Currents and Sediment Transport in Mangrove\rForests. *Estuarine, Coastal and Shelf Science*, 44:301–310.

Gilman, E. L., Ellison, J., Duke, N. C., and Field, C. (2008). Threats to mangroves from climate change and adaptation options: A review.

Hamm, L., Madsen, P. A., and Peregrine, D. H. (1993). Wave transformation in the nearshore zone: a review. *Coastal Engineering*, 21(1-3):5–39.

Kathiresan, K. (2003). How do mangrove forests induce sedimentation? *Revista de Biologia Tropical*, 51(2):355–359.

Kinsman, B. (2002). *Wind Waves: Their Generation and Propagation on the Ocean Surface*. Dover Phoenix Editions. Dover.

Larson, J. S. (2004). Shrimp Farming and Mangrove Loss in Thailand. *Wetlands*, 24(4):913–913.

List, J. H. (1991). Wave groupiness variations in the nearshore. *Coastal Engineering*, 15(5-6):475–496.

Longuet-Higgins, M. S. and Stewart, R. (1964). Radiation stresses in water waves; a physical discussion, with applications. In *Deep Sea Research and Oceanographic Abstracts*, volume 11, pages 529–562. Elsevier.

Makowski, C. and Finkl, C. (2018). *Threats to Mangrove Forests: Hazards, Vulnerability, and Management*. Coastal Research Library. Springer International Publishing.

Massel, S. R., Furukawa, K., and Brinkman, R. M. (1999). Surface wave propagation in mangrove forests. *Fluid Dynamics Research*, 24(4):219.

Masselink, G. (1995). Group bound long waves as a source of infragravity energy in the surf zone. *Continental Shelf Research*, 15(13):1525 – 1547. Nearshore and Coastal Oceanography.

Mazda, Y., Kanazawa, N., and Wolanski, E. (1995). Tidal asymmetry in mangrove creeks. *Hydrobiologia*, 295(1-3):51–58.

Neumann, B., Vafeidis, A. T., Zimmermann, J., and Nicholls, R. J. (2015). Future coastal population growth and exposure to sea-level rise and coastal flooding - A global assessment. *PLoS ONE*, 10(3).

Nordstrom, K. F. (2014). Living with shore protection structures: A review. *Estuarine, Coastal and Shelf Science*, 150(PA):11–23.

Phan, L. K., van Thiel de Vries, J. S., and Stive, M. J. F. (2015). Coastal Mangrove Squeeze in the Mekong Delta. *Journal of Coastal Research*, 300:233–243.

Polidoro, B. A., Carpenter, K. E., Collins, L., Duke, N. C., Ellison, A. M., Ellison, J. C., Farnsworth, E. J., Fernando, E. S., Kathiresan, K., Koedam, N. E., Livingstone, S. R., Miyagi, T., Moore, G. E., Nam, V. N., Ong, J. E., Primavera, J. H., Salmo, S. G., Sanciangco, J. C., Sukardjo, S., Wang, Y., and Yong, J. W. H. (2010). The loss of species: Mangrove extinction risk and geographic areas of global concern. *PLoS ONE*, 5(4).

Renaud, F. G. and Kuenzer, C. (2012). *The Mekong Delta System: Interdisciplinary Analyses of a River Delta*.

Schäffer, H. A. (1993). Infragravity waves induced by short-wave groups. *Journal of Fluid Mechanics*, 247:551–588.

Seto, K. C. and Fragkias, M. (2007). Mangrove conversion and aquaculture development in Vietnam: A remote sensing-based approach for evaluating the Ramsar Convention on Wetlands. *Global Environmental Change*, 17(3-4):486–500.

SIWRR (2010). Tien Estuary Investigation Report [in Vietnamese]. Technical report, Southern Institute of Water Resources Research, Ho Chi Minh, Vietnam: Ministry of Agriculture and Rural Development of Vietnam, 180 p.

Symonds, G., Huntley, D. A., and Bowen, A. J. (1982). Two-dimensional surf beat: Long wave generation by a time-varying breakpoint. *Journal of Geophysical Research: Oceans*, 87(C1):492–498.

Torio, D. D. and Chmura, G. L. (2013). Assessing Coastal Squeeze of Tidal Wetlands. *Journal of Coastal Research*, 290:1049–1061.

Truong, S. H., Ye, Q., and Stive, M. J. F. (2017). Estuarine mangrove squeeze in the mekong delta, vietnam. *Journal of Coastal Research*, 33(4):747–763.

Wolanski, E., Mazda, Y., King, B., and Gay, S. (1990). Dynamics, flushing and trapping in Hinchinbrook channel, a giant mangrove swamp, Australia. *Estuarine, Coastal and Shelf Science*, 31(5):555–579.

Yu, G. and Zhang, J. Y. (2011). Analysis of the impact on ecosystem and environment of marine reclamation-A case study in Jiaozhou Bay. In *Energy Procedia*, volume 5, pages 105–111.

Zhang, K. Q., Douglas, B. C., and Leatherman, S. P. (2004). Global warming and coastal erosion. *Climatic Change*, 64(1-2):41–58.

Chapter 2

Coastal Mangrove Squeeze in The Mekong Delta

When it hurts-observe;
Life is trying to teach you something.

Anita Krizzan

Along the Mekong eastern and southeastern coast, mangrove degradation and rapid coastline erosion are observed at many locations. At these locations, the mangrove forests usually consist of a narrow strip only, sometimes as narrow as 100 m. This mangrove squeeze is mainly due to the construction of sea dikes in a quest for the creation of space for cultivation and the prevention of salinity intrusion. The basic assumption behind our work is that there is a critical minimum width of a coastal mangrove forest strip to keep its ability to stay stable or, once surpassing the minimum width, to promote sedimentation. The larger the width the more efficient the attenuation of waves and currents will be, offering both a successful seedling and sedimentary environment. Our analysis of available data both from literature and from satellite observations supports our basic assumption: an average critical width of 140 m is found for the southeastern and eastern Mekong Delta coast as a minimum width to sustain a healthy mangrove forest. To further our insights into the efficiency of mangrove to attenuate wave energy as a function of their width we have applied a state-of-the-art wave propagation model that includes both short and long waves. Our results confirm earlier results from the literature that short waves are indeed attenuated very rapidly over distances shorter than the critical width, but as we show for the first time infragravity waves penetrate over much larger distances. We therefore hypothesize that the decay of long waves plays a crucial role in the health of the mangrove.

Parts of this chapter have been published in Journal of Coastal Research, Volume 31 , Issue 23, pages 243–253. Linh, K. Phan., Van Thiel de Vries, J. S . M. , and Stive, M. J. F (2015). Coastal mangrove squeeze in the Mekong Delta, Vietnam.

2.1 Introduction

The Mekong Deltaic River System (MDRS) in Vietnam (also known as the Cuu Long or the "Nine Dragons", because of the nine river outlets, although presently only now eight are left (see Figure 2.1) covers an area of 39 000 km^2 and is home to more than 17 million inhabitants. Although this is not very well known, this region is as populated as that of a country of similar size like the Netherlands, which is known as one of the most populated in the world. This is an important reason for the pressure on coastal land use.

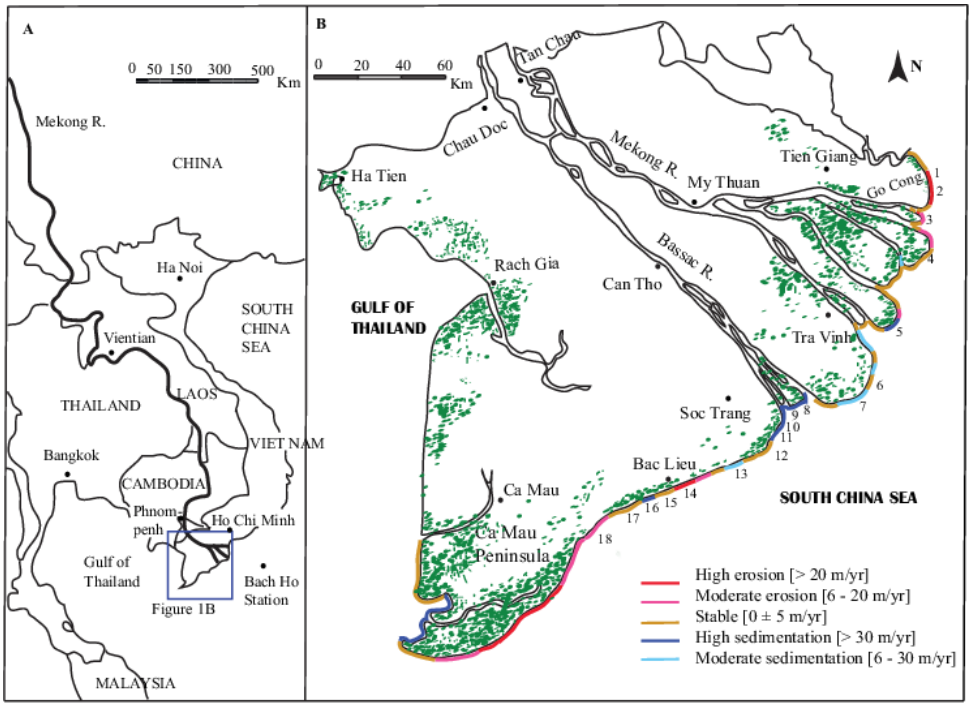

Figure 2.1: (A) Location of the study site in Southeast Asia. (B) Map of the Mekong Delta in Vietnam showing mangrove locations by green dots (after Spalding et al. (2010)); location of places mentioned in the text and the coastline evolution from 1989 to 2002. Places that were chosen to analyze coastline evolution in relation to mangrove space are numbered from 1 to 18. Place names are given in Table 2.1.

The MDRS shapes its initial course at Phnom Penh, Cambodia, where the river divides into two main distributaries, the Mekong (Tien River) and the Bassac (Hau River). The Tien then divides into five and formally six main channels and the Hau into three channels to form the original Nine Dragons of the MDRS. The Mekong deltaic coast, which has progressed in the Holocene from the Cambodian border to its present position, is historically rich in sediment with an overall sedimentation of both sand and fines (silt and clay), creating a coastline of both mangrove and non mangrove sections (Nguyen et al., 2000). The average suspended sediment concentrations (SSC) from 1993 to 2000 reach approximately 100 mg/L, 50 mg/L, and 80 mg/L at Tan Chau, Can Tho, and

My Thuan stations, respectively (Figure 2.1B) (Lu and Siew, 2005). Along the South China Sea, the Mekong Delta coast can be characterized respectively into the eastern zone from Tien Giang Province to Soc Trang Province featuring an estuarine environment, and the south eastern zone from Soc Trang Province to Ca Mau Cape featuring a transient tidal and coastal environment (Figure 2.1B).

Presently, sedimentation still prevails near the estuarine inlets (Figure 2.1B), but due to natural and human-induced causes, erosion is occurring away from the inlets and it is anticipated that erosion will increase in the future for several reasons: the increasing number of dams in the Mekong River capturing SSC, the increasing human-induced subsidence due to groundwater extraction, and climate-change-induced sea level rise (IUCN, 2011). The decrease of SSC and of mangrove health due to coastal mangrove squeeze is causing a high human-induced impact, which is our subject of interest. This coastal region experiences the compound impacts from climate change and human intervention most clearly. Coastal recession contributes to the loss of mangrove and land and increases salinity intrusion, creating problems for many functions, such as agriculture and aquaculture and coastal infrastructure. Although this is a very important area, the south eastern and eastern coasts are as yet quite understudied.

The recognition that coastal ecosystems will increase to retreat landward when relative sea level is rising has been noted abundantly in the literature (Gilman et al., 2007). However, whenever coastal development such as urbanization, agriculture, aquaculture, and infrastructure plays a role as a blocking barrier, this will stop this migration and lead to the loss of valuable coastal habitats (Feagin et al., 2010). This loss was recognized by Doody (2004) as "coastal squeeze" when this author realized the necessity of keeping space for "coastal habitats to operate". The term coastal squeeze then is used more frequently by other researchers Gilman et al. (2007); Torio and Chmura (2013) when coastal habitats such as mangrove and other tidal wetlands are in danger because of sea-level rise and limiting the available space for migration landward. We therefore adopt the term "coastal mangrove squeeze" in this paper to emphasize the very same situation that is now operating on the Mekong Delta coast in Vietnam.

2.2 Method

After our description of the study site and the mangrove forests in their local and international context, we first present our analysis of our observations of mangrove widths and coastal behavior and compare this with existing literature. We then apply numerical process-based models to investigate in more detail the decay of both high-frequency and low-frequency wave damping. This we consider as a new addition to the research that has been done today. The low-frequency wave damping has not been considered in the international literature and we hypothesize that this is an important process that cannot be ignored.

2.2.1 Study Site in Global and Regional Context

Mangroves can be classified according to quite different environmental factors. On a global scale mangroves are divided into six tropical regions on the basis of their conti-

nental border: western America, eastern America, western Africa, eastern Africa, Indo-Malesia, and Australia (Duke, 1992). Vietnam belongs to the Indo-Malesian class of the

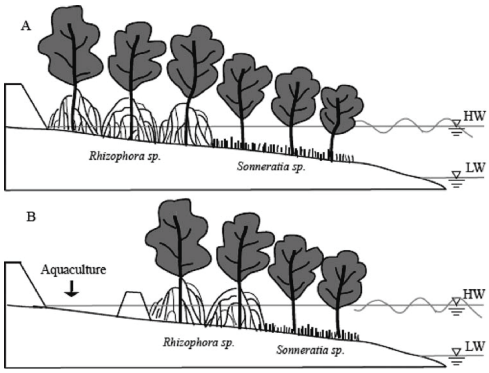

Figure 2.2: Two different systems of mangrove and sea dike locations along the southeastern coast and the eastern coast of MDRS. (A) Sea dikes are located right behind mangrove forest. (B) Human intervention is found in between sea dike and mangrove forest.

most biodiverse region in the world (Alongi, 2002). Mangroves can also be defined into six classes according to their physiognomy: fringing, riverine, overwash, basin, scrub, and hammock (Lugo and Snedaker, 1974), in which coastal mangrove distributed alongshore and often exposed to waves is recognized as fringing mangrove. Woodroffe (1992) created a ternary diagram by adding the dominant physical process of tide-dominated, river-dominated, and interior mangrove into this classification. Then Ewel et al. (1998) proposed a hybrid of these two systems above by referring to tide-dominated mangrove as fringe mangrove, river-dominated mangrove as riverine mangrove, and interior mangrove as basin mangrove.

According to these classifications, coastal mangrove in the MDRS can be characterized as fringe mangrove under tide dominance. It is estimated that nearly 40% of the mangrove forests in southern Vietnam were destroyed during the Vietnam War (1962–1971) (Hong and San, 1993). Over 20% of about 600,000 ha of the total mangrove-forested regions of South Vietnam was defoliated in 1968 by chemical spraying. Since 1975 mangrove forests initially recovered as a result of both natural regeneration and manual planting. However, in the 1980s and early 1990s the mangrove forests were again heavily destroyed because of timber overexploitation for construction, charcoal, and conversion of forest land into aquaculture-fisheries farming systems (Christensen et al., 2008). By the mid-1990s forest-felling bans were imposed and the forest enterprises were forced to replant and protect the forest rather than utilize it; however, by 1999 the felling ban ceased.

Nowadays, along the eastern (locations 1 to 7) and south eastern (locations 8 to 18) coasts, there are many locations where mangrove degradations are observed. At these locations, the mangrove forests usually consist of a narrow strip only, sometimes as narrow as 100 m. This mangrove squeeze is mainly due to the construction of primary sea dikes protecting the hinterland against flooding or smaller secondary sea dikes in front of the primary sea dikes protecting aquaculture (Figure 2.2). Government officials usu-

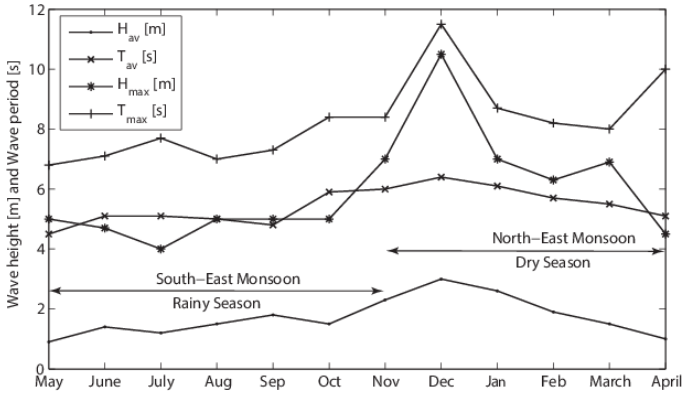

Figure 2.3: Monthly offshore wave parameters at Bach Ho station, situated 150 km offshore MDRS (see Fig 1A); the wave height and wave period reach their maximum value in December. Data were collected from 1986 until 2006.

ally blame the mangrove loss as well as dike collapse on sea-level rise and stronger wave action (IUCN, 2011). However, we hypothesize that mangrove squeeze due to the construction of the sea dikes is the main reason for mangrove loss and dike collapse. Subsidence due to natural causes and groundwater extraction may play a role as well. The basic assumption behind our work is that there is a critical minimum width of a coastal mangrove forest strip to keep its ability to stay stable or, once surpassing the minimum width, to promote sedimentation. The larger the width the more efficient the attenuation of waves and currents will be, offering a successful environment for both propagules and sedimentation.

The MDRS and its directly adjacent coasts have historically been under the influence of both the freshwater discharge and the actions of the tide. The freshwater discharge is very high during the flood season, especially during September and October, with an average maximum flow rate of 25 500 $m^3 s^{-1}$, whereas during the relatively long dry season the flow is quite low, with an average lowest monthly discharge of about 2300 $m^3 s^{-1}$ in April (Tri, 2012). Especially in the dry season the tidal flows dominate. Tides in this region of the South China Sea have a semi diurnal character with a high range (more than 2 m at mean tide, increasing to 4 m at spring tide). As the tidal range decreases toward Ca Mau Cape, the number of diurnal tidal days and the diurnal characteristics increase, causing the tide to display a more diurnal than semi diurnal appearance. This is due to non-linear interactions caused by the impact of the large shelf width on the tidal characteristics.

Although the coastal environment of the MDRS is traditionally classified as a tide-dominated environment this system is increasingly more influenced by waves as the SSCs discharged by the Mekong River are observed to decrease, which increases the impact of waves (Ta et al., 2002). Offshore winds and waves at the East Sea are measured at some 150 km offshore at Bach Ho station (Figure 2.1A) (Hoang and Nguyen, 2006). In winter (November to April) the NE monsoon is dominating and blowing from NE to SW; in summer (May to October) the SW monsoon is dominating and blowing from

Figure 2.4: Monthly offshore wave parameters at Bach Ho station, situated 150 km offshore MDRS (see Fig 1A); the wave height and wave period reach their maximum value in December. Data were collected from 1986 until 2006.

SW to NE. On the basis of the observed data, the average and maximum wave heights (H_{av},H_{max}) and wave period (T_{av}, T_{max}) for every month at Bach Ho station can be observed in Figure 2.3. In the dry season, the highest wave height and period are 10.5 m and 11.5 s, respectively. At this time strong wave energy with waves of 4 m significant height occur, whereas in the rainy season, wave heights are not larger than 3 m and T_s= 5 to 12 s. Although the waves offshore can be very high, we will show later in our modelling approach that the very gentle slopes of the foreshore cause a strong damping of the wave heights to arrive inshore. This also implies that annual variations in the wave data need not be considered.

2.2.2 Observations of Mangrove Width and Coastline Evolution

In this section we investigate our hypothesis that once mangrove width is under squeeze, i.e. when either the primary or the secondary dike is too close to the non vegetated foreshore, erosion is usually occurring and the health of the mangrove forest is under stress (see Figure 2.2 showing an illustrated schematization). The sections that we have chosen are near the estuarine inlets, so that sediment availability should not be a limiting factor. These two systems are found both along the south eastern coast and the eastern coast.

The first system is Google-illustrated at Go Cong 1 and 2 (Figure 2.4A and B; Vinh Trach Dong and Ganh Hao), where the primary sea dike is located right in front of the

Table 2.1: Coastal evolution rate over two periods of observation and Google-based estimated mangrove widths in 2002 at different locations along the southeastern coast and the eastern coast of the MDRS.

No.	Cross-Section	1965–1989		1989–2002		Mangrove Width (m) Converted to 2002	
		Coastline Change (m)	Evolution Rate (m/yr)	Coastline Change (m)	Evolution Rate (m/yr)	Range (m)	Representative Value (m)
1	Go Cong 1	-250	-10	-350	-25	160-260	240
2	Go Cong 2	-350	-15	-300	-20	-	90
3	Phu Tan	2500	105	-130	-10	-	40
4	Binh Dai	1200	50	0	0	30-40	30
5	Thanh Phu	600	25	900	70	320-570	520
6	Tra Vinh 1	0	0	0	0	30-70	50
7	Tra Vinh 2	0	0	130	10	0-50	0
8	Cu Lao 1	900	40	650	50	600-750	700
9	Cu Lao 2	1800	75	1000	80	740-890	790
10	Kinh Ba 1	-350	-15	550	40	380-530	480
11	Kinh Ba 2	0	0	1000	80	440-590	540
12	Vinh Hai	-280	-10	0	0	150-250	200
13	Vinh Chau	0	0	350	25	190-290	240
14	Vinh Trach Dong 1	0	0	-350	-25	150-290	260
15	Vinh Trach Dong 2	0	0	0	0	200-300	250
16	Vinh Loi 1	700	30	600	45	420-570	515
17	Vinh Loi 2	1600	65	0	0	100-300	200
18	Ganh Hao	-200	-15	-130	-10	140-240	190

squeezed mangrove forest. In the second system, human interventions are found between the sea dikes and the mangrove forest. Kinh Ba is an example of the second system where about 300 m width in between the sea dike and the mangrove forest is used for aquaculture (Figure 2.4C). To have land protected for cultivation, a smaller and discontinuous sea dike is constructed between the aquaculture area and the mangrove forest.

We have chosen to include observations from those regions where we infer that a sediment source is still available because of the near presence of the riverine outflow, so that sediment availability is not a limiting factor. These observations are taken at different locations that undergo either erosion or sedimentation from Go Cong to Ganh Hao (chosen locations are numbered from 1 to 18 in Figure 2.1B; location names can be found in Table 2.1). According to the scale classification of shores and shoreline variability presented by Stive et al. (2002), we are interested in evolutional trends based on the middle term scale with a time scale from years to decades and a space scale from 1 km to 5 km. On the basis of the observations the typical length scale along which the rate of erosion or sedimentation can be considered rather similar is about 2 km. Ca Mau Peninsula is not considered since no sea dikes are built along the coastline of this area. The rate of coastline evolution is calculated on the basis of the shoreline evolution maps provided by the SIWRR (2010). The evolution rates presented in Table 2.1 are calculated for two periods, from 1965 to 1989 and from 1989 to 2002. For each of the locations the estimated mangrove width in 2002 is also presented in Table 2.1. The mangrove widths, measured from Google Earth for the year 2006, were converted to 2002 by using the observed accretion and sedimentation rates. The error term involved in using this approach is not so much due to ground-referencing errors (the location of the primary or secondary sea dike is not influenced by water levels, for instance), but rather due to alongshore variability over the considered stretches that we have included in our data presentation (the horizontal error bars in Figure 2.5).

Before presenting our relation between coastal evolution and mangrove width, we first reflect on the erosion and accretion observations over the two periods. In the period 1965–1989 five (1, 2, 10, 12, and 18) of the 18 stretches experienced erosion. In the period 1989–2002 also five (1, 2, 3, 14, and 18) stretches experienced erosion; hence there exists variability. However, in general the erosive stretches experienced more erosion, whereas some stretches turned from stability to erosion. We refrain from making a general statement on the nature of the coastal evolution, realizing that this is also related to the supply of sediment from the MDRS and now present the relation between coastal evolution and mangrove widths.

Our suggested relationship between mangrove widths and the southeastern and the eastern coastline evolution is presented in Figure 2.5. In this figure the vertical axis shows the evolution rate from 1989 to 2002 (since our mangrove width observations are from 2002) and the horizontal axis shows the mangrove width. The uncertainty bars are applied in both vertical and horizontal directions. The vertical bar presents the uncertainty in determining the evolution rate, on average 5 m yr^{-1}, which is at most half but often much less than half the observed rate. The horizontal bar presents the uncertainty in quantifying the mangrove width. It is based on the range of the mangrove width that is measured within 2 km(Table 2.1). A linear trend line is added to show the tendency of the relationship.

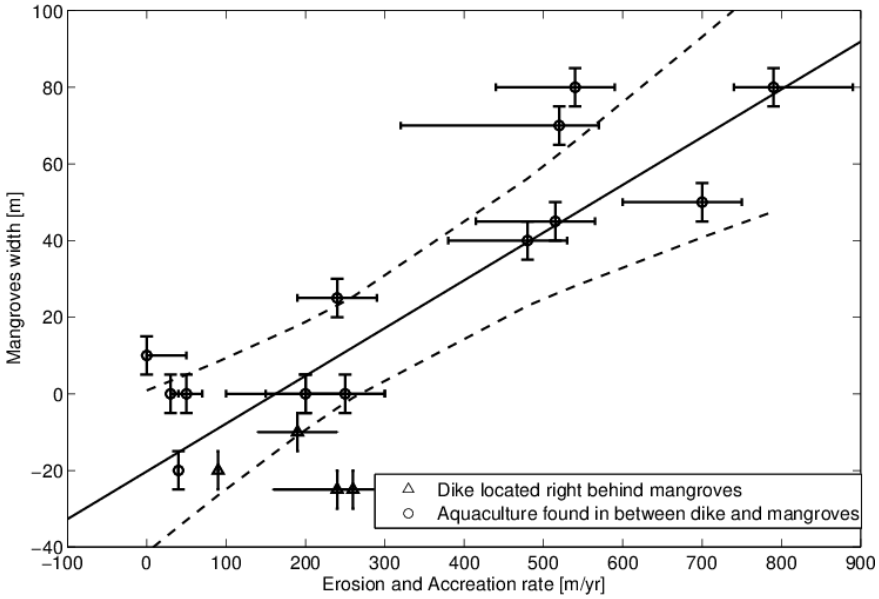

Figure 2.5: Relationship between mangrove width and coastline evolution along the east coast of the MDR, showing the best fit and the 90% confidence interval.

Although the interpretation of the results is somewhat subjective, we deduce from Figure 2.5 that the shoreline will remain stable with the presence of approximately 30 m to 250 m width of the mangrove forest, with an average value of 140 m. A larger width will lead to a higher sedimentation potential.

However, the coastline evolution also depends on many other factors such as sediment supply, hydraulic conditions (wave, wind, current), bathymetry, *etc.* Therefore, there is no unique critical mangrove width value that can be set for all shorelines. For instance, there will be a difference between the critical mangrove width of the south eastern coast and the eastern coast and that of the west coast. Even though the West Sea has smaller tidal amplitudes and smaller wave heights, the sediment supply in the West Sea is also weaker than in the South China Sea. Therefore, no significant erosion is observed along the west coast, nor is there much sedimentation found even at the location where the mangrove forest width is about 900 m. The quantitative relationship that we provide will therefore only be applicable for the southeastern coast and the eastern coast of the Mekong Delta, although the general principle will apply to many mangrove coasts.

2.2.3 Wave Attenuation as a Function of Mangrove Forest Width

We conjecture that the health of a coastal mangrove forest is determined by its effectiveness to attenuate wave energy, which is obviously related to its width. The purpose of this section is to achieve insight into the wave transformation in the mangrove forest and suggest a rough estimation for the necessary distance from the sea dike to the mangrove forests along the southern coast of Vietnam in relation to the wave attenuation. To further our insights into the efficiency of mangrove to attenuate wave energy as a function of their width we have applied a state-of-the-art wave propagation model that includes both short and long waves. On the basis of bathymetric maps available at Delft University of Technology's map room, Soc Trang coast is chosen to present a typical coastline profile in the southern coast of Vietnam. The foreshore of the southern coast of Vietnam has a quite gentle slope (1/30000). The water depth reaches 30 m at a distance of about 100 km offshore. Along this coast, mangroves are found to display a healthy development when a magnitude order of more than 1000 m width is present.

2.2.4 Mangrove Cross-Shore Distribution

For our modeling purposes we need to define more precisely our assumptions on mangrove cross-shore distribution. Mangrove marshes are distributed along the present coastline and are usually located behind a tidal flat. Mangrove-dominated intertidal environments are quite extensive in the south eastern part of the Ca Mau Peninsula and along the mainland margins of the estuaries (Figure 2.1B). Mangroves are typically distributed from mean sea level (MSL) to highest spring tide (Alongi, 2009; Hogarth, 2015), since below MSL the seedlings cannot settle and at higher levels the mangroves cannot compete with other plants (Schiereck and Booij, 1995). A succession of mangroves in the Mekong Delta is roughly described by three stages (Hong and San, 1993):

Pioneer stage: is typically found on tidal flats, which are flooded by the mean tide. *Sonneratia alba* and *Avicennia alba* are pioneers because these two species can tolerate extensive floods and high salinity. Also they share the same biological characteristics and have pneumatophore roots.

Transitional stage: is recognized by a community of *A. alba* and *Rhizophora apiculata*. Propagules of *Rhizophora* are protected by the pioneer against the waves. After 4–5

Figure 2.6: Mangrove root systems. (A) Stilt roots of Rhizophora sp. (Treknature). (B) Pneumatophores roots of Avicennia sp. and Sonneratia sp. (CMP).

years they can surpass A. alba and as a result the pioneer species are eliminated in the course of time.

Final stage: is only flooded with high tide and therefore includes other mangrove species, making the final stage a multispecies community.

The southern coast has favorable conditions, especially rainfall and the availability of alluvial sediment, for the growth and distribution of mangrove trees. Therefore, mangrove species are quite diverse in this area. For brevity in the numerical simulations we have divided mangrove species into two main families, *Rhizophora* sp. and *Sonneratia* sp., which means the pioneer stage is covered by *Sonneratia* sp. and the transitional stage and the final stage are covered by *Rhizophora* sp. This choice is based on the fact that mangroves are easily distinguished by their root systems, which are highly adapted to their specific habitat (Figure 2.6). *Rhizophora* sp. is typical for a prop root system (stilt roots) that arises from its trunk and its lower branches. *Avicennia* sp. and *Sonneratia* sp. are known by their pneumatophores, which are erect lateral branches of the horizontal cable roots, and are themselves growing underground (De Vos, 2004). *Sonneratia*, the pioneer species, is applied near the water line and *Rhizophora* sp. is applied farther inshore. Since there are no common rules for the transition from the pioneer species to the species associated with the transitional stage, it is assumed that *Sonneratia* sp. will be present from MSL to the middle of the forest (for example, x= 1000 m in case of 2000 m mangrove forest width) and *Rhizophora* sp. will be present from the middle to the edge of the forest at the landward side.

2.2.5 Xbeach Model

The effectiveness of wave attenuation by a mangrove forest depends mainly on vegetation properties and hydraulic boundary conditions as discussed by several researchers (Burger, 2005; De Vos, 2004; Meijer, 2005; Suzuki, 2011). Quite a limited number of studies on wave attenuation in the field in Vietnam have been published. Among these studies, four of them are about fringing mangrove (Bao, 2011; Mazda et al., 2006, 1997; Quartel et al., 2007), and one is about riverine mangrove at the southern coast of Vietnam

Table 2.2: Different scenarios for XBeach simulation, Soc Trang case study.

Mangrove Width	Mangrove Density
1. No sea dike + 2000 m mangrove width	1. Spare density
2. Sea dike + 1000 m mangrove width	2. Average density
3. Sea dike + 600 m mangrove width	3. Dense density
4. Sea dike + 400 m mangrove width	
5. Sea dike + 200 m mangrove width	

(Hong Phuoc and Massel, 2006). The field experiment on wave motion and suspended sediment transport of riverine mangrove at Can Gio (Hong Phuoc and Massel, 2006) was used to validate a theoretical model for wave propagation through a nonuniform forest of arbitrary water depth proposed by Vo-Luong and Massel (2008). On the basis of the field observations at Tong Kinh Delta and at Vinh Quang coast, Mazda et al. (2006, 1997) suggested a quantitative formulation of the relationship between vegetation characteristics, water depth, and incident wave conditions. This relationship once again confirmed the field study of Quartel et al. (2007) on wave attenuation in coastal mangrove in the Red River Delta. Bao (2011) collected data on wave height attenuation and mangrove characteristics from 32 mangrove plots located in two coastal regions in Vietnam: the Red River Delta and Can Gio mangrove forest. This research proved the importance of sufficient mangrove bandwidth for wave height attenuation. However, in all these studies only short waves are considered, whereas longer waves generated by wave groups are expected to play an important role in the hydrodynamics and sediment transport processes within mangrove systems as suggested by Brinkman et al. (1997). The mildly sloped mangrove beaches and their even more gently sloping foreshores create dissipative conditions in which the incident wind and swell waves dissipate most of their energy before reaching the shoreline. At the edge of the mangrove forests the longer infragravity band will therefore already substantially contribute to the water surface variance. Within the mangrove forest this effect is enhanced since longer-period waves such as swells and infragravity waves are subject to less attenuation, whereas short-period waves with frequencies related to wind waves lose substantial energy due to stronger interactions with the vegetation. To consider the effect of both incident waves and infragravity waves, the XBeach model was used in this study to provide insight into the wave attenuation in mangrove forests and to evaluate the critical value of mangrove width as found for the east coast of Vietnam in more quantitative terms.

XBeach is a two-dimensional model for wave propagation, long waves, and mean flow. The model consists of formulations for short-wave envelope propagation, non stationary shallow water equations, sediment transport, and bed update. Innovations include a newly developed time-dependent wave action balance solver, which solves the wave refraction and allows variation of wave action in x, y, time, and over the directional space, and can be used to simulate the propagation and dissipation of wave groups (Roelvink et al., 2009). Recently, the development teamhas been working on a very new application: “wave attenuation by vegetation on XBeach”. Wave attenuation by vegetation is successfully implemented in the simulating waves nearshore (SWAN)

Table 2.3: A set of flat bottom cases (Suzuki, 2011).

Case Name	Wave	h (m)	H_1(cm)	$T(s)$	C_d
F2I100516	Irregular	0.1	5.0(H_s)	1.6(T_p)	1.35
F9I100516	Irregular	0.1	5.0(H_s)	1.6(T_p)	0.8

model for short waves by Suzuki (2011). The implementation is based on an energy attenuation equation first provided by Dalrymple et al. (1984), which was further developed and validated by Mendez and Losada (2004):

$$D_v = \frac{1}{2\sqrt{\pi}} \rho C_D b_v N_v \left(\frac{k}{2\sigma}\right)^3 \frac{\sinh^3(k\alpha h) + 3\sinh(k\alpha h)}{3k\cosh^3(kh)} H^3{}_{rms} \tag{2.1}$$

where D_v is the time-averaged rate of energy dissipation per unit area; C_D, b_v, and N_v are the vegetation drag coefficient, diameter, and spatial density; k is the average wave number; r is the average wave frequency; αh is the mean vegetation height; h is the water depth (m); and H_{rms} is the significant wave height at that point (m).

In the XBeach model, the short-wave attenuation by vegetation is implemented in a comparable way, where k and r are respectively the wave number and wave frequency associated with the peak period of the incident waves. The long wave attenuation by vegetation is modeled with a Morrison type equation defined as:

$$F_v = 0.5 C_D b_v N_v \frac{\alpha h}{h} u|u| \tag{2.2}$$

where u is the orbital velocity.

The vegetation properties can be specified for multiple species and can vary per species over the vertical to mimic a mangrove tree. In XBeach a vegetation-file can be specified that contains a file list with vegetation properties including number of vertical sections, the height of a section (h), drag coefficient (C_D), number of plants per unit area (N_v), and plant area per unit height (b_v). To check the correct implementation and applicability of XBeach we have included a comparison with laboratory experiments.

The XBeach model was recently extended to simulate short and long-wave attenuation by vegetation. To validate the implementation the numerical result of short-wave attenuation over vegetation is compared with the experimental results of Suzuki (2011). The most relevant cases are the two flat-bottom cases with irregular incoming waves. In this experiment rigid artificial vegetation was used, made of smooth plywood cylinders with diameter D = 0.6 cm, cylinder height h_{veg} = 10 cm, and densities of 242 units/m2 (case F2) and 962 units/m2 (case F9). The input parameters are given in Table 2.3, in which h = 0.1 m is the water depth at the impermeable flat bottom. Wave period T and wave height HI are input values for the wave generation.

Figure 2.7 shows the experiment results and numerically calculated short-wave heights in two chosen cases F2 and F9. The vertical axis shows the wave-height attenuation and the horizontal axis shows the distance from the wave generation. The vegetation is located from x = 16.3 m to x = 19.3 m.

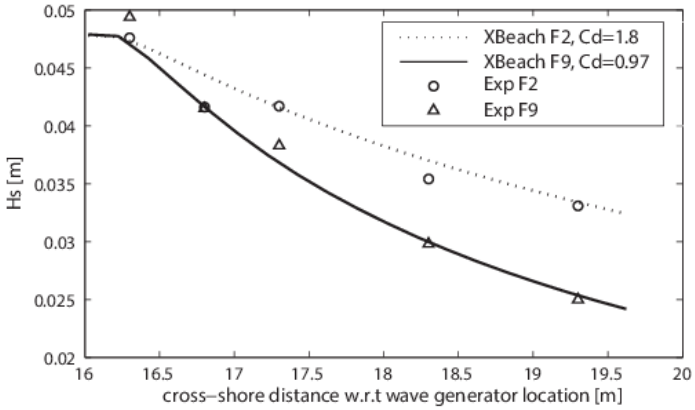

Figure 2.7: Short-wave attenuation over vegetation is validated on the basis of experiment of Suzuki (2011).

As shown in Figure 2.7, it is confirmed that the wave height calculated by the numerical model is in good accordance with the flume experiment of Suzuki (2011). It has to be noted that there is a difference in drag coefficients that are used in XBeach model and in results of Suzuki (2011). The drag coefficients are CD=1.8 and CD=0.97 in case F2 and case F9 respectively with XBeach model, differing only 10 to 20% from those used by Suzuki (2011). These differences of the drag coefficients used in the XBeach model and in results of Suzuki (2011) are not significant and are acceptable. Drag coefficients from results of Suzuki (2011) are obtained from the SWAN calculations. XBeach and SWAN have different approaches to calculate wave-height attenuation therefore it might create a slightly different drag coefficient than that used by each model.

2.2.6 Different Scenarios and Input Parameters

Five scenarios of mangrove width are considered, including a case without a sea dike on which mangroves are expected to healthily develop from MSL up until mean high water (MHW) (Table 2.2). In four other cases the mangrove width is limited by the presence of a sea dike. For each case three scenarios of mangrove density (spare density, average density, and dense density) were considered. No variations in vegetation height are taken into account since the water depth is quite small compared with the mangrove height.

The simulations discussed are executed with XBeach revision range 3234:3237 and default settings were used as much as possible. Specific settings are explained below and are related to bathymetry, hydraulic boundary conditions, and vegetation properties.

The one-dimensional cross-shore bathymetry was estimated using hydro-graphic maps from the Delft University of Technology map room. Three depth contours from 10 to 30 m (extending up to 100 km offshore) were digitised manually from the maps. Intermediate contours were interpolated using a simple Matlab script. The tidal levels at Mekong Delta are recorded for every hour at two stations. Hon Ba is the offshore station, located at Con Dao Island (883805400 N, 10683301800 E). The nearshore station is lo-

Table 2.4: Vegetation parameters (Ranasinghe et al., 2010)

Parameters	*Sonneratia*	*Rhizophora*
Stem diameter (m)	0.3	0.25
Root diameter (m)	0.02	0.075
Canopy diameter(m)	0.5	0.5
Stem height (m)	6	6
Root height (m)	0.5	0.8
Canopy height (m)	2	2
Density variations		
Stem (m-2)		
Spare	0.5	0.5
Average	0.7	0.7
Dense	1.7	1.7
Root (m-2)		
Spare	25	30
Average	50	60
Dense	100	130
Canopy (m-2)		
Spare	50	50
Average	100	100
Dense	100	100

cated at Vung Tau (1082404300 N, 1078801100 E).The spring tidal ranges at Hon Ba and Vung Tau are 0.4–3.5 m and 0.3–3.5 m respectively. In this study the tidal range chosen is 0.4–3.5 m. From this range, MSL is found to be 1.95 m. Since there is no available information about the slope of mangrove forest at Mekong Delta, the slope was estimated as follows. Mangroves are only found between MSL and MHW, which means from 1.95 m to 3.5 m above ordnance datum. Observations from Google Earth show that the mangrove width at Soc Trang coast is in the order of approximately 1500 m. Therefore the slope of the mangrove forest at Soc Trang is estimated to be about 1/1000.

The nine vegetation parameters—three for each of the three layers that had to be estimated or measured on the basis of the requirements of the XBeach model—are the diameters (b_v), densities (N_v) and heights (αh) of the roots, stem, and canopy. The characteristics of *Rhizophora* sp. and *Sonneratia* sp. are fully described by Ranasinghe et al. (2010) for mangrove in India, which we have adopted here. We defend applying these parameters for mangrove species in Vietnam because of the similarities between the mangrove species in the Mekong Delta and those in India (including *Sonneratia* sp. and *Rhizophora* sp.) (Table 2.4).

A representative wave height to be applied as offshore boundary condition in our simulations is derived as follows. An important part of the cross-shore sediment transport rate is proportional to the odd moment $\langle u|u^2|\rangle$ (Bosboom and Stive, 2011), where u is the instantaneous cross-shore velocity and the brackets indicate time averaging. The term u^2 can be interpreted as representing the sediment concentration stirred up by the

oscillatory wave motion. In shallow water this motion is proportional to the wave height. This we have used to derive a representative wave height by weighing the square of the wave height with its frequency of occurrence, which resulted in a representative offshore wave height of 3 m.

2.3 Results

Here we discuss the results of our simulations of wave transformation from offshore to nearshore for the various cases considered. The reference case is a situation with no mangroves,which is compared with various mangrove density cases. Finally, the effect of a sea dike at various distances from the waterline is discussed.

2.3.1 Wave Transformation from Offshore to Nearshore

The wave height transmission for both long and short waves from offshore to nearshore is shown in Figure 2.8. Because of wave breaking, the short wave height (H_{hf}) decreases gradually to less than 0.5 m at the seaward edge of the mangrove forests. The long wave height (H_{lf}) first slightly increases toward the shoreline until x=−4000 m and then starts to decrease slowly. At the seaward edge of the mangroves the long wave height exceeds the short wave height.

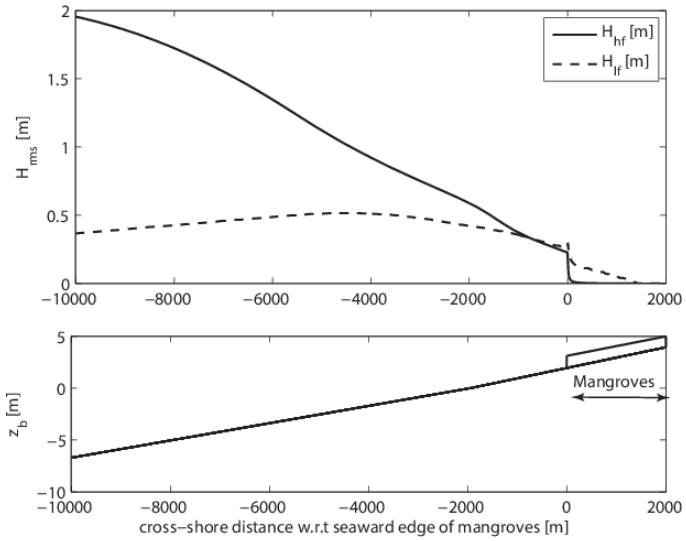

Figure 2.8: Example of wave height transmission from offshore to nearshore in case of 2000 m mangrove width; H_{rms} is the root mean square wave height and z_b is the bed level, relative to MSL.

2.3.2 Wave Transformation without Mangrove

Figure 2.9 shows the normalized wave energy transformation over a profile without mangrove. The vertical axis shows the normalized wave energy and the horizontal axis shows the cross-shore distance with respect to the shoreline position at MSL (this location is commonly associated with the seaward edge of mangrove vegetation).

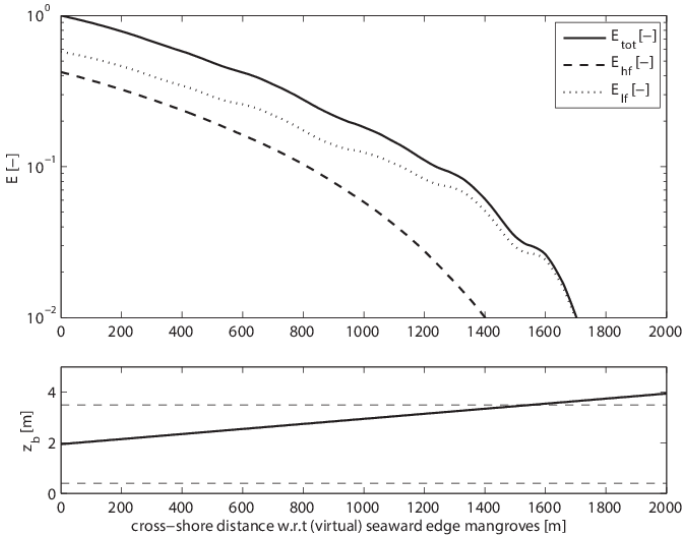

Figure 2.9: Normalized wave energy transformation in case of no mangrove, in which E_{tot} is the total wave energy, E_{hf} is the high-frequency energy or short-wave energy, E_{lf} is the low-frequency energy or long-wave energy, and z_b is the bed level.

The normalized wave energy at a specific location x is defined as the ratio between the wave energy at this location divided by the wave energy at x=0 and is a measure for attenuation. It can be seen from Figure 2.9 that at x=60% of the incoming wave energy is in the long waves (E_{lf}) and only 40% of the energy is in the short waves (E_{hf}). On the basis of this finding it is anticipated that the penetration of long waves cannot be neglected in understanding mangrove hydrodynamics.

2.3.3 Wave Transformation in Case of Different Mangrove Densities

The wave transformation in a 2000 m-wide mangrove forest is examined for sparse, average, and dense vegetation. The results are presented in Figure 2.10 and show an overall increase in the degree of wave attenuation from low to high vegetation density. Splitting out the overall wave height transformation (upper panel) into the attenuation of short waves (middle panel) and long waves (lower panel), respectively, reveals some interesting insights. First, the mangrove forest is very effective in attenuating the short-wave energy, which is in line with previous studies about short-wave attenuation into the mangrove forests (Burger, 2005; De Vos, 2004; Meijer, 2005). The short waves rapidly decrease after entering the mangrove forest and reduce until less than 1% of the incoming wave

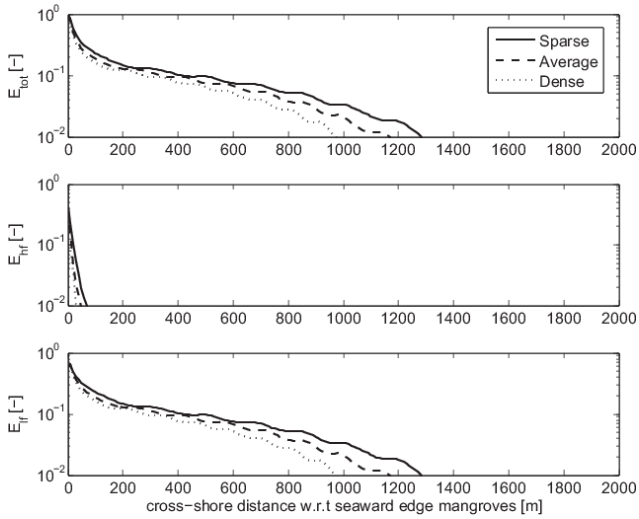

Figure 2.10: Normalized wave energy transformation in case of different mangrove density.

height is within the first 100 m, independent of the vegetation density. The long waves, on the other hand, are attenuated much less effectively by the vegetation and they can penetrate 950-1300 m into the forest depending on the vegetation density. We note that at a distance of 300 to 400 m the longwave energy is 10% of that at the start of the forest. As a result the hydrodynamics farther into the mangrove forest are controlled by the tide and long waves (tidal variance not shown here). Another observation in Figure 2.10 is that the long-wave height transformation shows modulations in wave height where the length scale of the modulations seems to be related to the vegetation density and increases for lower-density waves. We hypothesize that long-wave reflection both at the shoreline and on the vegetation stems is responsible for creating these modulations.

2.3.4 Effect of a Dike in the Profile (for Average Mangrove Density)

The presence of a sea dike can limit the width of a mangrove forest from the landward side and its presence is expected to play an important role in the stability of mangrove forests. The influence of five different sea dike locations on wave transformation into the mangrove forest is presented in Figure 2.11. On the basis of this figure, it seems that the short-wave transformation is independent of the cross-shore location of the dike since all incident band energy is attenuated by the mangrove within 50 to 100 m. The long-wave height transformation instead is strongly affected by the cross-shore location of the dike. The more seaward the dike the higher the long wave variance, which is likely related to long-wave reflections on the sea dike.

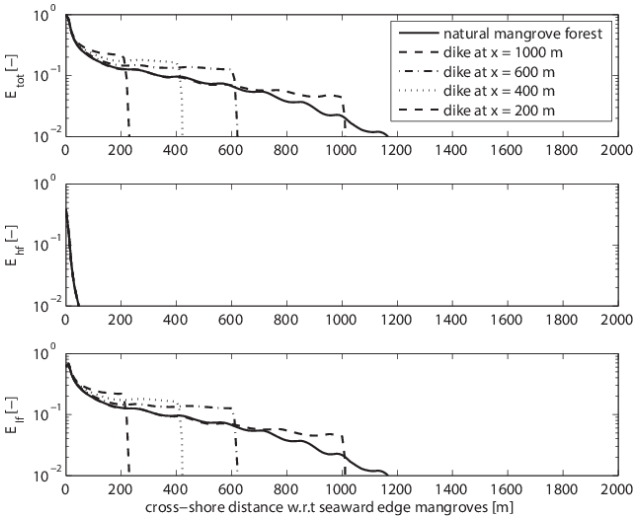

Figure 2.11: Effect of sea dike location on normalized wave energy transformation in case of average mangrove density.

2.4 Conclusions

Since the past few decades erosion has been observed at various locations along the southern coast of the Mekong Delta, where sedimentation has been observed in the past. Planting mangrove forest is so far the best solution to mitigate coastal erosion in the southeastern coast and the eastern coast of the MDRS since the coast is rich in sediment supply from the Mekong River system. Mangroves can reduce wave energy and trap sediment, and therefore enhance sedimentation. It was found that the southeastern coast and the eastern coast of the MDRS was stable with a mangrove width range of approximately 30 to 250 m and 140 m on average. This result is estimated on the basis of our empirical relationship of mangrove forest width and coastline evolution from 1989 to 2002.

Results from the XBeach model for the Soc Trang case study show the effectiveness of short-wave attenuation in a mangrove forest. After passing through less than 100 m of mangrove width, the short-wave height is significantly reduced to virtually zero. Therefore it is hypothesized that short waves do not really play a role in the health of a mangrove forest. Long waves, on the other hand, need more distance for attenuation. Even for the case of dense mangrove, long waves can still penetrate in the order of 1000 m into the forest, but after 300 to 400 m the long-wave energy is only 10% of the wave height at the seaward edge of the mangroves. A qualitative explanation could be that the long-wave energy needs to be attenuated (reflections should be limited) to create a sedimentation friendly environment. In addition, wave reflections will potentially increase long-wave energy within the mangrove forest, dependent on the position of a sea dike. We hypothesize that long waves play an important role in creating a favorable environment for seedlings and sedimentation.

References

Alongi, D. M. (2002). Present state and future of the world's mangrove forests. *Environmental Conservation*, 29(03).

Alongi, D. M. (2009). *The energetics of mangrove forests*. SpringerLink: Springer e-Books. Queensland, Australia: Springer.

Bao, T. Q. (2011). Effect of mangrove forest structures on wave attenuation in coastal vietnam. *Oceanologia*, 53(3):807–818.

Bosboom, J. and Stive, M. (2011). *Coastal Dynamics I*. VSSD, 573p, Delft, the Netherlands.

Brinkman, R. M., Massel, S. R., Ridd, P. V., Furukawa, K., et al. (1997). Surface wave attenuation in mangrove forests. In *Pacific Coasts and Ports' 97: Proceedings of the 13th Australasian Coastal and Ocean Engineering Conference and the 6th Australasian Port and Harbour Conference; Volume 2*, page 909. Centre for Advanced Engineering, University of Canterbury.

Burger, B. (2005). Wave attenuation in mangrove forests. Master's thesis, Delft University of Technology.

Christensen, S. M., Tarp, P., and Hjortsø, C. N. (2008). Mangrove forest management planning in coastal buffer and conservation zones, vietnam: A multimethodological approach incorporating multiple stakeholders. *Ocean & Coastal Management*, 51(10):712–726.

Dalrymple, R. A., Kirby, J. T., and Hwang, P. A. (1984). Wave diffraction due to areas of energy dissipation. *Journal of Waterway, Port, Coastal, and Ocean Engineering*, 110(1):67–79.

De Vos, W. (2004). Wave attenuation in mangroves wetlands, red river delta, vietnam. delft, the netherlands: Delft university of technology. Master's thesis, Master?s thesis, 107p. http://repository. tudelft. nl/view/ir/uuid% 3A4d8f93b5-8efa-4663-a29a-448a50c45525.

Doody, J. P. (2004). ?coastal squeeze?–an historical perspective. *Journal of Coastal Conservation*, 10(1):129–138.

Duke, N. C. (1992). Mangrove floristics and biogeography. *Tropical mangrove ecosystems*, pages 63–100.

Ewel, K. C., Twilley, R. R., and Ong, J. E. (1998). Different Kinds of Mangrove Forests Provide Different Goods and Services. *Global Ecology and Biogeography Letters*, 7(1):83.

Feagin, R. A., Martinez, M. L., Mendoza-Gonzalez, G., and Costanza, R. (2010). Salt marsh zonal migration and ecosystem service change in response to global sea level rise: A case study from an urban region. *Ecology and Society*, 15(4).

Gilman, E., Ellison, J., and Coleman, R. (2007). Assessment of mangrove response to projected relative sea-level rise and recent historical reconstruction of shoreline position. *Environmental Monitoring and Assessment*, 124(1-3):105–130.

Hoang, V. and Nguyen, H. (2006). Result on study of wave field on dong nai, sai gon estuaries and suggestion of sea bank and river mouth protection methods. In *Proceedings of theVietnam–Japan Estuary Workshop (Ha Noi, Vietnam)*, page pp. 140–150.

Hogarth, P. J. (2015). *The Biology of Mangroves and Seagrasses, Third Edition*. Oxford University Press, Oxford, 3 edition.

Hong, P. and San, H. (1993). *Mangroves of Vietnam*. IUCN wetlands programme. IUCN.

Hong Phuoc, V. and Massel, S. R. (2006). Experiments on wave motion and suspended sediment concentration at nang hai, can gio mangrove forest, southern vietnam. *Oceanologia*, 48(1).

IUCN (2011). Why healthy ecosystems matter: the case of mangroves in the Mekong Delta.

Lu, X. X. and Siew, R. Y. (2005). Water discharge and sediment flux changes over the past decades in the Lower Mekong River: possible impacts of the Chinese dams. *Hydrology and Earth System Sciences*, 10:181–195.

Lugo, A. E. and Snedaker, S. C. (1974). The Ecology of Mangroves. *Annual Review of Ecology and Systematics*, 5(1):39–64.

Mazda, Y., Magi, M., Ikeda, Y., Kurokawa, T., and Asano, T. (2006). Wave reduction in a mangrove forest dominated by sonneratia sp. *Wetlands Ecology and Management*, 14(4):365–378.

Mazda, Y., Magi, M., Kogo, M., and Hong, P. N. (1997). Mangroves as a coastal protection from waves in the tong king delta, vietnam. *Mangroves and Salt marshes*, 1(2):127–135.

Meijer, M. (2005). Wave attenuation over salt marsh vegetation.

Mendez, F. J. and Losada, I. J. (2004). An empirical model to estimate the propagation of random breaking and nonbreaking waves over vegetation fields. *Coastal Engineering*, 51(2):103–118.

Nguyen, V. L., Ta, T. K. O., and Tateishi, M. (2000). Late holocene depositional environments and coastal evolution of the mekong river delta, southern vietnam. *Journal of Asian Earth Sciences*, 18(4):427–439.

Quartel, S., Kroon, A., Augustinus, P., Van Santen, P., and Tri, N. (2007). Wave attenuation in coastal mangroves in the red river delta, vietnam. *Journal of Asian Earth Sciences*, 29(4):576–584.

Ranasinghe, R., Narayan, S., Suzuki, T., Stive, M., Ursem, W., and Verhagen, H. (2010). On the effectiveness of mangroves in attenuating cyclone induced waves. In *Proceedings of the 32th International Conference on Coastal Engineering, ICCE 2010, June/July, Shanghai*. ASCE-Texas Digital Library.

Roelvink, D., Reniers, A., van Dongeren, A., van Thiel de Vries, J., McCall, R., and Lescinski, J. (2009). Modelling storm impacts on beaches, dunes and barrier islands. *Coastal Engineering*, 56(11):1133 – 1152.

Schiereck, G. J. and Booij, N. (1995). Wave transmission in mangrove forests.pdf. In *International Conference on Coastal and Port Engineering in Developing Countries*, pages 1969–1983.

SIWRR (2010). Tien Estuary Investigation Report [in Vietnamese]. Technical report, Southern Institute of Water Resources Research, Ho Chi Minh, Vietnam: Ministry of Agriculture and Rural Development of Vietnam, 180 p.

Spalding, M., Kainuma, M., and Collins, L. (2010). *World Atlas of Mangroves*. Earthscan.

Stive, M. J., Aarninkhof, S. G., Hamm, L., Hanson, H., Larson, M., Wijnberg, K. M., Nicholls, R. J., and Capobianco, M. (2002). Variability of shore and shoreline evolution. *Coastal Engineering*, 47(2):211–235.

Suzuki, T. (2011). *Wave dissipation over vegetation fields*.

Ta, T. K. O., Nguyen, V. L., Tateishi, M., Kobayashi, I., Saito, Y., and Nakamura, T. (2002). Sediment facies and Late Holocene progradation of the Mekong River Delta in Bentre Province, southern Vietnam: An example of evolution from a tide-dominated to a tide- and wave-dominated delta. *Sedimentary Geology*, 152(3-4):313–325.

Torio, D. D. and Chmura, G. L. (2013). Assessing Coastal Squeeze of Tidal Wetlands. *Journal of Coastal Research*, 290:1049–1061.

Tri, V. K. (2012). Hydrology and Hydraulic Infrastructure Systems in the Mekong Delta, Vietnamong Delta System. In *The Mekong Delta System: Interdiciplinary Analyses of a River Delta*, pages 49–81.

Vo-Luong, P. and Massel, S. (2008). Energy dissipation in non-uniform mangrove forests of arbitrary depth. *Journal of Marine Systems*, 74(1-2):603–622.

Woodroffe, C. (1992). Tropical mangrove ecosystems. *Coastal and Estuarine Studies*, 41:7–41.

Chapter 3

The effects of wave non-linearity on wave attenuation by vegetation

The true method of knowledge is experiment.

William Blake

Wave attenuation through mangrove forests has received more and more attention, especially in the context of increasing coastal erosion and sea-level-rise. Numerous studies have focused on studying the reduction of wave height in a mangrove forest. However, the understanding of this attenuation process is still in its infancy. In order to obtain more insight, a laboratory experiment, mimicking the processes of wave attenuation by coastal mangroves in the Mekong Delta, Vietnam was conducted. The reduction of wave height for different scenarios of mangrove densities and wave conditions was investigated. A new method to quantify vegetation attenuation induced by vegetation is presented. The wave height reduction is presented over a relative length scale (viz. the number of wavelengths), instead of an absolute length scale of the forest (e.g per meter or per 100 meter). The effects of wave non-linearity on the wave height attenuation over the mangrove forest were investigated using the Ursell number. It is suggested that the non-linear character of waves has a strong influence on the attenuation of the waves inside the mangrove forest. A numerical model, mimicking the experiment was constructed in SWASH and validated using the experimental data. Finally, the data set was extended through numerical modelling so that a larger ranging relationship between wave attenuation per wave length and the Ursell number could be formulated.

Parts of this chapter have been published in Coastal Engineering. Linh, K. Phan., Stive, M.J.F, Zijlema, M, Truong, H.S., and Aarninkhof S.G.J (2019). The effects of wave non-linearity on wave attenuation by vegetation.

3.1 Introduction

In recent decades, many coastal and estuarine regions around the world have been recorded to suffer from accelerated erosion due to the effects of global warming, sea-level-rise and subsidence. In this context, the defensive role of ecosystems in general and mangrove forests in particular for coastal areas has been increasingly recognized. The complex system of roots, stems and canopies enables mangroves to absorb external forces such as due to waves and currents.

Understanding the mechanism of wave height reduction by mangroves is an important step in understanding the hydrodynamic, sedimentation and exchange processes in mangrove forests. Numerous studies have been published focusing on this topic (Augustin et al., 2009; Bao, 2011; Brinkman, 2006; Brinkman et al., 1997; Massel, 2006; Mazda et al., 2006, 1997; Quartel et al., 2007). It is accepted that waves travelling through a mangrove forest perform work on vegetation roots, stems and canopies, thereby losing their energy and reducing their wave height (Dalrymple et al., 1984; Mork, 1996).

The reduction of wave height depends on the vegetation characteristics *i.e.* the density, stiffness etc. and the wave characteristics *i.e.* at least the wave height and wave period (Mendez and Losada, 2004). However, the effect of the wave characteristics on the wave height reduction through a mangrove forest is less clarified than that of the cylinder density. While Bradley and Houser (2009) suggested that the wave attenuation through the vegetation reduces with increasing wave height, Cavallaro et al. (2011) observed more wave height reduction when the wave height increases.

The effect of wave characteristics in general and wave non-linearity in particular on the attenuation rate of wave height due to vegetation is not fully understood. As a result, although many physical models have been conducted, combined with calibration or validation of advanced numerical models, most studies only focus on the attenuation of regular waves, and only over a limited distance of vegetation length in the range of 1 to 4 m). Data sets for model validation in this context are also lacking.

Therefore, the main objectives of this study are to (1) study the role of wave characteristics on the wave attenuation processes, (2) to provide and extend the data sets for advanced analyses and validation, using both a physical and a numerical model.

3.2 Methodology

In order to achieve the research objectives, physical and numerical modelling were chosen as major approaches. Their set-up and configurations are described in this section of the paper. First, a physical experiment mimicking the wave attenuation processes by mangroves in the Mekong Delta was conducted. Second, a numerical model was constructed and validated with the experimental data. The combined results were analysed to study the effects of wave characteristics and non-linearity on the wave attenuation by the vegetation.

3.2.1 Physical modelling

A laboratory experiment of wave attenuation through cylinder arrays, mimicking wave attenuation processes through a coastal mangrove forest was conducted in a flume of the Fluid Mechanics Laboratory at Delft University of Technology. The effective length, height and width of the flume is 40m, 1m and 0.8m respectively.

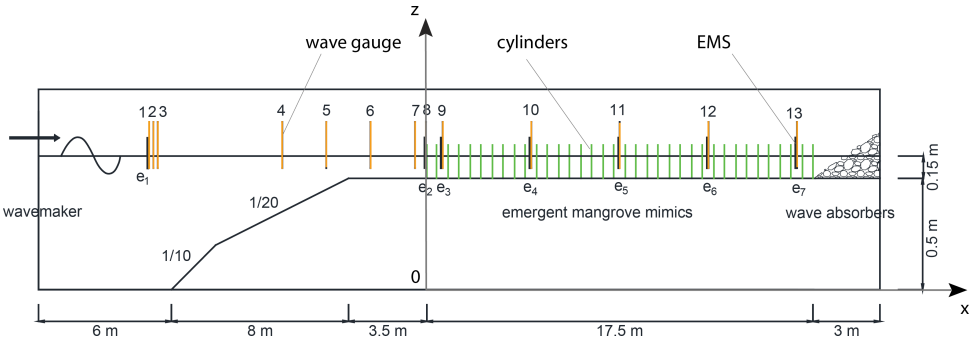

Figure 3.1: Schematic view of the experiment set up, including the locations of wave gauges, EMSs and vegetation. Not to scale.

Figure 3.1 gives a cross-section of the experimental set up. The wave generator with an active wave absorption system was placed at the beginning of the flume to prevent reflected waves from reflecting again into the flume. The 2nd order wave steering was always active during the experiment.

Because the Mekong Delta coast has generally a very gentle slope of about 1/10000, waves propagating towards the mangroves are usually broken before entering the mangrove forests (Phan et al., 2014). As a result, they have lost their primary spectral energy and long wave energy has developed. Therefore a steep wooden slope with a combination slope of 1/10 and 1/20 was used to simulate the processes of shoaling and breaking waves. This situation was considered in the experiments named broken wave scenarios. In addition to that, there are also situations where waves are not broken such as waves generated by strong local wind. This circumstance also was considered in the experiment regarding the so named non-broken wave scenarios. It is noticed that the broken or non-broken wave conditions described in this study represent the wave modes before entering the mangrove forest. It is observed that wave breaking processes did virtually not occur inside the mangrove forests in all experimental scenarios.

Over a length of 17.5 m cylinder arrays were installed along a horizontal bottom. The wave height and the depth-averaged velocity were measured by 13 wave gauges and seven electromagnetic velocity meters (EMS) with a sampling rate of 100 Hz. Representative locations of the equipment are indicated in Figure 3.1. The experiments were repeated with different locations of the equipment to obtain more data inside the vegetation. Wave height and velocity measurements were taken over a long time interval so at least 100 waves in scenarios of regular waves and 1000 waves in scenarios of irregular waves so that representative statistical data could be achieved. Typical values in the experiment are: a water depth in front of the wave paddle of 65 cm; wave heights ranging

from 1 to 10 cm; and wave periods ranging from 1 to 3s. In most experiments, a wave absorber was placed at the end of the flume to reduce wave reflections. Some additional experiments were done with a wooden sea-dike at the end with slope 1:5, representing the sea-dikes usually constructed right behind the mangrove forests along the Mekong Delta coast (Phan et al., 2014).

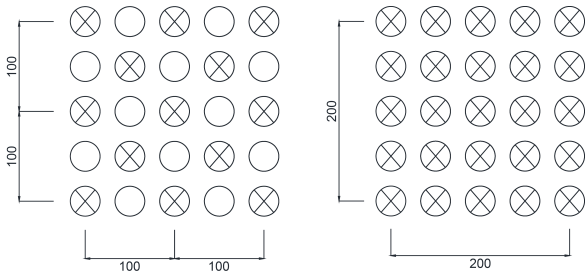

Figure 3.2: Cylinder distribution used in the experiment (unit in mm). Not to scale.

Figure 3.2 shows the arrangements of the cylinder arrays which were considered in the experiment. The density of the cylinder arrays was based on the solid volume fraction of the mangrove forest . The solid volume fraction per unit volume can be calculated according to : $V_s = N\frac{\pi d^2}{4}$ where d is the diameter of the cylinder : d =0.012 m and N is the density of mangroves. In this way, there are 2 densities of mangroves considered, which are 200 cylinders/m^2 (sparse cases) and 400 cylinders/m^2 (dense cases), yielding V_s values of 2% and 4% respectively.

Table 3.1: Experimental scenarios

Vegetation	Wave characteristics	Regular (Re)		Irregular (Ir)	
		H (cm)	T(s)	Hs (cm)	Tp (s)
without mangroves	Broken (Type 2)	10	2.0; 2.5; 3.0	10	2.0; 2.5; 3.0
with mangroves	Non-broken (Type 1)	1; 2; 3; 4; 5	2.0; 2.5; 3.0	3; 5	2.0; 2.5; 3.0
	Broken (Type 2)	7; 10	2.0; 2.5; 3.0	7; 9; 10; 13; 15	2.0; 2.5; 3.0

Based on the set up described above, the experiments were performed for different cases of wave heights and wave periods, including regular and irregular, non-broken waves (Type 1) and broken waves (Type 2). Further details are given in Table 3.1.

3.2.2 Numerical model

A numerical model mimicking the experiment was constructed based on the SWASH model. The SWASH model is a time domain model for simulating non-hydrostatic, free surface, rotational flows, in which the governing equations of the model are the shallow water equations including a non-hydrostatic pressure term (Zijlema et al., 2011b). The presence of vegetation in SWASH was modelled through Morrison's equation:

$$F_x = \frac{1}{2}\rho C_D h_v b_v N_v u|u| \tag{3.1}$$

in which ρ is gravitational acceleration, C_D is a bulk drag coefficient, $h_v$is the height of the cylinder, b_v is the diameter of the cylinder.N_v is the number of plants per square meter and u is the horizontal velocity due to wave motion.

The numerical model was constructed based on the physical model in such a way that the numerical results can be directly compared with the experimental results. Specific settings described below are related to boundary conditions and vegetation properties. The minimum grid size is 0.01 m. This results in about 4000 active grid points. The time step was chosen as small as 0.001 s. The hydraulic boundary conditions of the numerical model were prescribed based on the experimental configurations. At the end of the model, three different types of constructions were applied which are (1) a sponge layer in which there is no wave reflection, (2) a permeable slope corresponding to the cases with wave absorber(stone size 0.03 m and (porosity 40%) and (3) an impermeable slope representing the case with a sea dike at the end of the flume (slope 1/5).

The predictive skill of SWASH was calculated using the bias and the scatter index SI, which are given by:

$$bias = \frac{1}{N}\sum_{i=1}^{N}\left(\varphi^i_{comp} - \varphi^i_{obs}\right) \tag{3.2}$$

and

$$SI = \frac{\sqrt{\frac{1}{N}\sum_{i=1}^{N}\left(\varphi^i_{comp} - \varphi^i_{obs}\right)^2}}{\frac{1}{N}\sum_{i=1}^{N}\varphi^i_{obs}} \tag{3.3}$$

In which, N is the total number of data points in a given data set, φ_{comp} is the wave parameter computed by SWASH and φ_{obs} is the corresponding observed wave parameter (Zijlema, 2012). The simulation time in cases of irregular waves is 60 min and in cases with regular waves 20 min.

3.3 Incoming and reflected wave separation

The methodology of Guza et al. (1985) was used to separate incoming and reflected wave for irregular and regular wave in cases without mangroves. This method is based on surface time series signal and velocity time series signal collected at the same locations.

Wave conditions were performed for two different boundaries conditions *i.e.* with the wave absorber or with the sea dike at the end. The incoming wave signal determined in these both cases are the same indicating the accuracy of the method (see Figure 3.3)

The incoming wave heights determined by Guza's method for different wave conditions (H=10 cm; T=2 s; 2.5 s and 3 s) in cases with wave absorber at the end were compared with that in cases with sea dikes at the end (Figure 3.4). It is shown that this separation method achieves more than 90% accuracy.

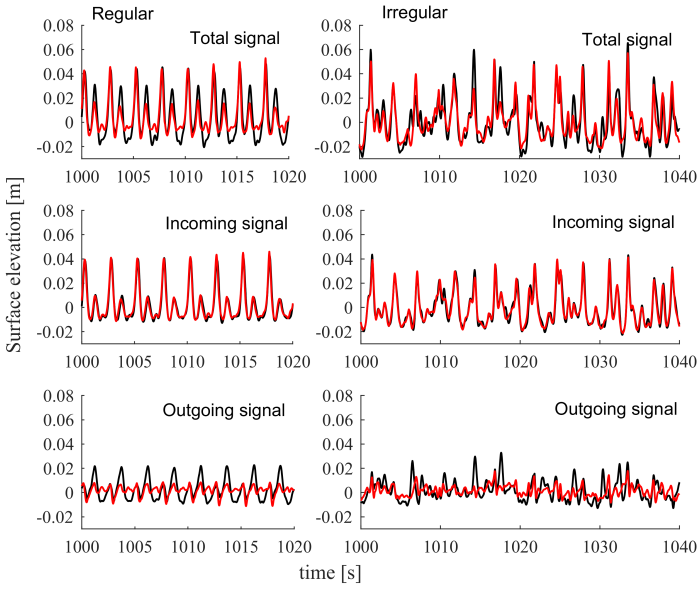

Figure 3.3: Comparisons time series signal in case of sea dike in the end (black line) and wave absorber in the end (red line) for regular wave (left hand side) and irregular wave (right hand side) at x=2.75[m] from the virtual seaward edge of the mangroves. Upper panels show total time series signal. Middle panels and lower panels showing incoming and outgoing time series signal separated by Guza method respectively. Wave condition: H=10 cm; T=2.5 s.

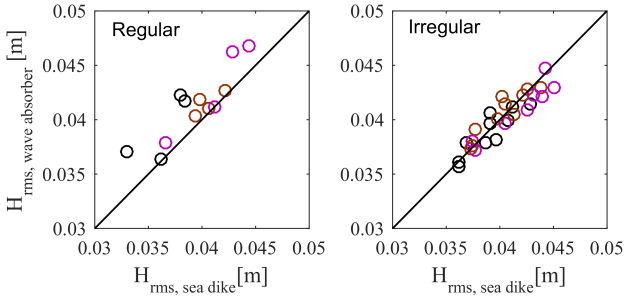

Figure 3.4: Comparisons between incoming wave height in case of wave absorber in the end (vertical) and in case of sea dike in the end (horizontal) for irregular and regular wave.

3.4 Experimental results

In this section, wave attenuation is evaluated using different attenuation coefficients. The relationship between wave non-linearity and wave attenuation is examined using the Ursell number, which is an indicator of wave non-linearity.

3.4.1 Wave attenuation per unit distance of the mangrove forest

In the literature, the reduction of wave heights inside the vegetation is usually presented through the wave transmission coefficient (K_t). It is the ratio between the transmitted wave height (H_x) and the wave height at the starting location of the mangroves (H_0 at x=0 m). H_x is the root mean squared wave height at location x inside the mangrove forest.

$$K_t = \frac{H_x}{H_o} \tag{3.4}$$

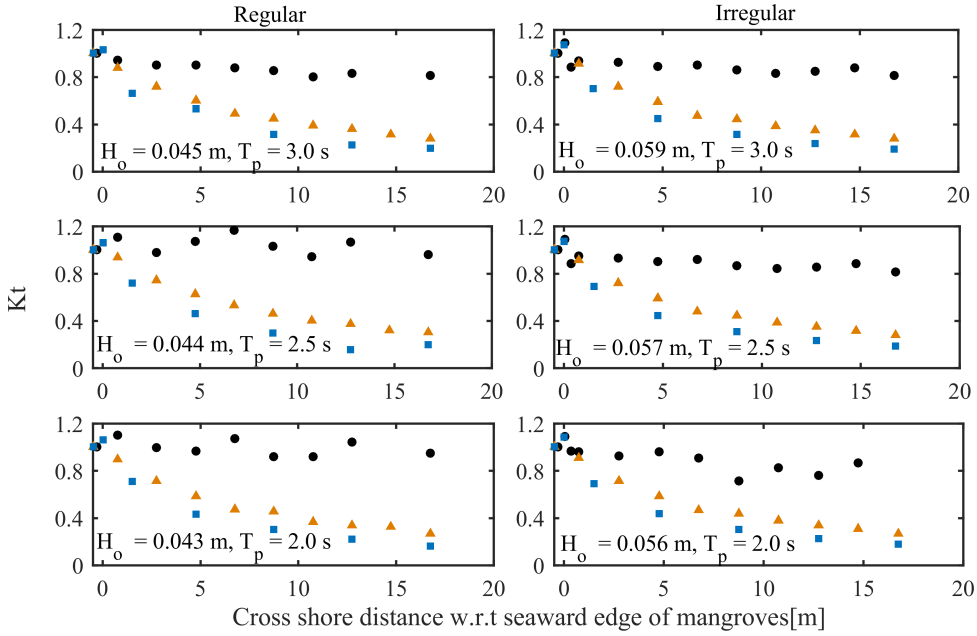

Figure 3.5: Wave transmission coefficient Kt in cases of different mangroves densities: no mangroves (circles), V1=200 units/m2 (triangles) and V2= 400 units/m2 (squares). A wave height of 10cm, with different wave periods of 3.0s(upper panels); 2.5s(middle panels) and 2.0s(lower panels). Left-hand side: regular waves. Right-hand side: irregular waves. H_0 is the wave height measured at the vegetation edge.

The impacts of vegetation on the transformation processes can be revealed by comparing this wave transmission coefficient along the forest in cases of different vegetation densities (no vegetation: $N = 0$; sparse: $N = 200$ cylinders/m^2 and dense: N =400 cylinders/m^2). Figure 3.5 shows the wave transmission coefficient (Kt) along the mangrove forest in cases of 10 cm wave height at the wave paddle with different wave periods (Tp =2.0; 2.5 and 3 s), wave conditions (regular and irregular), and with different mangrove densities (no mangroves, sparse and dense).

In scenarios without vegetation, it can be seen that the wave transmission coefficient remains almost the same along the bare horizontal bottom. The wave height is slightly reduced probably due to bottom friction. Moreover, there is a fluctuation of K_t along the flume. Waves reflected from the end of the flume are the possible reason for this

fluctuation. However, this phenomenon is not observed in cases with vegetation. K_t does not fluctuate but continuously reduces toward the end of the forest. This means that the reflected waves in the flume are also damped. This result reveals the capability of vegetation in reducing not only the incoming waves but also the wave reflection from the sea dike.

In scenarios with sparse vegetation, the wave height was damped about 60 percent after passing through 17.5 m length of mangroves. In scenarios with dense cylinder arrays, around 70 percent of the wave height was damped at the end of the forest. In this sense, the denser the vegetation, the smaller the wave transmission coefficient Kt and vice versa. It is noted that although the density of mangroves was doubled from 200 stems/m^2 to 400 stems/m^2 (V_s increases from 2% to 4%), the attenuation wave increased only 10 percent. In this context, 1% of V_s appears to corresponds to about 5% of wave height reduction, which means that if the solid volume fraction (V_s) increases to 20%, the wave height could be nearly total damping.

3.4.2 Wave attenuation per wave length

In the above section of this paper, the result of wave height reduction in the experiment is examined through the wave transmission coefficient K_t. In the literature, it is noticed that the evaluation of the wave attenuation according to K_t appears to be not consistent. For example, the wave attenuation was calculated per 100 m (Mazda et al., 1997), per 1 m (Bao, 2011; Bradley and Houser, 2009; Cooper, 2005; Lövstedt and Larson, 2009; Massel, 2006; Mazda et al., 2006; Möller, 2006; Möller and Spencer, 2002; Möller et al., 1999; Quartel et al., 2007) or per length of the forest (Brinkman, 2006; Brinkman et al., 1997). As a result, the rate of wave attenuation in the literature is hardly informative.

Moreover, one should bear in mind that the attenuation of waves by mangroves does not only depend on vegetation characteristics such as diameter, density and distribution of roots, stems and canopies, but also on the characteristics of incoming wave groups *i.e* broken and non-broken, long and short, large and small waves. Therefore, in order to include more physics in studying the wave attenuation processes, the reduction of waves is presented over a relative distance, viz the number of wavelengths instead of the length of the mangrove forest or an arbitrary absolute length. In this way, the influences of wave characteristics on the wave attenuation processes can be interpreted more easily and the observed large variation in the wave attenuation in the literature is expected to be reduced.

The total wave attenuation per meter of wavelength (K_L), or the effective wave transmission coefficient is defined as :

$$K_L = \frac{H_L}{H_o} \tag{3.5}$$

Where H_L is the root mean squared wave height after a certain number of wavelength (n) and H_o is the root mean squared wave height at the mangrove edge (n=0).

Figure 3.6 shows the correlation between the effective wave transmission coefficient (K_L) and the number of wavelengths in scenarios of non-broken waves (upper panels) and broken waves (lower panels) with the same wave height and different wave periods. It can be seen that the larger the number of wave lengths, the smaller the effective

wave transmission coefficient (K_L). Moreover, in all considered scenarios, although the wave height was damped 15% to 20% after the first wavelength, only about 40% of the wave height was damped in the next four wave lengths *i.e.* 8% per wavelength. In this sense, wave damping over the first wave length is the most effective. Furthermore, it can also be seen that the larger the wave period, the smaller the effective wave transmission coefficient *i.e.* the more wave damping.

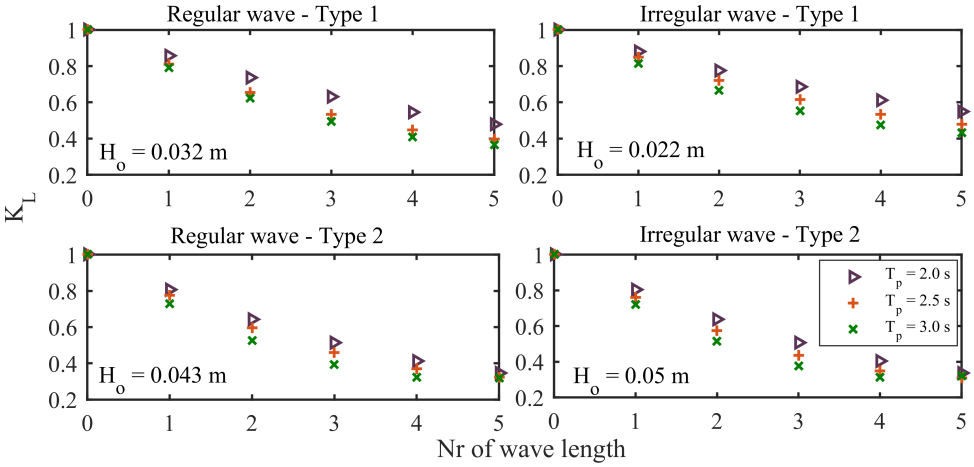

Figure 3.6: Effective wave transmission K_L in cases of sparse mangroves, different wave periods: $T_p = 2$ s (black triangles), $T_p = 2.5$ s (red pluses) and $T_p = 3$ s (green crosses).

The influence of wave height on wave attenuation was revealed by comparing the K_L in non-broken cases of the same wave period, but with different wave height, (Figure 3.7). In scenarios of non-broken regular waves (upper left panel), it is suggested that the larger the wave height, the larger the wave attenuation and vice versa. In the case with 5 cm wave height at the mangrove edge (orange crosses), wave height was damped about 20% after the first wave length and more than 62% in the next four wave lengths. However, in the case of 1 cm wave height (blue left-pointing triangles), only about 5% of the wave height is damped after the first wave length, while up to 25% of the wave height is damped after the next four wave lengths. It appears that larger waves of the same period attenuate stronger. Similar results were also observed in cases of non-broken irregular waves (upper right panel).

In scenarios of broken regular waves (lower left panel), the incoming waves have already reduced their height due to the breaking process before entering the mangrove forest. As a result, even when the wave height at the wave paddle is quite different ($H = 0.07$ m and 0.1 m), the wave height at the edge of the mangrove forest is almost the same ($H_0 = 0.043$ m and 0.044 m, respectively) which results in a similar attenuation process inside the mangrove forest. In scenarios of broken irregular waves (lower right panel), although the wave height at the wave paddle are the same as that in cases of broken regular waves ($H = 0.07$ m and 0.1 m), the wave height at the mangrove edge are slightly different ($H_0 = 0.043$ m and 0.05 m, respectively). This is due to the differences in the breaking processes between the regular and irregular waves. However, the wave

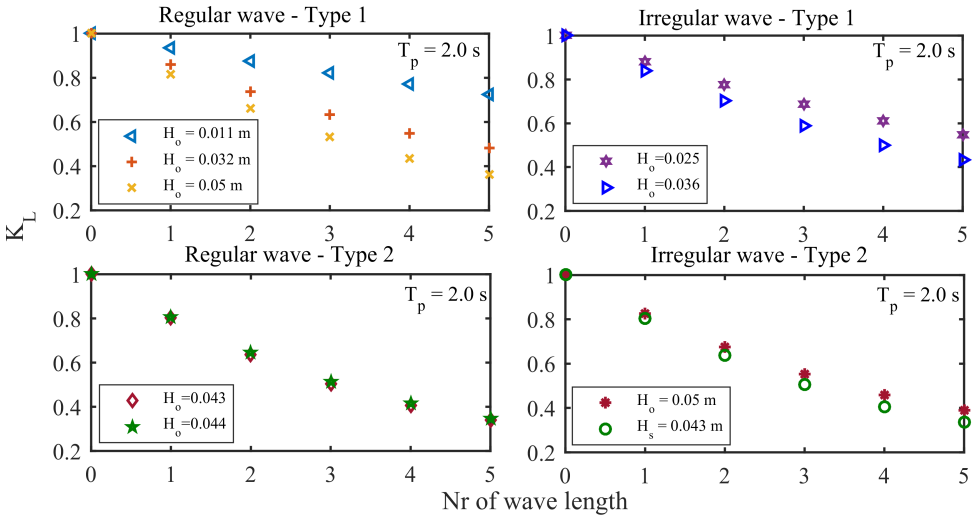

Figure 3.7: Effective wave transmission K_L in cases of sparse vegetation, wave period of 2 s, different wave height.

attenuation processes inside the mangroves in regular and irregular cases appears to be similar.

Overall, by presenting the effective wave transmission coefficient, the variation of wave attenuation rate appears to be reduced as being expected. The small scatter that remains is possibly caused by the non-linearity of the wave characteristics, which is examined in the following section.

3.4.3 Effect of wave non-linearity on wave attenuation by mangroves

By determining the reduction of the wave height according to a relative length scale *i.e.* wave length, it is suggested that the damping of the waves depends on the wave characteristics. In this sense, an overall indicator accounting for the wave characteristics in studying the wave attenuation processes is required. In the literature, most studies on wave height attenuation processes through the vegetation are usually simplified by adopting the four main assumptions: (1) vegetation consists of rigid plants (2) waves are regular, (3) vegetation is emerged and uniform and (4) waves follow linear theory. The effects of wave characteristic in general and wave non-linearity in particular on the attenuation processes have received less attention. In this section, the influence of wave non-linearity on the wave attenuation through a mangrove forest are examined.

The influences of wave non-linearity on the wave damping through vegetation were studied in Wu and Cox (2015). A relationship between the Ursell number (varied from 0 to 60) and the drag coefficient was shown based on an experiment of the damping of non-broken, irregular waves through an 1.8 m long stretch of cylinder arrays. It is suggested that the wave steepness influences the wave attenuation by vegetation. In this study, Ursell numbers (in the range of 20 to 250) were used to clarify the impact of wave

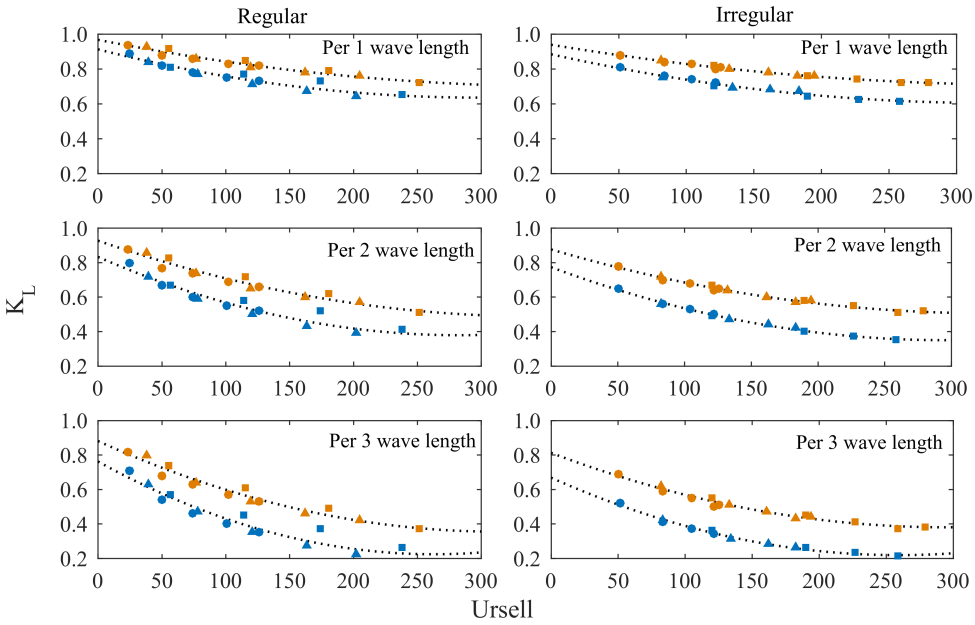

Figure 3.8: Relationship between the effective transmission coefficient K_L and Ursell number for different wave height and periods: $T_p = 2$ s (circles), $T_p = 2.5$ s (triangles), $T_p = 3$ s (squares), different mangrove densities: sparse (orange), dense (blue) per one wave length (upper panels), per two wave lengths (middle panels), per three wave lengths (upper panels). The trend lines (dot lines) are second order polynomial lines.

non-linearity on the wave damping through mangroves for both non-broken and broken irregular wave and non-broken regular waves. The Ursell number is defined as:

$$Ursell = \frac{\text{wave steepness}}{\text{relative depth}} = \frac{H_s L^2}{h^3} \tag{3.6}$$

where H_s is the significant wave height (m); h is the water depth (m); and L is the wave length (m), with all parameter values at the mangrove edge.

Figure 3.8 shows the relationship between the effective wave transmission coefficient and the Ursell number for a varying number of wave lengths. It can be clearly seen that as the Ursell number increases, K_L reduces implying an increase in the wave reduction. This result means that the wave dissipation by vegetation appears to be more effective as the waves are more non-linear. Moreover, as the Ursell number increases to above 150, the declination of the K_L reduces. K_L appears to achieve an equilibrium value when the Ursell number is larger than 250. This means that the wave heigh reduction no longer depends on the wave non-linearity. This characteristic can be observed for both regular and irregular waves.

It can be seen that the influence of mangrove density on the wave attenuation process is different for different numbers of wave length. For the first wave length, the difference of K_L between the sparse cases and dense cases is about 10% (upper panels in Figure 3.8). However, after three wave lengths, this difference increases to about 20% (lower

panels in Figure 3.8). Furthermore, it is suggested that the effect of wave-nonlinearity on the wave height reduction also depends on the numbers of wave length. For instance, over the first wave length, the wave attenuation increases about 20% (K_L reduce from about 0.9 to 0.7) as the Ursell increases from 50 to 250. However, after 3 wave lengths, the wave attenuation increases about 35% when the Ursell number increases from 50 to 250. A similar trend was observed for both regular and irregular waves.

3.5 Numerical results

The capability of the SWASH model in the reproduction of the wave transformation in cases without vegetation has been well validated (Buckley et al., 2014; Zijlema et al., 2011a,a), but cases with vegetation have received more attention only recently (Cao et al., 2016). Data sets presenting wave transformation over a long vegetation distance are needed. In this section, the capability of the SWASH model in the simulation of the wave transformation processes over an elongated 24 m foreshore with and without vegetation was validated using experimental results. Moreover, the model was used to extend the experimental data set so that the rate of wave attenuation can be evaluated over a larger number of wave lengths.

3.5.1 SWASH performance for wave transformation without mangroves

The SWASH model can improve its frequency dispersion by increasing the number of vertical layers. However, increasing the number of layers also means that the model becomes more computational costly in terms of practical engineering. Usually, a vertical coarse resolution (1-3 layers) is sufficient to describe the wave physics outside the surf zone (Van den Berg et al., 2015). In this study, a two layer model was chosen because it provides better prediction for wave transformation processes. Figure 3.9 compares the root mean square wave height and the mean water level between the physical and numerical model with a different number of vertical layers in both regular and irregular cases. The predictive skill for different numbers of layers is presented in Table 3.2. The results suggest that the SWASH model with 2 or 3 vertical layers provide better agreement with the physical model than with 1 layer.

Increasing the number of layers from 1 to 2 layers significantly improves the predictive skill for the wave set up, especially in cases with irregular waves (the SI of the wave set up for 1 layer and 2 layer are 0.62 and 0.41, respectively). Moreover, increasing the number of layers from 2 to 3 layers does not substantially improve the predictive skill of the model. For example, the scatter index of $Hrms$ for two and three layers in cases with regular waves are 0.09 and 0.07 and in cases with irregular waves are 0.12 and 0.11, respectively. Based on these results, a two layer model was considered sufficient for this study.

As mentioned in the previous section, different boundary conditions at the end of the model can be imposed into the SWASH model. They include a sponge layer, a permeable slope and an impermeable slope. These options are sufficient to mimic the wave absorber and sea dike, which were considered in the physical model.

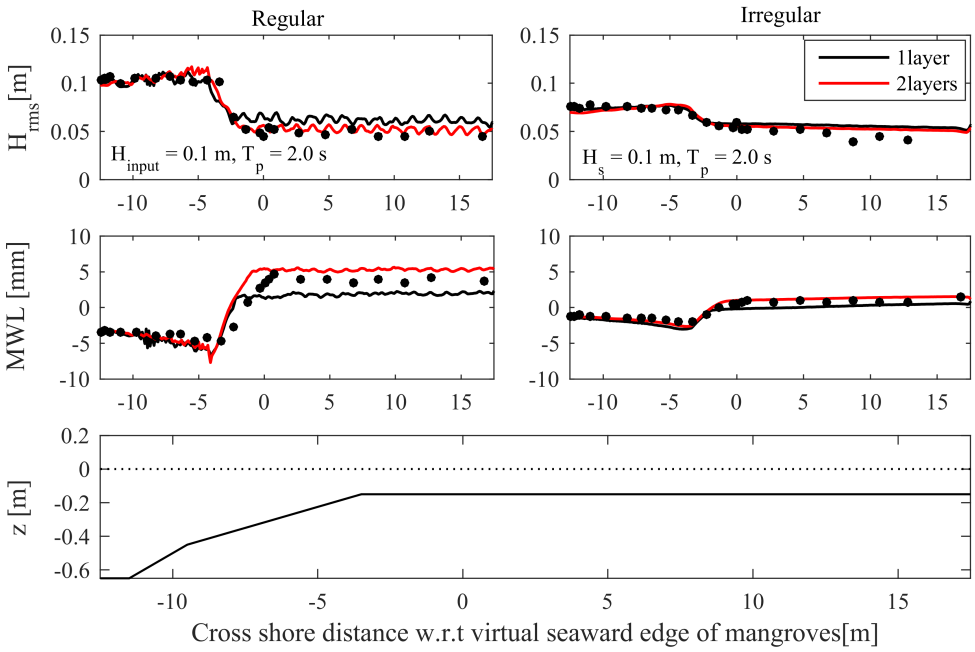

Figure 3.9: Comparisons between numerical model with 1 vertical layer (black line) and numerical model with 2 vertical layers (red line) and physical model (markers) for both regular (left hand side) and irregular wave (right hand side).

Table 3.2: Swash model skill for different number of vertical layers

Case	ReH10T20			IrH10T20		
	1 layer	2 layers	3 layers	1 layer	2 layers	3 layers
BIAS Hrms [mm]	5.4	1.8	0.4	4.4	2.7	1.1
SI Hrms	0.15	0.09	0.07	0.14	0.12	0.11
BIAS set up [mm]	-0.1	-0.008	-0.008	-0.5	0.08	0.16
SI set up	0.44	0.43	0.43	0.62	0.41	0.46

The upper panels (Figure 3.10A,B) show the incoming wave height separated from the physical model and the associated results extracted from the numerical model with sponge layer. It can be seen that the wave height is slightly overestimated by the numerical model. The BIAS and Scatter index in cases with regular and irregular waves are 9.3 mm, 0.25 and 9.3mm, 0.23 respectively. Because there is no wave reflection in the numerical model with a sponge layer, in order to compare the physical model with the numerical model the wave signal measured from the physical model was firstly separated incoming and reflected waves using Guza method (Guza et al., 1985). It is shown that this method can be used to separate the incoming and reflected waves in shallow water with an uncertainty of less than 10% (see Section 3.3). This uncertainty may be the reason for a small difference in wave height between the physical and numerical model

with the sponge layer. Although the simulation with sponge layer has larger BIAS and Scatter index than other cases (with wave absorbers and sea dikes), it is still in an acceptable range (less than 10 %) and the SWASH model with sponge layer can be used to mimic scenarios without reflection waves.

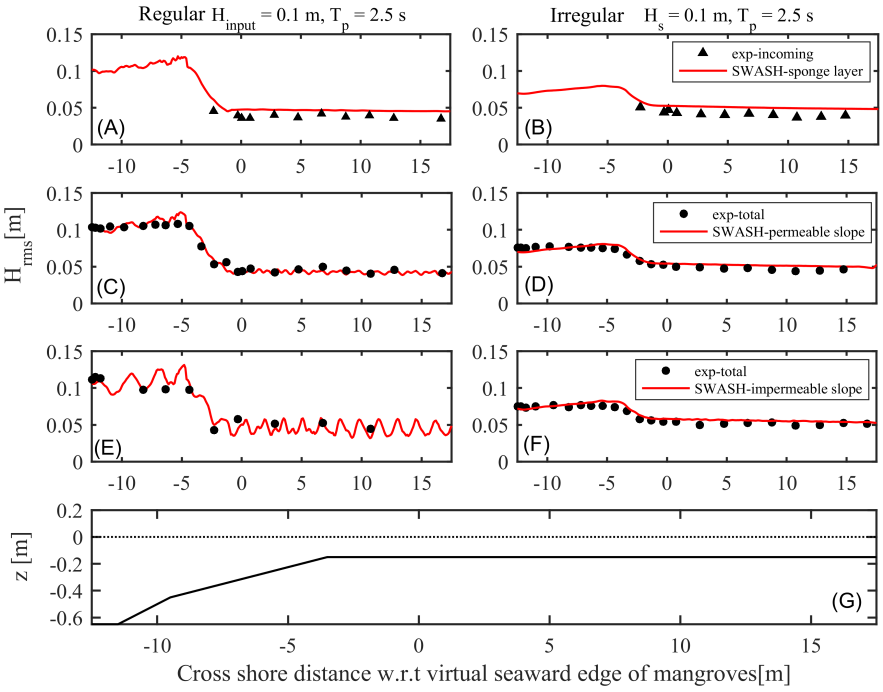

Figure 3.10: broken wave. Wave height comparisons between numerical model (red line) and physical model (markers) for 2 wave conditions ReH10T25 (left hand side) and IrH10T25 (right hand side) for 3 boundaries cases in SWASH.

The SWASH model with default values in cases with permeable and impermeable slopes can well reproduce the wave height transformation processes determined from the physical model (see Figure 3.10C,D and Table 3.3). For example, for regular and irregular cases with permeable slopes (wave absorber) there is only a small BIAS difference of 0.12 mm and 1.7 mm between physical model and numerical model, respectively. The scatter index numbers in those cases are also small (0.074 and 0.076 respectively).

Table 3.3: Statistic measures computed for wave height in case of different boundaries conditions.

Case	ReH10T25			IrH10T25		
	Sponge	Permeable	Impermeable	Sponge	Permeable	Impermeable
BIAS Hrms [mm]	9.4	0.12	-2	9.3	1.7	3.1
SI Hrms	0.25	0.074	0.1	0.22	0.076	0.068

Looking at the breaking processes (from x=−5 m to x=0 m), it is noticed that in cases with regular waves (Figure 3.10C,E), the numerical model can well capture the breaking processes. However, in cases with irregular waves (Figure 3.10D,F) the waves appear to start breaking later than in the physical model. If only a few vertical layers (one to three layers) are implemented in SWASH, the amount of wave energy dissipation due to wave breaking may be underestimated, which can be compensated using a "breaking command" (Van den Berg et al., 2015). This command allows to initiate the wave breaking through a threshold parameter α and stop wave breaking through a threshold parameter β. In this study, α was varied in a range from 0.6 (default value) to 0.2 to get a better prediction of the breaking processes for irregular waves. It is shown that the predictive skill of SWASH can be improved by reducing α from 0.6 to 0.4 (BIAS reduce from 1.8mm to 1mm and SI reduce from 0.09 to 0.06 in case of wave absorber in the end) (see Table 3.4). Similar results can be observed in cases with a sea dike at the end of the flume (Table 3.4). Hence, the simulation of the breaking processes in cases with irregular waves can be improved by tuning the breaking parameter α in the "breaking command". However, it is not really necessary because the difference is not significant (3% improvement). In conclusion, the above results confirm that the SWASH model using only default values can well reproduce the wave transformation and set up in the scenarios without vegetation.

Table 3.4: Statistic measures computed for wave height in case of different broken parameter alpha for irregular wave IrH10T20.

Case	Wave absorber			
	α=0.6	α=0.4	α=0.3	α=0.2
BIAS Hrms [mm]	1.8	1	-1.9	-0.7
SI Hrms	0.09	0.06	0.07	0.15
Case	Slope in the end			
BIAS Hrms [mm]	3.1	1.3	-2.1	-7.8
SI Hrms	0.075	0.055	0.08	0.16

3.5.2 SWASH performance for wave transformation with mangroves

It is difficult to choose an appropriate bulk drag coefficient (C_d) to calculate the wave attenuation by vegetation due to the complexity of turbulence structures in and around the vegetation. Theoretically, in cases with rigid cylinder arrays and irrotational flow, C_d =1.

In this part, the sensitivity of the SWASH model to the drag coefficient was studied. Five different irregular cases and five different regular cases with two mangroves densities from the physical model were simulated with different values of C_d (from 1 to 1.6 with with an interval of 0.2). It is suggested that the root-mean squared wave height measured in the experiment for both regular and irregular waves can be well reproduced in the simulations in sparse and dense cases with a bulk drag coefficient of 1.6 and 1.4, respectively (Figure 3.11). It is noted that the 1D SWASH model does not account for

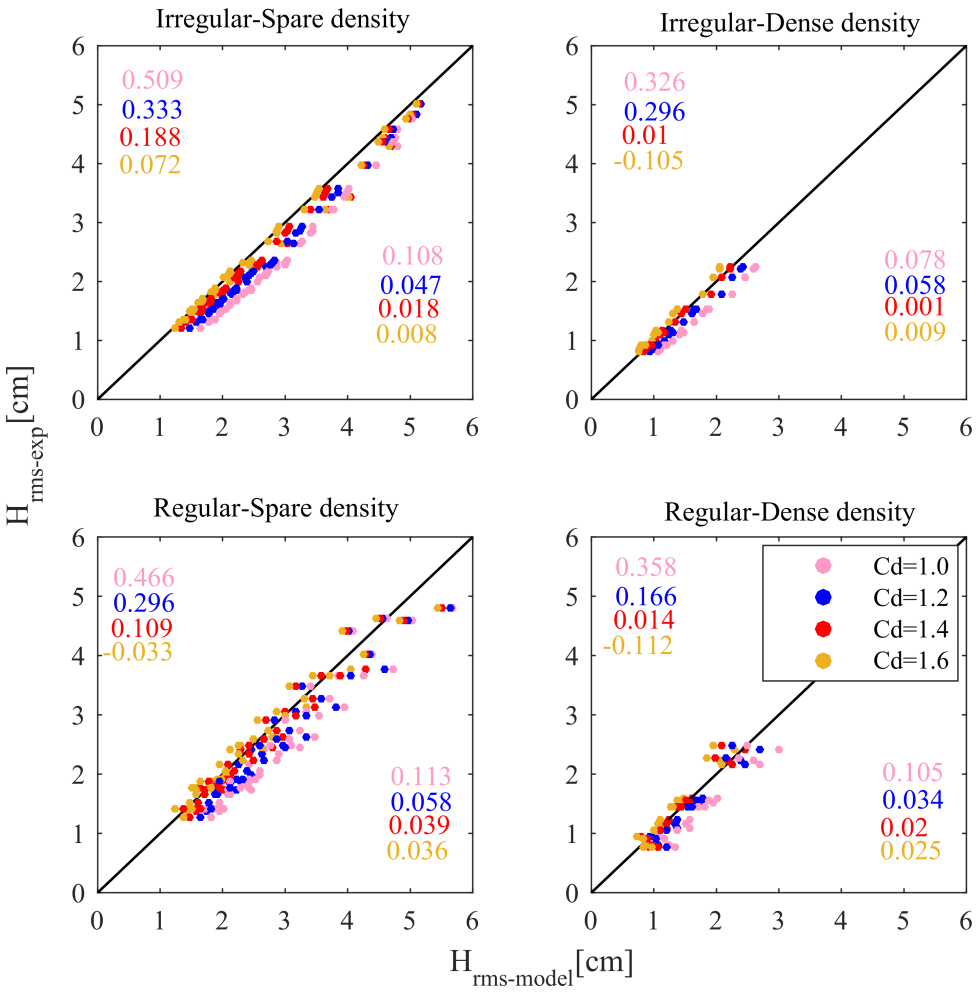

Figure 3.11: Comparison of physical model (vertical) and numerical model (horizontal) root mean square wave height for irregular (A,B) and regular wave (C,D) in case of different mangroves densities: sparse density (A,C) and dense density (B,D). Four different values of the drag coefficient are used. The predicting skill of the model is represented by the bias (top left) and scatter index (bottom right) in each plot.

the energy dissipation caused by turbulence processes in and around vegetation. In this sense, the increase in the magnitude of the C_d value can be interpreted to compensate for this missing mechanism of energy dissipation. In this study, an average drag coefficient of 1.5 was adopted in all cases.

Figure 3.12 illustrates the wave height transformation processes measured in the physical model and the associated results determined by the SWASH model with different densities of vegetation (no, sparse and dense mangrove). The results suggest that the wave height attenuation by cylinder arrays can be well predicted by the SWASH model (Figure 3.12A,B,E,F,I,J). Although the wave height continues to reduce inside the vegeta-

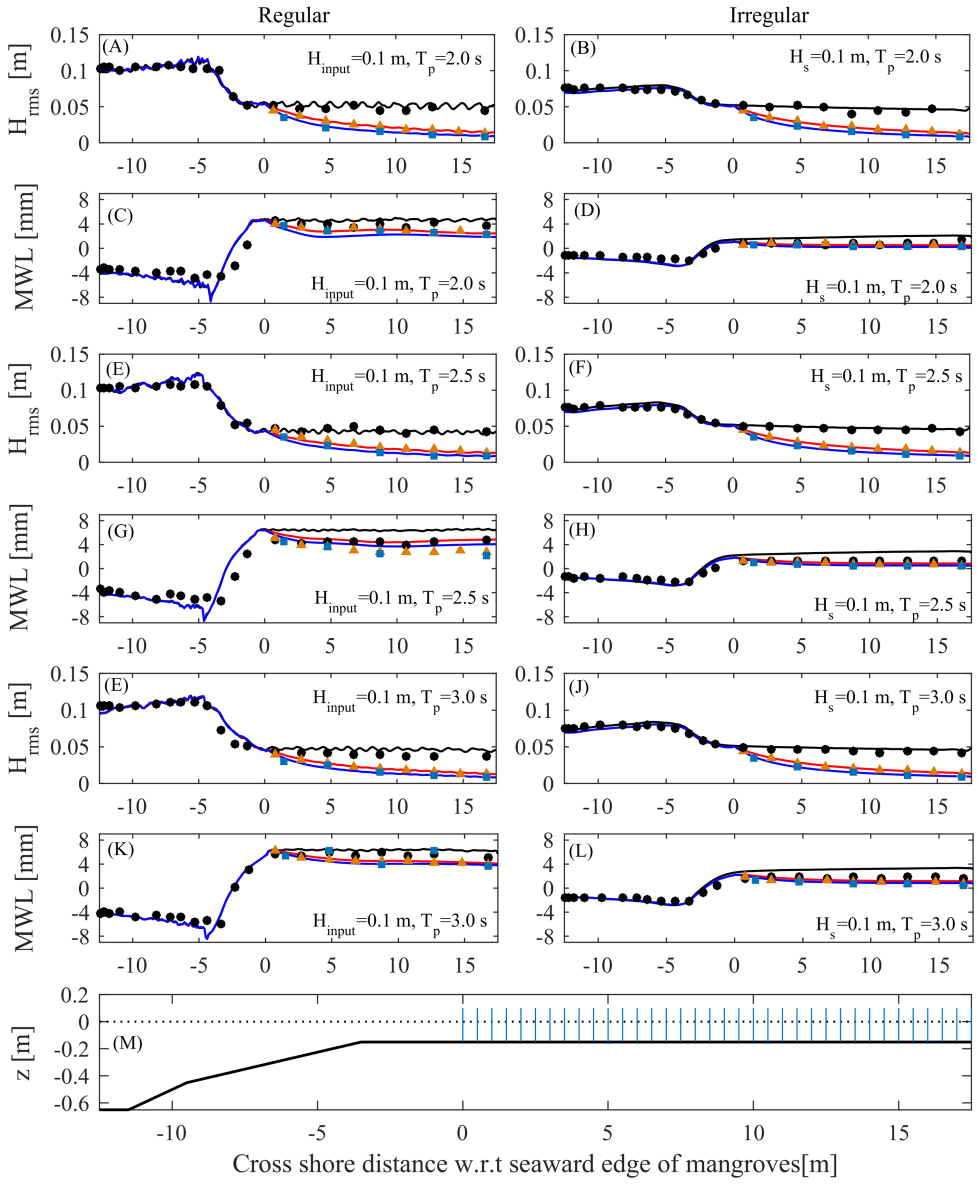

Figure 3.12: Wave height transformation comparisons between physical model: without mangroves (black circles), sparse mangroves (orange triangles), dense mangroves (square blues) and numerical model: without mangroves (black line), sparse mangroves (red line), dense mangroves (blue line) for different wave height conditions. Regular waves are represented in the left hand side and irregular waves are represented in the right hand side.

tion, it can be clearly seen that there is a wave set-down instead of set-up in the case of both regular and irregular waves. The balance of momentum flux and the drag force in-

duced by the presence of cylinder arrays is the main reason of this phenomenon (Dean and Bender, 2006). It is noticed that in all cases, this phenomenon of wave set-down in stead of set-up inside the mangrove forest is also well reproduced by the numerical model (Figure 3.12C,D,G,H,K,L).

3.5.3 Experimental data extended using thenumerical model

In this section, the numerical model was used to extend the length of mangroves in the experiment from 17.5 m to 40 m (from five wave lengths to ten wave lengths). The wave conditions (wave height and wave periods) were taken the same as in the experiment. Representative cases with sparse vegetation and irregular waves with a wave absorber in the end was considered.

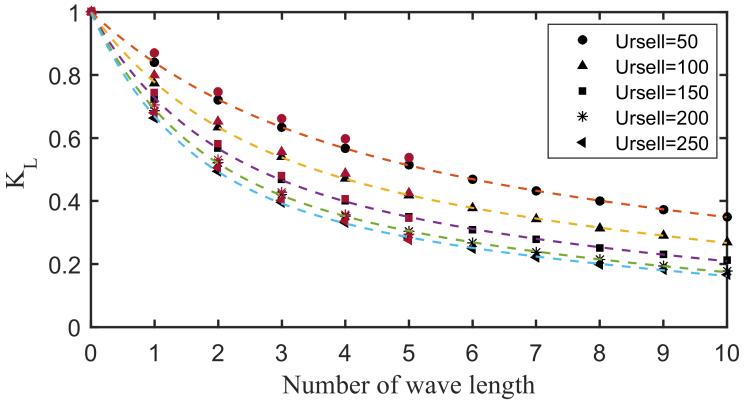

Figure 3.13: Comparision the effective wave transmission K_L determined from physical model(red markers) and predicted from the numerical model (black markers). In cases of irregular waves, sparse vegetation with different Ursell numbers. Ursell =50 (circles), Ursell =100 (triangles), Ursell =150 (squares), Ursell =200 (stars), Ursell =250 (left-pointing triangles).

Figure 3.13 shows the final extended results of wave attenuation determined for the effective transmission coefficient (K_L). The first part (first five wave lengths) includes the original experimental results (red markers) and that determined by the model (black markers). It can be clearly seen that the model can well predict the wave attenuation for the first five wave lengths. Therefore, the extended part (next five wave lengths) is expected to be trustworthy. According to the numerical simulation, it is predicted that the rate of wave attenuation rate appears to be constant after about eight wave lengths where the changes in the wave attenuation rate become less than 5 % in all cases for different Ursell numbers.

In this sense, the rate of wave attenuation by vegetation can be understood as a function of the number of wave lengths and Ursell numbers which can be generalized in an exponential equation:

$$K_L = ae^{bn} + ce^{dn} \tag{3.7}$$

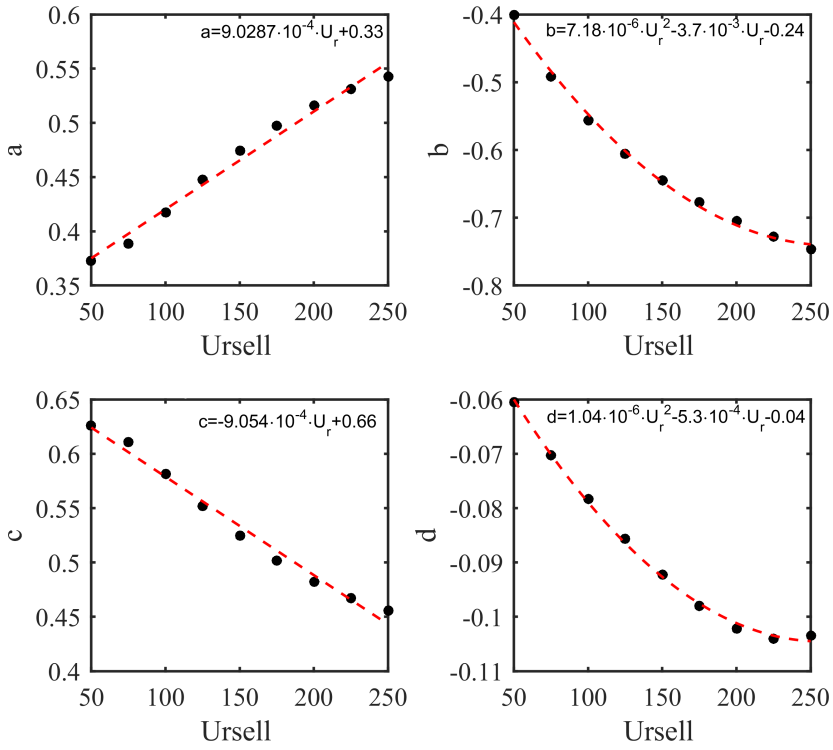

Figure 3.14: Relationship between parameters a,b,c,d from Equation (3.7) and Ursell number.

where n is the number of wave lengths and a, b, c, d are proportionality coefficients depending on the Ursell number. The relationship between these four coefficients and the Ursell numbers is presented in Figure 3.14. In this way, the wave height attenuation rate per number of wave length for a specific mangrove density can be presented as a function of the wave non-linearity presented by the Ursell number.

3.6 Conclusions

In this study, the wave attenuation process due to rigid vegetation was investigated, particularly focusing on the effect of wave non-linearity on the attenuation processes. Although many studies have been published on this topic, it is unclear how and to what extent the wave characteristics affect this phenomenon. As a result, the attenuation rate of wave height in the literature is commonly presented and evaluated as a function of an arbitrary absolute length.

In order to obtain more insight, an experiment was performed with different scenarios covering a large range of wave characteristics, including regular, irregular, broken, and non-broken waves with different wave heights and wave periods. The results confirm the role of vegetation in attenuating the wave height. Moreover, a wave set-down

instead of wave set-up due to the effect of vegetation was also observed.

The experimental data were used to evaluate the effects of the wave-non linearity on the wave reduction processes. An effective wave transmission coefficient is proposed, in which the wave height reduction is evaluated according to a relative length, i.e the number of wave lengths. Moreover, the wave characteristics are assessed through the Ursell number. It is shown that as the Ursell number increases from 0 to 250, the wave attenuation processes are also significantly affected. It is found that, the stronger the wave non-linearity , the stronger the attenuation of the wave height. For Ursell larger than 250, the wave attenuation processes appear to be independent of the wave characteristics. In this sense, if the characteristics of wave height (represented by Ursell) and vegetation (density, drag coefficient) are known, the attenuation rate of the waves can be derived.

Furthermore, a numerical model mimicking the physical model was constructed with the SWASH model. The numerical model then was validated using the experimental data. It is suggested that the model with only default values can well capture the transformation processes of the wave heights observed and measured in the physical model. A drag coefficient of 1.5 for all experiments is adopted to account for the turbulent energy dissipation processes that can not resolved in the simulations. Finally, the numerical model was used to extend the attenuation distance of the mangroves in the experiment so that the wave attenuation rate over up to ten wave lengths could be assessed. Based on that, the wave attenuation rate for a specific mangrove density can be presented as a function of the number of wave lengths and the Ursell number.

References

Augustin, L. N., Irish, J. L., and Lynett, P. (2009). Laboratory and numerical studies of wave damping by emergent and near-emergent wetland vegetation. *Coastal Engineering*, 56(3):332–340.

Bao, T. Q. (2011). Effect of mangrove forest structures on wave attenuation in coastal vietnam. *Oceanologia*, 53(3):807–818.

Bradley, K. and Houser, C. (2009). Relative velocity of seagrass blades: Implications for wave attenuation in low-energy environments. *Journal of Geophysical Research: Earth Surface*, 114(F1).

Brinkman, R. M. (2006). *Wave attenuation in mangrove forests: an investigation through field and theoretical studies*. PhD thesis, James Cook University.

Brinkman, R. M., Massel, S. R., Ridd, P. V., Furukawa, K., et al. (1997). Surface wave attenuation in mangrove forests. In *Pacific Coasts and Ports' 97: Proceedings of the 13th Australasian Coastal and Ocean Engineering Conference and the 6th Australasian Port and Harbour Conference; Volume 2*, page 909. Centre for Advanced Engineering, University of Canterbury.

Buckley, M., Lowe, R., and Hansen, J. (2014). Evaluation of nearshore wave models in steep reef environments. *Ocean Dynamics*, 64(6):847–862.

Cao, H., Feng, W., and Chen, Y. (2016). Numerical modeling of wave transformation and runup reduction by coastal vegetation of the south china sea. *Journal of Coastal Research*, 75(sp1):830–835.

Cavallaro, L., Re, C. L., Paratore, G., Viviano, A., and Foti, E. (2011). Response of posidonia oceanica to wave motion in shallow-waters-preliminary experimental results. *Coastal Engineering Proceedings*, 1(32):49.

Cooper, N. J. (2005). Wave dissipation across intertidal surfaces in the wash tidal inlet, eastern england. *Journal of Coastal Research*, pages 28–40.

Dalrymple, R. A., Kirby, J. T., and Hwang, P. A. (1984). Wave diffraction due to areas of energy dissipation. *Journal of Waterway, Port, Coastal, and Ocean Engineering*, 110(1):67–79.

Dean, R. G. and Bender, C. J. (2006). Static wave setup with emphasis on damping effects by vegetation and bottom friction. *Coastal engineering*, 53(2-3):149–156.

Guza, R., Thornton, E., and Holman, R. (1985). Swash on steep and shallow beaches. In *Coastal Engineering 1984*, pages 708–723.

Lövstedt, C. B. and Larson, M. (2009). Wave damping in reed: Field measurements and mathematical modeling. *Journal of Hydraulic Engineering*, 136(4):222–233.

Massel, S. (2006). Experiments on wave motion and suspended sediment concentration at nang hai, can gio mangrove forest, southern vietnam. *Oceanologia*, 48(1).

Mazda, Y., Magi, M., Ikeda, Y., Kurokawa, T., and Asano, T. (2006). Wave reduction in a mangrove forest dominated by sonneratia sp. *Wetlands Ecology and Management*, 14(4):365–378.

Mazda, Y., Magi, M., Kogo, M., and Hong, P. N. (1997). Mangroves as a coastal protection from waves in the tong king delta, vietnam. *Mangroves and Salt marshes*, 1(2):127–135.

Mendez, F. J. and Losada, I. J. (2004). An empirical model to estimate the propagation of random breaking and nonbreaking waves over vegetation fields. *Coastal Engineering*, 51(2):103–118.

Möller, I. (2006). Quantifying saltmarsh vegetation and its effect on wave height dissipation: Results from a uk east coast saltmarsh. *Estuarine, Coastal and Shelf Science*, 69(3-4):337–351.

Möller, I. and Spencer, T. (2002). Wave dissipation over macro-tidal saltmarshes: Effects of marsh edge typology and vegetation change. *Journal of Coastal Research*, 36(1):506–521.

Möller, I., Spencer, T., French, J. R., Leggett, D., and Dixon, M. (1999). Wave transformation over salt marshes: a field and numerical modelling study from north norfolk, england. *Estuarine, Coastal and Shelf Science*, 49(3):411–426.

Mork, M. (1996). Wave attenuation due to bottom vegetation. In *Waves and nonlinear processes in hydrodynamics*, pages 371–382. Springer.

Phan, L. K., van Thiel de Vries, J. S. M., and Stive, M. J. F. (2014). Coastal mangrove squeeze in the mekong delta. *Journal of coastal Research*, 31(2):233–243.

Quartel, S., Kroon, A., Augustinus, P., Van Santen, P., and Tri, N. (2007). Wave attenuation in coastal mangroves in the red river delta, vietnam. *Journal of Asian Earth Sciences*, 29(4):576–584.

Van den Berg, F., Beltman, W., Adriaanse, P., de Jong, A., and Te Roller, J. (2015). Swash manual 5.3: user's guide version 5. Technical report, Statutory Research Tasks Unit for Nature & the Environment (WOT Natuur & Milieu).

Wu, W.-C. and Cox, D. T. (2015). Effects of wave steepness and relative water depth on wave attenuation by emergent vegetation. *Estuarine, Coastal and Shelf Science*, 164:443–450.

Zijlema, M. (2012). Modelling wave transformation across a fringing reef using swash. *Coastal Engineering Proceedings*, 1(33):26.

Zijlema, M., Stelling, G., and Smit, P. (2011a). Simulating nearshore wave transformation with non-hydrostatic wave-flow modelling. In *Conference Proceedings, 12th Int. Workshop on Wave Hindcasting and Forecasting, Hawai'i, USA*.

Zijlema, M., Stelling, G., and Smit, P. (2011b). Swash: An operational public domain code for simulating wave fields and rapidly varied flows in coastal waters. *Coastal Engineering*, 58(10):992–1012.

Chapter 4

A laboratory study of long wave attenuation through mangrove forests

No amount of experimentation can ever prove me right;
a single experiment can prove me wrong.

Albert Einstein

As understanding the attenuation of low frequency waves inside the vegetation is still limited, a unique laboratory experiment was conducted to examine the attenuation through vegetation of three main types of infragravity waves including free long waves, bound long waves and mixed bound and free long waves. The experimental results were analysed and presented in terms of cross-correlation functions, damping rates per unit number of wave lengths and wave non-linearity effects. The results confirmed the role of mangroves in the absorption of the long wave reflections and suggested that different types of low frequency waves attenuate differently inside the mangrove forest. The free long waves damp fastest and the bound long waves damp slowest inside the vegetation. Both high and low frequency waves damp most effectively over the first wave length. Moreover, the larger the wave height or the wave period, the faster the wave attenuation. Furthermore although longer waves can penetrate further inside the vegetation than short waves, the damping rate per wave length of the short waves is smaller than the long waves. Additionally, it is found that bound long waves and mixed bound and free long waves strongly depend on the wave non-linearity as expressed by the Ursell number, while free long waves are only weakly dependent on this parameter. Last but not least, it is shown that the wave non-linearity is the primary parameter governing the attenuation of low frequency waves inside the vegetation.

A modified version of this chapter is planned to be submitted to Coastal Engineering. Phan, L.K., Stive M.J.F., Tissier, M.F.S., Truong, H.S., and Reniers A.J.H.M (2019). A laboratory study of infragravity wave attenuation by vegetation.

4.1 Introduction

Over the last decade, ecological wetland systems have received many attention because of their efficient protective role in sustainable coastal development. Due to increasing sea levels and the human exploitation, the degradation of tidal wetland vegetation in general and mangrove forests in particular is of major concern in many coastal areas. These issues are also true for the Mekong Delta coast, where usually only a narrow strip of about 100 m-200 m coastal mangroves remained. At those locations, the degradation of coastal mangrove is usually observed together with the erosion of the shoreline with erosion rates of up to 30 m yr^{-1} (Phan et al., 2014).

The degradation of mangrove forests is usually blamed on the effects of sea level rise or the impacts of human intervention. While the former impacts from the sea side, the latter impacts from the land-side and is often related to the construction of sea dikes or fish-farms. Wherever the impacts come from the sea or land side, the mangrove forests are usually squeezed, *i.e.* only a narrow strip of mangroves is remained and they usually degrade along with the erosion of the coastal shore line. This phenomenon is known as "mangrove squeeze". (Phan et al., 2014) and (Truong et al., 2017) investigated that the degradation of mangroves is strongly related to their available development space. From the physical perspective, the hydrodynamic forces, *i.e.* the attenuation of waves and flows through mangrove forests were shown to be important factors that can explain this phenomenon. While flows are usually relevant for the estuarine mangroves Truong et al. (2017), waves are of primary importance for coastal mangroves (Phan et al., 2014) which is the major focus of this paper.

Numerous studies have focused on studying the attenuation of waves through mangroves (Augustin et al., 2009; Brinkman, 2006; Massel, 2006; Mazda et al., 2006; Quartel et al., 2007). It is suggested that by performing work on vegetation roots, stems and canopies, waves travelling in a mangrove forest lose their energy and thereby their wave height decreases (Mork, 1996). In those previous studies, primarily the attenuation of high frequency waves were considered and that of low frequency waves has received much less attention. Furthermore, the wave attenuation is usually presented through a wave transmission coefficient (K_t), also named a wave height damping coefficient, calculated based on an absolute length scale, *i.e.* per meter length of the forest. Using an absolute length scale causes a large variation in results, especially as Phan et al. (2014) investigated the attenuation of infra-gravity waves inside the forests using a numerical model constructed in X-beach, and suggested that long waves penetrate over a longer distance inside the vegetation compared to high frequency waves. In order to obtain more insight, a new presentation method, in which the wave height reduction is presented through a relative length scale, *i.e.* a unit number of wave lengths (Phan et al., 2018). It is suggested that the longer waves need a longer distance to attenuate in the mangrove forest compared to shorter waves. Furthermore, the effect of wave nonlinearity was revealed using the Ursell number (Phan et al., 2018). These findings have motivated this study, based on a unique laboratory study of both low and high frequency wave attenuation through a mangrove forest.

In the Mekong Delta, the shoreline slope is usually gentle of about 1/10000 and the waves are mostly wind waves (Phan et al., 2014). In this condition, the bound long waves

can be generated by the grouping of natural incident random waves. Low frequency waves or so called long waves, which were also known as infra-gravity waves are waves generated by the transfer of energy from high frequency waves or so called short waves (Hamm et al., 1993). When short waves propagates toward foreshore, changing their amplitude because of the variation in the water depth, lose their energy and break over depth changes, *i.e.* bars (Agnon, 1993; Longuet-Higgins and Stewart, 1964), bound low frequency waves can be released to propagate freely. This processes of energy transfer from high frequency waves can be caused by different mechanisms. For example, the fluctuation of wave set-up in response to fluctuations in incident wave amplitude (List, 1991) or the movement of break points (Schäffer, 1993; Symonds et al., 1982). In reality, these two mechanisms can occur simultaneously, but, depending on the local and external boundary conditions, one of the two mechanisms can dominate. A number of studies has shown that the breakpoint forcing mechanism for infragravity waves was mainly relevant for steep beaches, and that over mild sloping beaches the bound long wave mechanism was dominating (Baldock and Huntley, 2002; Battjes et al., 2004). Thus the breakpoint mechanism is likely to be an important generation mechanism for the lab experiments but not over real mangroves due to their very mild slopes. How relevant the generation mechanism is regards the behaviour of the released long waves is an unresolved issue. However, despite the difference in the generation mechanism, it must be concluded that low frequency waves can include bound long waves, free long waves and a mixture between the two.

It is noticed that free long waves and bound long waves can have different effects on mass transport, for instance while the negative mass transport is related to bound long waves, free long waves are related to positive mass transport (Longuet-Higgins and Stewart, 1964). However, despite of their importance, understanding the generation and propagation of infra-gravity waves is limited, especially in terms of the presence of a mangrove forest. Therefore, the main purpose of this study is: (1) to understand how these types of long waves attenuate differently inside the vegetation and (2) to clarify which factor is important for the attenuation processes of low frequency waves.

4.2 Methodology

4.2.1 Experimental set up and wave conditions

In order to achieve the research objectives, a unique experiment including up to 17.5 m length of cylinder arrays was constructed, allowing the propagation of up to five wave lengths. The experimental set up is presented in Figure 4.1. Because of the very gentle slope of the Mekong Delta coast (1/10000), waves propagating towards the mangroves are usually broken before entering the mangrove forests (Phan et al., 2014). As a result, they have lost their primary spectral energy and long wave energy has developed. Therefore a horizontal deeper part and a steep wooden slope with a combination slope of 1/10 and 1/20 was used to simulate the processes of shoaling and breaking waves.

Different mangrove densities were considered including cases without mangroves ($AV0$), with sparse mangroves ($AV1$, 200 cylinder/m^2) and with dense mangroves ($AV2$, 400 cylinder/m^2). Phan et al. (2018) used the same experimental configuration to study

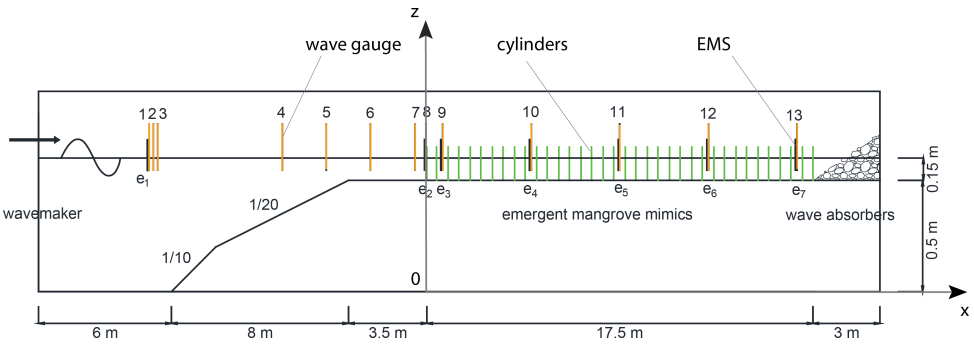

Figure 4.1: Schematic view of the experiment set up, including the locations of wave gauges, EMSs and vegetation. The vegetation starts from x=0 in the positive direction. The vegetation starts from x=0 in the positive direction. Not to scale.

the wave attenuation of high frequency waves, emphasizing the effects of wave nonlinearity.

This study focuses on the generation and the attenuation of the low frequency waves. Two main wave input conditions, *viz.* irregular waves with JONSWAP spectrum (wave type 1) and irregular waves with a double peaked spectrum (wave type 2) were considered at the wave paddle. Figure 4.2 illustrates time series signals and their associated spectra for these two wave types. Wave generation cases with predominant bound long waves in the offshore (wave type 1) where if no breaking occurs a limited amount of free long waves will emerge due to shoaling and interaction with vegetation (Scenario 1N) and when breaking occurs a substantial amount of free long waves will emerge (Scenario 1B). Wave generation cases of predominant free long waves in the offshore (Scenario 2) where the wave groups will generate bound long waves which persist in the absense of breaking (Scenario 2N) but will be released when breaking occurs (Scenario 2B). In this context, three main different wave conditions were recorded in the experiment which are (1) predominant bound long waves (Scenario 1N); (2) predominant free long waves (Scenario 2N and 2B); and (3) a mixed of bound and free long waves (Scenario 1B).

In scenarios of wave type 1, significant wave height (H_s) ranges from 3 to 10 cm at the wave paddle, peak period (T_p) ranges from 2 to 3 s. In scenarios of wave type 2, the wave height ranges from 2 to 6 cm at the wave paddle, the peak period is 2.5 s and for low frequency waves, the peak period (Tp_{lf}) ranges from 10 to 15 s which is comparable with that observed from scenarios of wave type 1.

Table 4.1: Experiment scenarios with wave characteristics at the wave paddle (significant wave height and peak period) and calculated incoming total waves, low and high frequency wave at the edge of the mangroves. Legend explanation presented in the end of the table.

Case		At the wave paddle (total waves)			At the seaward edge of the mangroves (incoming waves)				
	Wave type	x= -17.5 [m]			0 [m]				
		H_s [cm]	Tp_{hf} [s]	Tp_{lf} [s]	H_{t0} [cm]	H_{hf0} [cm]	H_{lf0} [cm]	H_{hf0}/H_{t0}	H_{lf0}/H_{t0}
AV1/AV2*IrH03T20	1N	3	2	8	2.5	2.48	0.32	0.992	0.128

AV1/AV2*IrH03T25	1N	3	2.5	10	2.71	2.69	0.33	0.993	0.122
AV1/AV2*IrH03T30	1N	3	3	12	2.59	2.58	0.3	0.996	0.116
AV1/AV2*IrH05T20	1N	5	2	8	4.16	4.09	0.76	0.983	0.183
AV1/AV2*IrH05T25	1N	5	2.5	10	4.23	4.17	0.73	0.986	0.173
AV1/AV2*IrH05T30	1N	5	3	12	4.14	4.08	0.66	0.986	0.16
AV0/AV1/AV2*IrH07T20	1B	7	2	8	4.98	4.86	1.08	0.976	0.217
AV0/AV1/AV2*IrH07T25	1B	7	2.5	10	5.24	5.12	1.12	0.977	0.213
AV0/AV1/AV2*IrH07T30	1B	7	3	12	4.8	4.71	0.94	0.981	0.196
AV0/AV1/AV2*IrH10T20	1B	10	2	8	5.75	5.55	1.49	0.965	0.259
AV0/AV1/AV2*IrH10T25	1B	10	2.5	10	5.85	5.64	1.56	0.964	0.267
AV0/AV1/AV2*IrH10T30	1B	10	3	12	5.5	5.31	1.43	0.965	0.26
AV1/AV2*2peak21	2N	2	2.5	12.5	1.48	1.04	1.05	0.703	0.71
AV1*2peak22	2N	2	2.5	10	1.34	0.97	0.93	0.724	0.694
AV1*2peak23	2N	2	2.5	15	1.53	1.09	1.07	0.712	0.699
AV1/AV2*2peak41	2B	4	2.5	12.5	3.8	2.82	2.55	0.742	0.671
AV1*2peak42	2B	4	2.5	10	3.01	2.21	2.04	0.734	0.678
AV1*2peak43	2B	4	2.5	15	3.82	2.86	2.53	0.749	0.662
AV0/AV1/AV2*2peak61	2B	6	2.5	12.5	5.21	3.95	3.4	0.758	0.653
AV0/AV1/AV2*2peak62	2B	6	2.5	10	6.62	5.05	4.27	0.763	0.645
AV1/AV2*2peak63	2B	6	2.5	15	6.47	4.92	4.2	0.76	0.645

AV0/AV1/AV2: no mangroves/sparse mangroves/dense mangroves.
IrH10T25: Irregular wave with Jonswap spectrum, Hs=10cm; Tp=2.5s.
2peak21: irregular wave with double peak spectrum.
Wave type 1N: Jonswap spectrum input at the wave paddle, non-broken wave
Wave type 1B: Jonswap spectrum input at the wave paddle, broken wave
Wave type 2N: double peak spectrum as input at the wave paddle, non-broken wave
Wave type 2B: double peak spectrum as input at the wave paddle, broken wave
H_{t0}: total incoming wave height at the edge of the mangroves.
H_{hf0}: incoming high frequency wave height at the edge of the mangroves.
H_{lf0}: incoming low frequency wave height at the edge of the mangroves.

These different scenarios of wave characteristics at the wave paddle (H_s and T_p) and their corresponding calculated incoming total, low and high frequency wave heights at the mangrove edge are presented in Table 4.1. The incoming waves are determined according to the method of Guza et al. (1985) which was proven to be applicable for irregular wave with same bathymetry and wave conditions (Phan et al., 2018).

It is noticed that in scenarios of wave type 1, at the seaward edge of the mangrove forest, the energy of long waves obtained in cases of broken waves (H_{lf0}/H_{t0} ranges from 0.21 to 0.27, Table 4.1) is larger than in cases of non-broken waves (H_{lf0}/H_{t0} ranges from 0.12 to 0.18, Table 4.1). This can be interpreted in terms of the breaking mechanism. In cases of broken waves, long wave energy was generated by two mechanisms which are (1) the release of the bound long wave (Longuet-Higgins and Stewart, 1964) and (2) the generation of free long waves by the movement of the break points (Symonds et al., 1982). However, in cases of non-broken waves, long wave energy stems mainly from the bound long wave energy.

Furthermore, in cases of wave type 2, free long waves may behave as short waves, i.e. shoaling and then breaking on the transition slope. Therefore, in case of broken waves, long waves also break and reduce their energy before they enter the mangroves. Consequently, at the seaward edge of the mangroves, free long wave energy in cases of broken waves (H_{lf0}/H_{t0} ranges from 0.65 to 0.68, Table 4.1) is smaller than in case of non-broken waves (H_{lf0}/H_{t0} ranges from 0.69 to 0.71, Table 4.1).

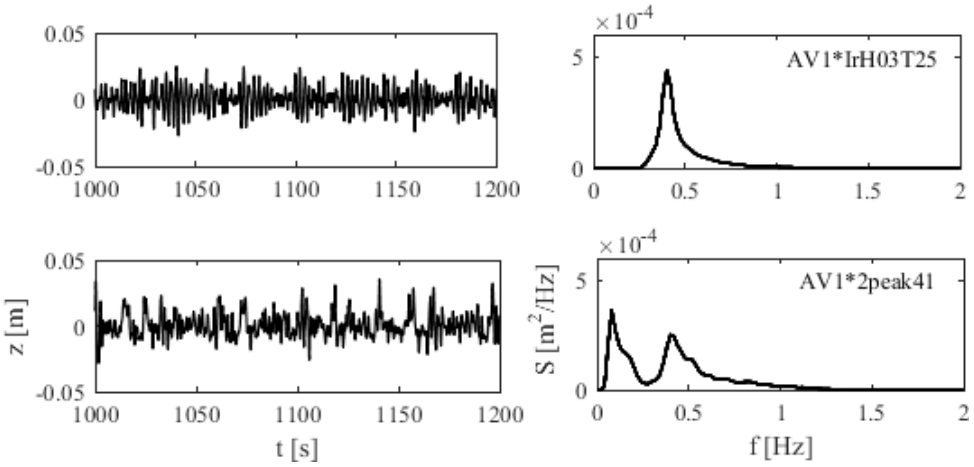

Figure 4.2: Representative time series signal (left hand side) and its associated wave spectrum (right hand side) at the wave paddle corresponding to irregular JOHNSWAP spectrum (upper panels) and double peak spectrum (lower panels).

4.2.2 Infragravity wave transformation

Three interaction modes of the low and high frequency waves in cases of dense mangroves are examined in five different experiment scenarios using the cross-correlation between the short waves envelope and long waves. These interaction modes are (1) the interaction between the free waves and short wave group inside the mangroves (case AV2*2peak21-double peak spectrum with significant wave height at the wave paddle is 2 cm, peak period of high frequency wave is 2.5 s and peak period of low frequency is 12.5 s); (2) the interaction between the bound long waves and the short wave group inside the mangroves (case AV2*IrH03T25-irregular wave with wave height at the wave paddle is 3 cm, peak period is 2.5 s, and case AV2*IrH05T25-irregular wave with wave height at the wave paddle is 5 cm, peak period is 2.5 s); and (3) the interaction between the mixed bound and free long waves and short wave group inside the mangroves (case AV2*IrH07T25-irregular wave with wave height at the wave paddle is 7 cm, peak period is 2.5 s, and case AV2*IrH10T25-irregular wave with wave height at the wave paddle is 10 cm, peak period is 2.5 s). In order to highlight the influence of mangroves on the wave transformation, the cross-correlation of the mixed bound and free long wave and the short wave group in two cases without mangroves (AV0*IrH07T25 and AV0*IrH10T25) are presented as the reference cases.

The cross-correlation can be determined according to the definition of Bendat and Piersol (2011):

$$R_{X_i X_r}(\tau) = \frac{\langle X_i(t) X_r(t+\tau) \rangle}{\sigma_{Xi} \sigma_{Xr}} \tag{4.1}$$

Where $X_i(t)$ and $X_r(t)$ are the harmonic signals, σ_{Xi} and σ_{Xr} are the standard deviations of $X_i(t)$ and $X_r(t)$, τ is the phase lag and $R_{x_i x_r}$ is the cross-correlation for these two signals.

The low and high frequency waves were split using band pass filtering ($f_{split} = f_{peak}/2$). The envelope of the high-frequency wave is determined using the Hilbert transform operator (Equation (4.2)):

$$|A(t)| = \left|\eta^{hf}(t) + i\Gamma\{\eta^{hf}\}\right|^{lf} \tag{4.2}$$

In which, $|A(t)|$ is the high-frequency envelop, which can be interpreted as the envelope of the short-wave group (Janssen et al., 2003) and Γ is the Hilbert transform operator. Representative bandpass filtered low-frequency waves (black line), bandpass filtered high-frequency waves (blue line) and their associated envelope (red line) derived following this methodology are illustrated in Figure 4.3.

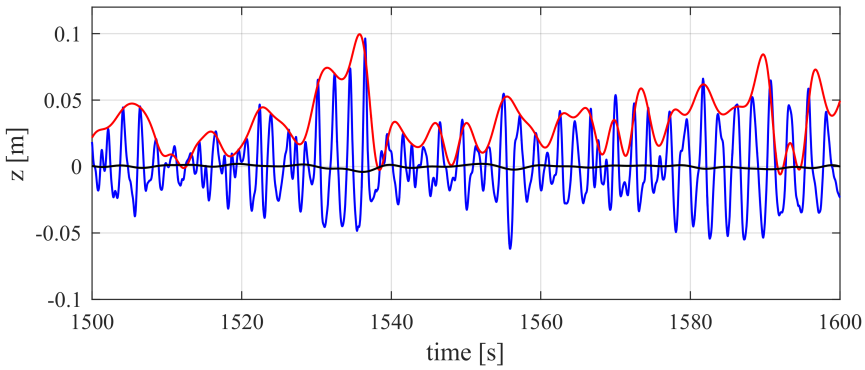

Figure 4.3: Example of bandpass filtered high-frequency signal (blue line) and the corresponding low-frequency signal (black line). Wave envelope (red line) was obtained using the Hilbert transform of high frequency wave signal measured at 5 m from the wave paddle for case IrH10T25.

4.3 The generation of infragravity waves

In this section, different mechanisms of generating infra-gravity waves were examined through the autocorrelation of short wave envelopes and long waves as well as the cross-correlation between them. The cross-correlation function (Equation (4.1)) is used to analyse the generation of infragravity waves in front of and inside the mangrove forest.

4.3.1 Propagation of short wave envelope

Figure 4.4 shows the cross-correlation between the squared envelop signal across the flume with respect to the location 12.5 m in front of the vegetation edge $R_{AA}(T, x_i, x_r{=}{-}12.5\,\text{m})$ in case of dense mangroves. It can be clearly seen that there is a band of positive correlation with increasing phase lag (T) towards the shoreline for all five cases. The dashed line in this figure indicates time lag values for waves which propagate at the group velocity c_g and the peak frequency T_p. This confirms the expected propagation of the wave groups (wave envelop). It is also suggested that the cross-correlation varies along

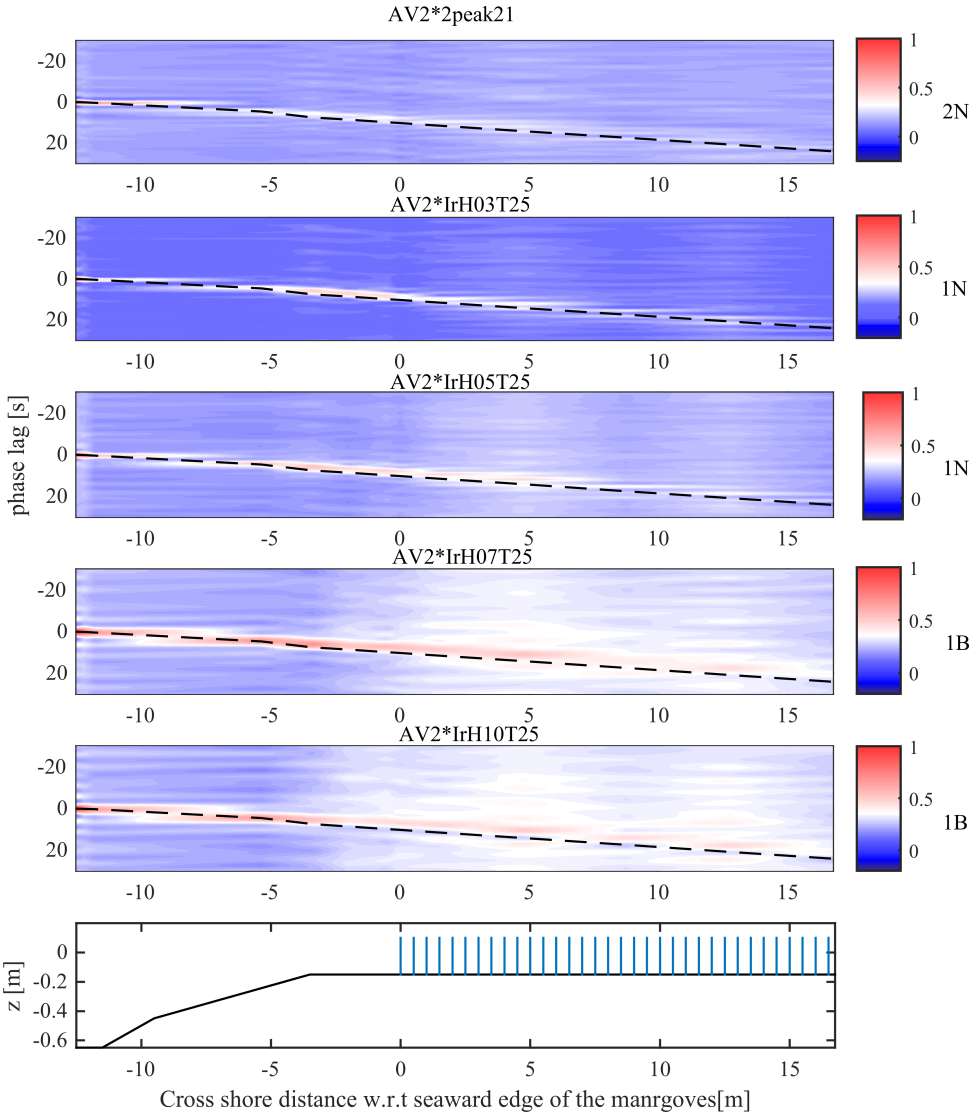

Figure 4.4: Cross-correlation of the squared short wave envelope (auto correlation) in case of dense mangroves. The dashed line shows the phase difference based on the group celerity c_g.

with the changes of the water depth (or bathymetry). At the beginning of the slope (x=−12.5 m), as the waves travel on the slope, the water depth decreases and the cross-correlation regularly decreases. However, along the flat bottom where the water depth remain unchanged (from x=−5 m to x=5 m), the cross-correlation increases. Finally when the waves penetrate into the forest and propagate toward the end of the flume (from x >5 m) the cross-correlation slowly reduces again. The results show that there is a good

agreement between the computed lags and the observed lags of the maximum correlation

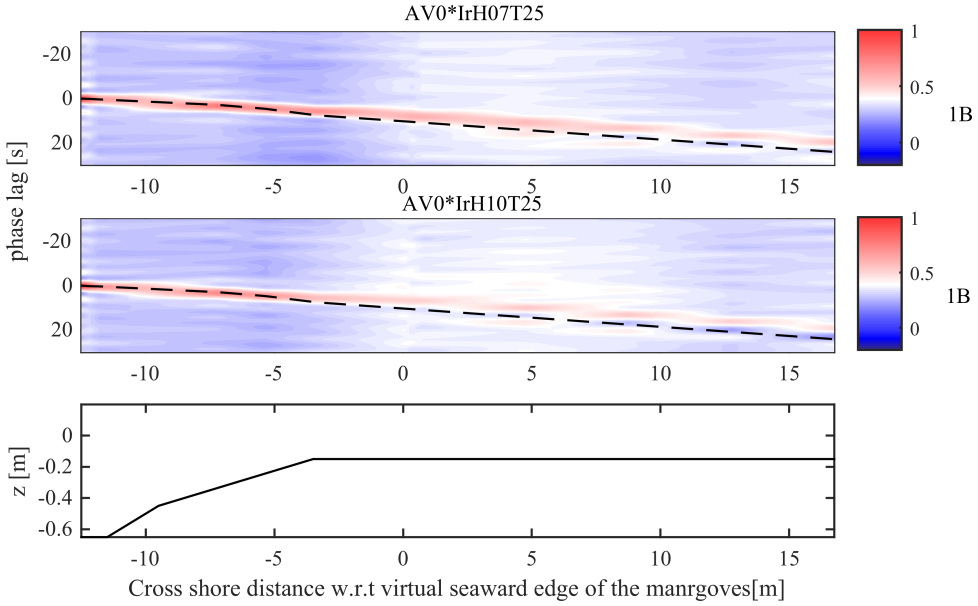

Figure 4.5: Cross-correlation of the squared short wave envelope in case without mangroves. The dashed line shows the phase difference based on the group celerity c_g.

Figure 4.5 presents the cross-correlation of the squared short wave envelope in case without mangroves. It can be seen that the cross-correlation reduces continuously from the beginning toward the end of the flume in cases without vegetation. Moreover, the values of cross-correlation in case of no mangroves appear to be larger than in cases with dense mangroves (darker red colour - in the same scenarios: AV0*IrH07T25 and AV0*IrH10T25). This can be interpreted in terms of the influence of mangroves on the propagation of short waves. Because mangroves are very effective in damping higher waves, the presence of mangroves in cases with dense mangrove causes deformation of the short wave group. In another words, mangroves reduce the groupiness of the waves. Consequently, the cross-correlation of the short wave envelop in case of dense mangroves is smaller than in cases without mangroves.

4.3.2 Propagation of infragravity wave

The low frequency wave signal at 12.5 m in front of the mangrove edge is compared to the low-frequency wave signal at different locations along the flume through the auto correlation coefficients ($R_{ll}(T, xi, xr)$) of the low-frequency wave signal in cases of dense mangroves (Figure 4.6). Similar to the propagation of the short wave envelope, a band of positive correlation can also be observed confirming the onshore propagation of the low-frequency waves for all the conditions tested. Furthermore, the evolution of the

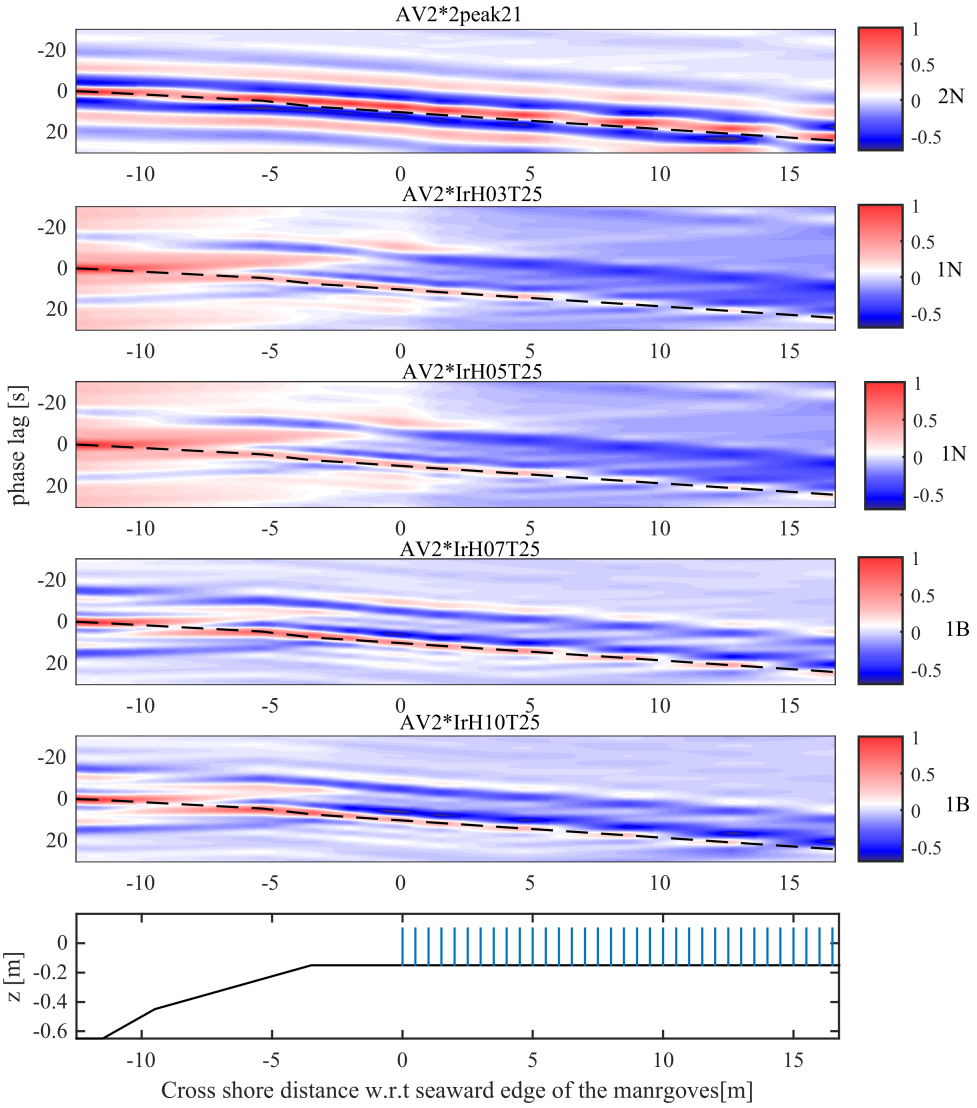

Figure 4.6: Auto-corelation of the low-frequency waves R_{ll}(T,xi,xr) in case of dense mangroves. The dashed line shows the phase difference based on the group celerity c_g.

band with positive correlation, corresponding to the propagation of the low-frequency waves is well described by the computed phase lags based on the group celerity c_g.

It is noted that a zero value of cross-correlation implies that the wave structure group is disappeared. In this context, it is found that the disappearance of the wave structure group can be explained regarding the presence of mangroves and the breaking processes of waves. In cases with mangroves, for both non-broken and broken waves, the cross-correlation value is about zeros after about 5 m inside the mangrove forest (see

Figure 4.6-1N and 1B).

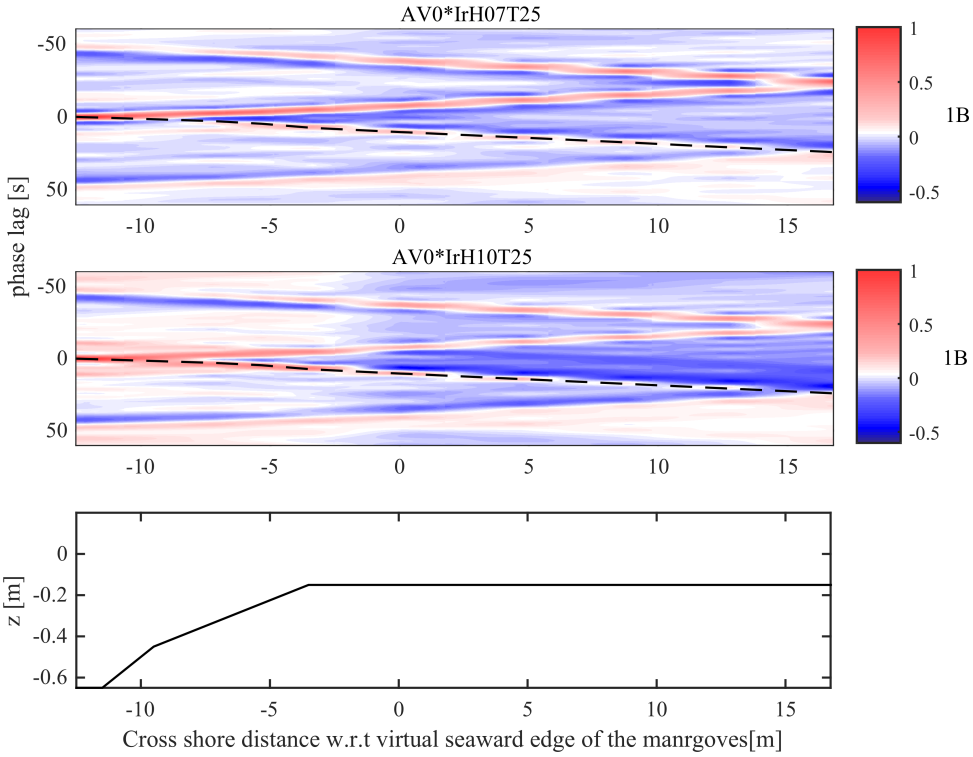

Figure 4.7: Auto-correlation of the low-frequency waves R_{ll}(T,xi,xr) in case of no mangroves. The dashed line shows the phase difference based on the group celerity c_g.

Figure 4.7 illustrates the autocorrelation of the low-frequency waves $R_{ll}(T, xi, xr)$ in case without mangroves. A band of positive correlation from the end of the flume toward the wave paddle can be clearly observed in this figure. It is noticed that this ridge in cases without mangrove corresponding to the reflection of the low frequency wave at the end of the flume cannot be observed in cases with dense mangroves (Figure 4.6). This result again confirms the role of vegetation in general and mangroves in particular on the absorption of the long wave reflection.

4.3.3 Interaction between short wave envelope and infra-gravity waves

Figure 4.8 illustrates the cross-correlation coefficients between the short wave envelope at 12.5 m in front of mangroves edge and the low-frequency waves at each location along the flume R_sl $(T, xi, xr = -12.5\,\text{m})$ in case of dense mangroves. The dashed line shows the phase difference based on the group celerity c_g. Three different modes of interaction mentioned previously can be clearly observed. Firstly, in the case of predominant free long waves (AV2*2peak21), there is no connection between low frequency waves and the wave group. As a result, there is a band of constant positive cross-correlation

with a value of about 0.1 observed along the flume. Secondly, in cases of predominant

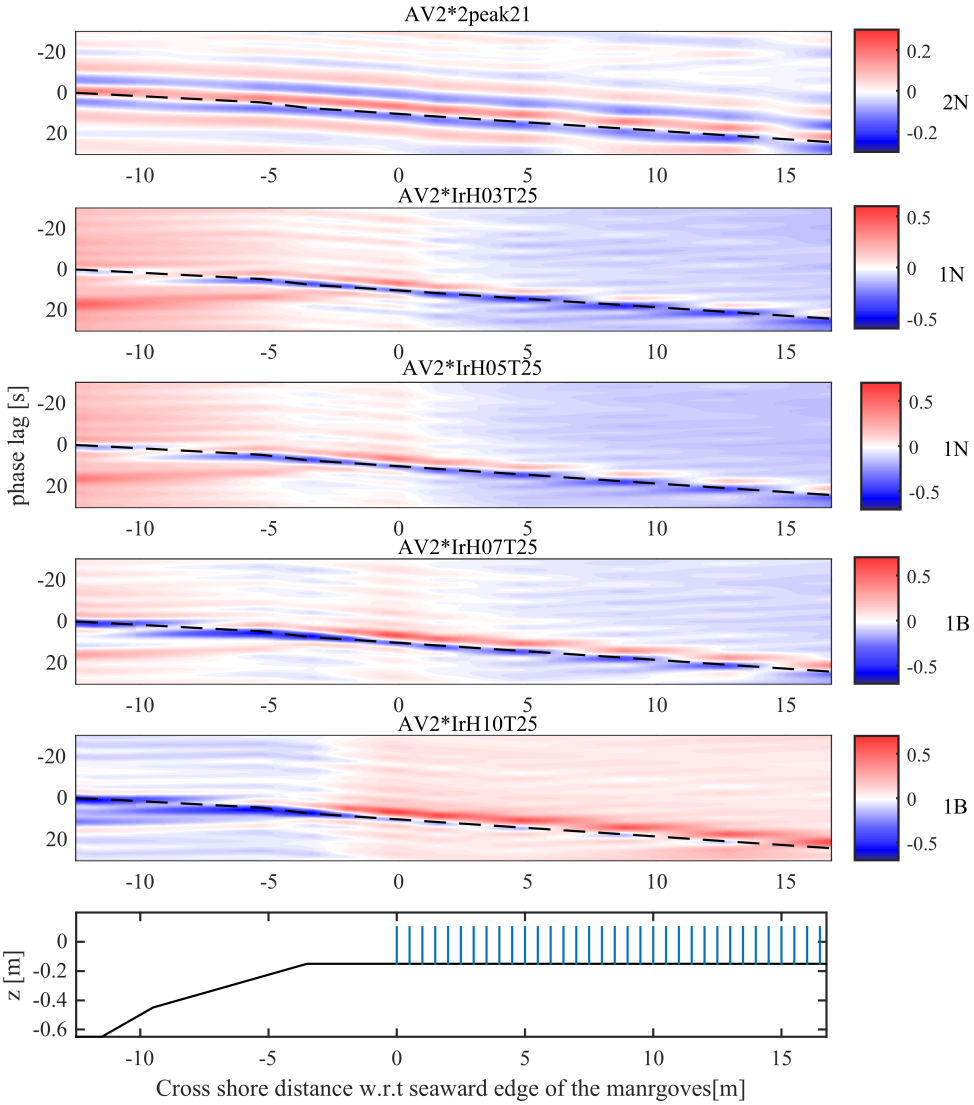

Figure 4.8: Cross-correlation function between the short wave envelope and the low-frequency waves $R_{sl}(T, xi, xr = -12.5\,\mathrm{m})$ in case of dense mangroves. The dashed line shows the phase difference based on the group celerity c_g.

bound long waves (AV2*IrH03T25 and AV2*IrH05T25), because the bound long waves are not yet generated at the wave paddle, the cross-correlation starts around zero, after that, as the bound long waves develop along with the wave group, the cross-correlation starts reaching negative values. The negative cross-correlation between the short wave envelopes and bound long waves implies that as the value of short waves group increase

at the beginning, the value of bound long waves will decrease in this region. Inside the mangroves, the cross-correlation remains negative towards the end of the flume. The propagation of the low-frequency wave is also well described by the computed phase lags based on the group celerity (cg) (dashed line).

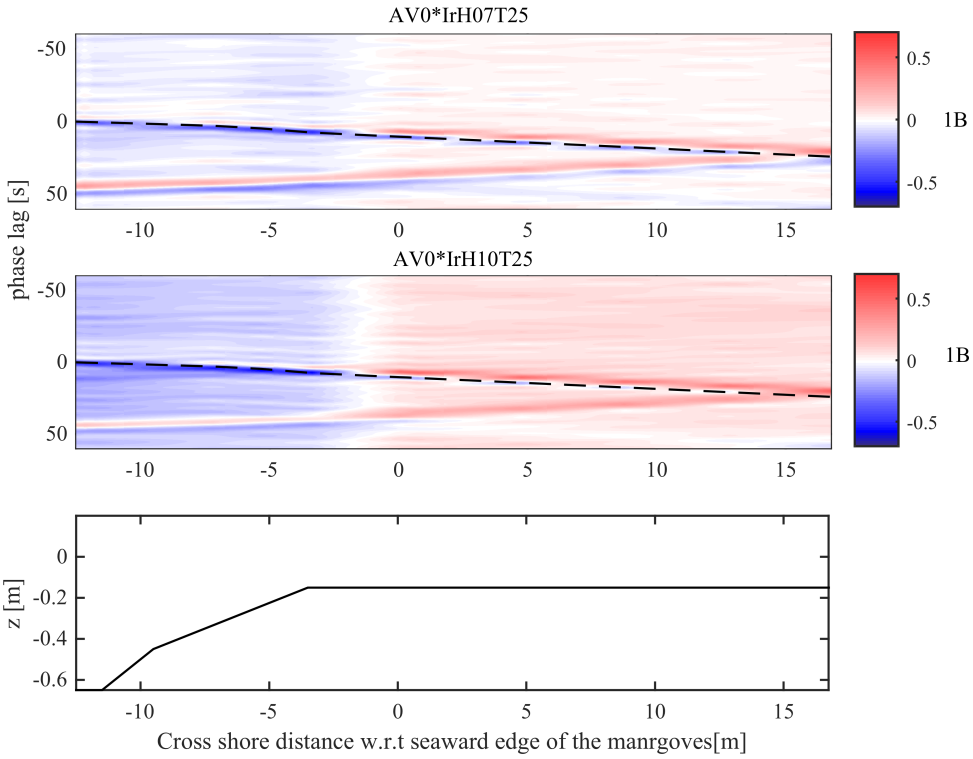

Figure 4.9: Cross-correlation function between the short wave envelope and the low-frequency waves $R_{sl}(T, xi, xr = -12.5\,\mathrm{m})$ in case without mangroves. The dashed line shows the phase difference based on the group celerity c_g.

Thirdly, when the mixed bound and free long waves presented inside the mangrove forest (AV2*IrH07T25 and AV2*IrH10T25), the cross-correlation coefficient was negative at the beginning and then switched to positive values after the breaking area. This indicates that outside the breaking region, the low frequency waves are bound with the wave group. After that, the interaction between low frequency waves and short wave group reduced, and the bound long waves were released as free waves. These released bound long waves propagated slightly faster than the wave group with the velocity $c = \sqrt{gh}$. The cross-correlation in the scenarios with the same wave conditions but without mangroves (AV0*IrH07T25 and AV0*IrH10T25) are presented in Figure 4.9. It can be clearly seen that the cross-correlation coefficient in both cases changed from negative to positive values after the breaking point.

In order to obtain more insight into the interaction between low frequency wave and the wave groups, the local cross-correlation is computed (Figure 4.10). In the case of

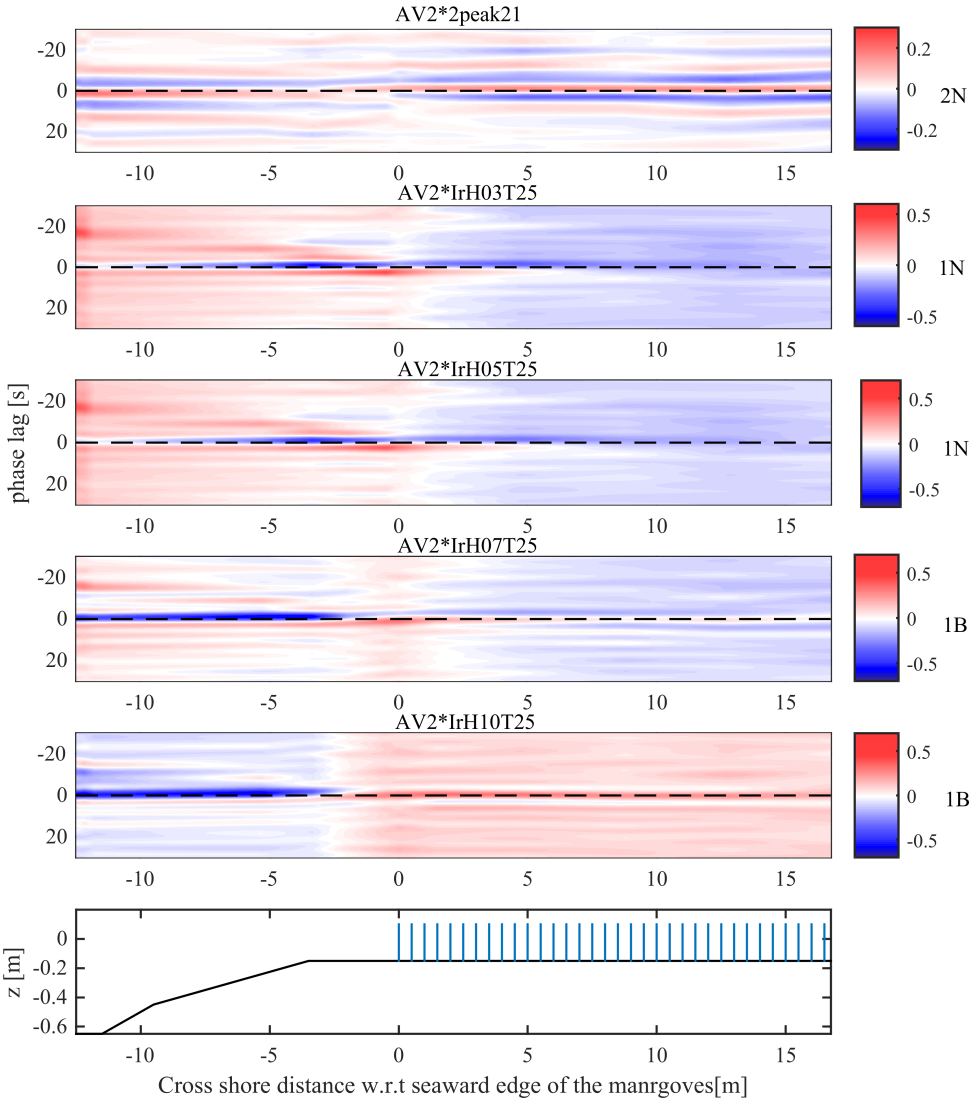

Figure 4.10: Cross-correlation function between the short wave envelope and the low frequency waves $R_{sl}(T,i,i)$.

predominant free long waves (case AV2*2peak21), a constant positive value of cross-correlation can be observed. Once again, a constant negative value of cross-correction can be observed in case of predominant bound long wave (case AV2*IrH03T25 and case IrH05T25). A negative cross-correlation between the bound long waves and the short wave groups was found to develop before the breaking sets in the two cases AV2*IrH07T25 and AV2*IrH10T25. The cross-correlation coefficient smoothly switched from negative to positive values, indicating that a part of the bound long wave outside the surf zone is

released to become free long waves before entering the mangrove forest.

4.4 Low and high frequency wave attenuation through mangroves

In this section, the attenuation of low and high frequency waves through mangroves is presented and the effects of wave non-linearity on the wave attenuation is examined.

4.4.1 Low and high frequency wave transformation

Figure 4.11 presents the transformation of low and high frequency waves along the flume for cases of different wave types including wave types 1N (orange markers), wave type 1B (purple markers), and wave type 2B (green markers) in the cases of dense mangroves.

Firstly, it can be seen that in cases of broken waves (wave type 1B and wave type 2B), although the height of low frequency waves at the mangrove edge (location $x = 0$ m) in the case of wave type 2B of about 4 cm is larger than that in the case of wave type 1B of about 2 cm, the height of the low frequency waves at the end of the mangroves is almost the same. This result suggests that inside the mangrove forest, free long waves are dampened faster than the mixed type of broken bound and free long waves.

Moreover, it can also be seen that the wave type of predominant bound long waves (orange triangles) and predominant free long waves (green triangles) attenuate differently inside the mangrove forest. Inside the mangroves, free long waves appear to be damped faster than bound long waves. In general, by comparing the wave height of different scenarios, i.e. (1) predominant free long waves, (2) predominant bound long waves and (3) mixed bound and free long waves, it is suggested that mangroves appear to be more effective in damping free long waves than mixed bound and free long waves and bound long waves. The wave height attenuation inside mangroves in these three different wave conditions will be focused on in more detail in the next section of the paper.

4.4.2 Low frequency and high frequency wave attenuation per unit wave length

It is suggested that examining wave attenuation through a relative length scale, i.e. per unit wave length instead of an absolute length scale, e.g. per meter length of mangrove forest, provides a better understanding of the influence of the wave characteristics on the wave attenuation processes (Phan et al., 2018). Therefore, in this section, wave attenuation inside mangroves is presented in terms of the the number of wave lengths for low frequency and high frequency waves.

Figure 4.12 illustrates the relationship between the normalized wave energy of high frequency waves (circle markers) and low frequency waves (triangle markers) for wave type 1 and the dimensionless number of wave length (x/L) for different wave periods, *i.e.* $T_p = 2$ s (orange markers), $T_p = 2.5$ s (purple markers), $T_p = 3$ s (green markers) and different wave heights at the wave paddle, *i.e.* $H_s = 3$ cm (panel A), $H_s = 5$ cm(panel B),

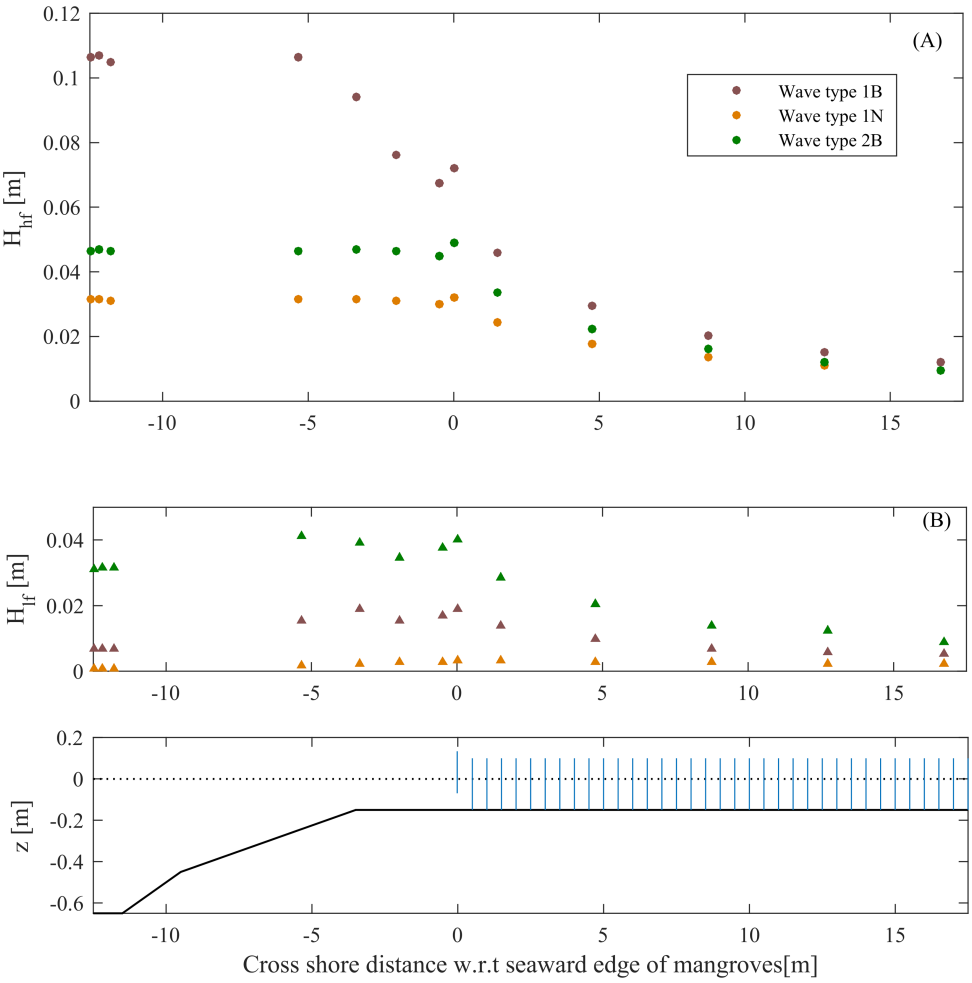

Figure 4.11: High frequency wave height (circle markers) and low frequency wave height (triangle markers) transformation in cases of dense mangroves for wave type 1B (purple markers), wave type 2B (green markers), wave type 1N (orange markers).

$H_s = 7$ cm(panel C) and $H_s = 10$ cm (panel D). In which, x is the measured location and L is the wave length determined based on the peak frequency. The normalized wave energy E is calculated according to: $E = E_x/E_o$; In which, E_x is the energy at the location x inside the mangrove forest and E_0 is the energy at the seaward edge of the forest ($x = 0$ m). In cases of wave type 1N (panel C and D), significant wave height at the wave paddle (H_s) is 3 and 5 cm, due to the shoaling process the significant wave height at the mangrove edge (H_{t0}) ranges from about 2.5 – 2.7 cm and 4.1 –4.2 cm due to wave period differences.

In this figure, it can be clearly seen that both low and high frequency waves damp most effectively over the first wave length (from $x/L = 0$ to $x/L = 1$). Long wave energy

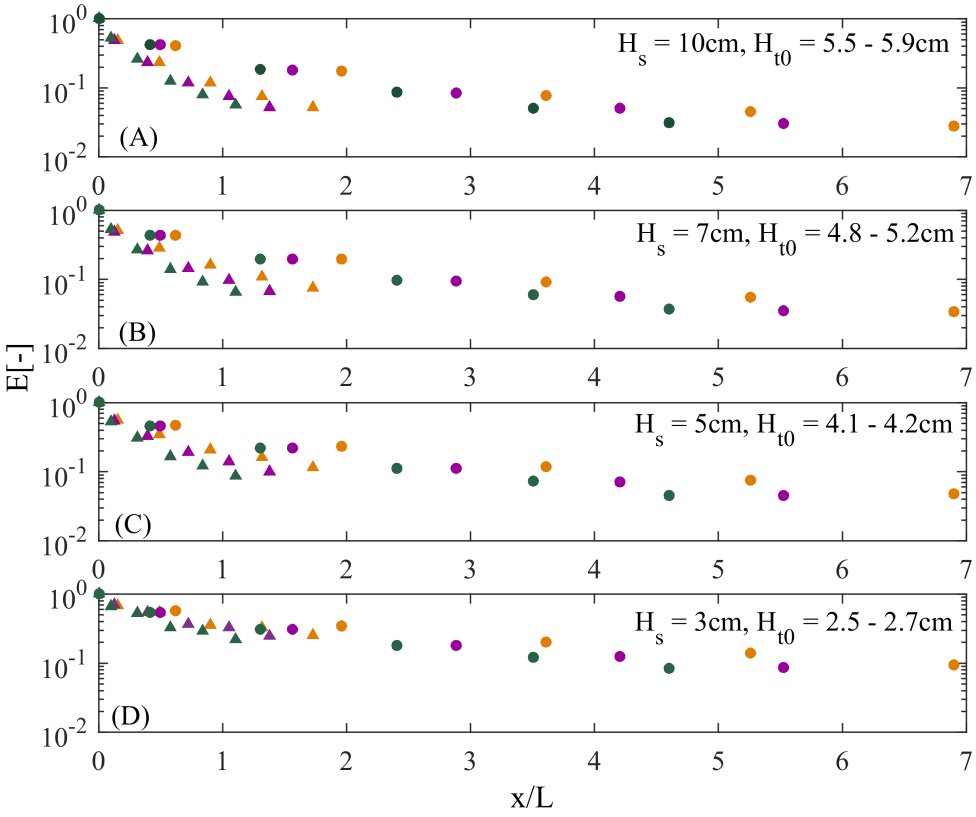

Figure 4.12: Normalized high frequency wave energy (circle markers) and low frequency wave energy (triangle markers) attenuation with respect to the dimensionless parameter x/L in case of dense mangroves for different wave height of wave type 1: panel A (Hs at the wave maker is 3cm, Hto at the edge of the mangroves range from 2.5 to 2.7cm), panel B(Hs at the wave maker is 5cm, Hto at the edge of the mangroves range from 4.1 to 4.2 cm), panel C (Hs at the wave maker is 7cm, Hto at the edge of the mangroves range from 4.8 to 5.2cm), panel D (Hs at the wave maker is 10cm, Hto at the edge of the mangroves range from 5.5 to 5.9 cm) and different wave period: Tp =2.0 s (orange markers), Tp=2.5s (purple markers), Tp=3.0s(green markers).

damps faster than short wave energy, especially in cases of wave type 1B. For example, after one wave length ($x/L = 1$), high frequency energy damped about 80% while low frequency energy damped about 90% in case of wave heights at the edge of the mangroves in the range 5.5 – 5.9 cm (panel A). The results suggest that the higher the waves the faster the damping. This finding is also true for both long and short waves. For example after one wave length, there is only about 70% of long waves damped in cases when the wave height at the mangrove edge are in the range 2.5 – 2.7 cm. However, when the wave heights at the mangrove edge are 5.5 – 5.9 cm, more than 90% of long waves damped. Furthermore, the results also suggest that mangroves are more effective in damping a mix of bound and free long waves (panel A and B) than in damping only bound long waves (panel C and D). It is also noted that in all conditions tested, the higher the wave period, the faster the wave damping.

In order to examine the influence of mangroves on the attenuation processes of free long waves, similar results between the normalized energy and dimensionless length (x/L) were also plotted in cases of wave type 2 (Figure 4.13). It can be seen that in cases when free long waves are predominant inside the mangroves, the higher the waves, the faster the wave damping. For example, in cases of 5.2 cm wave height at the edge of the mangroves (blue triangles), after one wave length there was only about 4% of wave energy is left. In cases when the wave height at the mangrove edge is 1.7 cm (black triangles), more than 10% of wave energy was left.

Furthermore, in cases when the wave heights at the mangrove edge are similar, for example H_{t0} = 5.2 cm (triangle purples, panel A, Figure 4.12) and 5.8 cm (blue triangles, Figure 4.13), about 8% of long wave energy was left after one wave length in cases of the mixed of bound and free long waves (triangle purples, panel A, Figure 4.12), while only about 4% of energy was left in cases of the predominant free long waves (blue triangles, Figure 4.13). This means that the free long waves appear to damp faster than the mixed bound and free long waves.

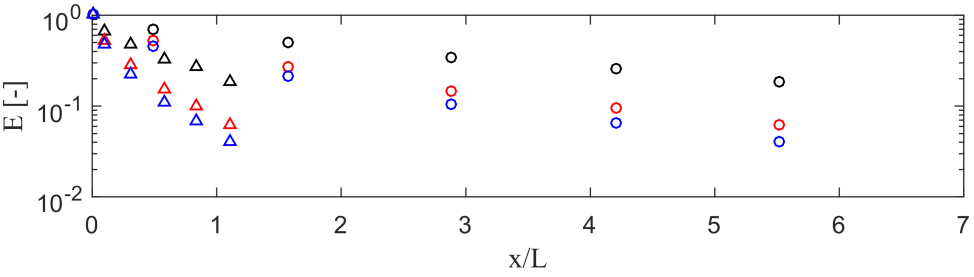

Figure 4.13: Normalized high frequency wave energy (circle markers) and low frequency wave energy (triangle markers) attenuation with respect to the dimensionless parameter x/L in case of dense mangroves for different wave height of wave type 2: Hs at the wave maker is 2cm, Hto at the edge of the mangroves is 1.7 cm (black markers), Hs at the wave maker is 4cm, Hto at the edge of the mangroves is 3.8 cm (red markers) and Hs at the wave maker is 6cm, Hto at the edge of the mangroves is 5.2 cm (blue markers). Short wave period is 2.5s and long wave period is 12.5s.

In conclusion, it can be seen that the attenuation of both long and short waves inside the mangroves are affected by wave heights and wave periods. The larger the wave height and the wave period, the faster the wave damping is. This is true for both cases of long and short waves. Furthermore, the type of long waves also has influence on the long wave attenuation inside the mangroves. The results show that free long waves seem to damp faster than a mixed of bound and free long wave or bound long waves. And the mixed bound and free long waves appear to damp faster than bound long waves.

4.4.3 Effect of wave non-linearity on low frequency and high frequency wave attenuation by mangroves

Phan et al. (2018) examined the influence of wave non-linearity on the total wave height attenuation inside the mangrove forest using the Ursell number. As shown in previous sections, it is suggested that the attenuation of both long and short waves inside mangroves is affected by the wave characteristics, *i.e.* wave heights and wave periods. This

suggests that the Ursell number can also be applied to illustrate the influences of the wave characteristics on the damping processes for both long and short waves.

Figure 4.14 shows the relationship between the Ursell number and normalized wave energy after the first wave length (E_{1L}) for both long (triangle markers) and short waves (circle markers). The normalized wave energy after the first wave length was calculated based on: $E_{1L} = E_1 / E_0$. In which E_1 is the wave energy after one wave length inside mangroves and E_0 is the energy at the edge of the mangroves. It can be seen that when the

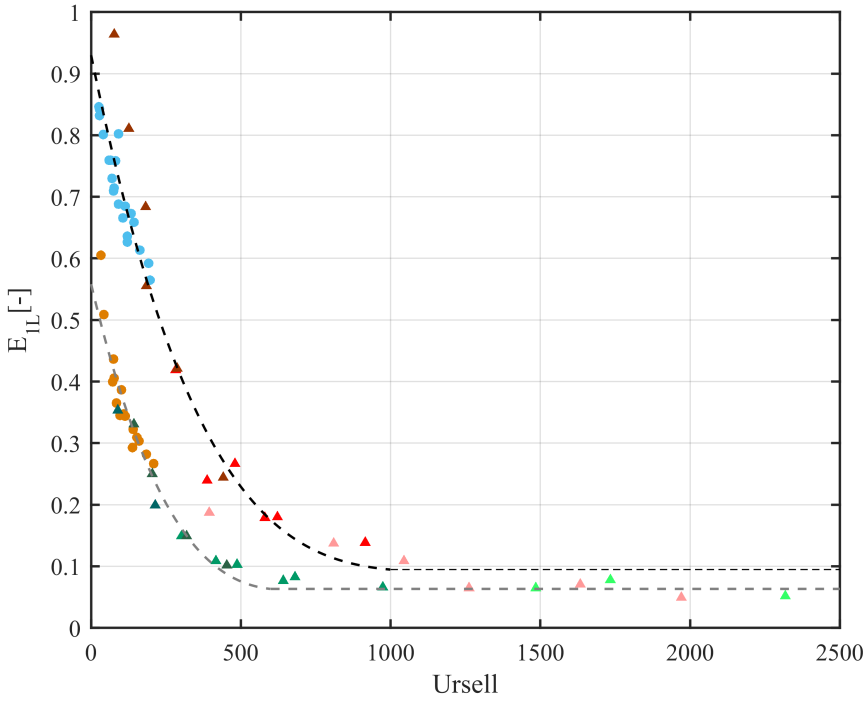

Figure 4.14: Relationship between normalized wave energy after the first wave length E_{1L} and Ursell number for high frequency waves (blue circle markers in case of sparse mangroves and orange circles markers in case of dense mangroves) and low frequency waves (different intensity red triangle markers for sparse mangroves density and different intensity green triangle markers for dense mangroves). The intensity of the colour range from darkest to lightest represent for bound long wave, mixed of bound and free long wave and free long wave. The trend lines for the sparse density cases (black dash line) and for dense density cases (grey dash line) are fourth order polynomial lines.

Ursell number is smaller than 1000, the normalized wave energy of both low and hight frequency waves reduce significantly when the Ursell number increases. This means that the non-linearity of the waves appear to have the same effects on the attenuation of the low and high frequency waves as for that of total wave height. However, when the Ursell number is larger than 1000, the results suggested that the normalized wave energy no longer depends on the wave non-linearity.

Additionally, in cases of sparse mangroves, if the Ursell number is smaller than 200, the attenuation rate of long waves (darkest-red triangles) is different with that of short waves (blue circles). However, in cases of dense mangroves, there is no difference between the attenuation rate of long and short waves (darkest-green triangles and orange circles, respectively). This means that mangrove density plays a significant role, especially when Ursell number is smaller than 200. Furthermore, when Ursell number is increased ($200 < Ursell < 1000$), the normalized wave energy is reduced by about 15% for low frequency waves by increasing the mangrove densities from 200 to 400 sticks/m2. However, when Ursell is increased ($500 < Ursell < 1000$), it can be seen that the influences of mangrove density on the wave energy dissipation E appear to be weaker. When Ursell is larger than 1000, the results in cases of two different densities are merged indicating that low frequency wave energy dissipation is independent of the mangrove density.

Figure 4.14 includes three types of long waves, i.e. the predominant bound long waves, predominant free long waves and the mixed bound and free long waves. These different types of long waves are represented with different colour intensity ranging from dark to light red in cases of sparse mangrove density and from dark to light green in cases of dense mangrove density. The result suggests that while wave with predominant bound long waves and mixed bound and free long waves are significantly affected by the wave non-linearity and mangroves density, wave with predominant free long waves are less dependent of these two factors.

In general, although the wave conditions in front of the mangroves are different in types, *i.e.* broken and non-broken wave, predominant bound long waves, mixed bound and free long waves and predominant free long waves, the wave energy dissipation for both low and high frequency waves is increased together with increasing Ursell number. In this context, wave non-linearity is a main factor controlling the wave attenuation process inside mangroves of short waves and long waves, especially when the Ursell number is smaller than 1000.

4.5 Conclusions

This study investigates the attenuation of three main types of infragravity waves through mangrove forests using a large data set obtained in a unique laboratory experiment. The results are examined in terms of the cross-correlation functions, the wave energy dissipation per number of wave lengths and the Ursell number. The cross-correlation function reveals the mechanisms in which different types of long waves are created, propagated and penetrated into the mangrove forest. The attenuation rate of wave height presented according to the number of wave lengths reveals the dependence of the low frequency wave attenuation through mangroves on the length of waves. Finally, the Ursell number shows the influence of wave non-linearity on the damping processes of low frequency waves.

Specifically, using cross-correlation allows to confirm and clarify the generation of long waves in the flume. While the long waves develop with the short wave group allows to create bound long waves, free long waves can be generated by adding additional long wave energy together with the short wave group at the wave paddle. The mixed

bound and free long waves can be reproduced by forcing part of bound long waves to break. Furthermore, comparing the auto-correlation of long waves, short waves and the cross-correlation between them in cases with and without mangroves confirms the effect of mangroves on the absorption of the low frequency wave energy. In cases with dense mangroves, the reflection of low frequency waves, that can clearly observed in cases without mangroves, can not be observed. In other words, most of the reflected long waves were absorbed by the mangroves.

By presenting the low frequency wave energy dissipation according to the number of wave length, it is suggested that both high and low frequency waves damp significantly over the first wave length. Furthermore, the wave height attenuation determined according to an absolute length scale (*i.e.* per meter of mangrove width) suggested that the long waves can penetrate further inside mangrove forest than short waves. This can actually be interpreted by determining the wave height attenuation according to a relative length scale, *i.e.* the number of wave length, in which the attenuation rate of the wave depends on its length. This means that longer waves require further distance depending on their corresponding lengths to damp to the same attenuation rate achieved by short waves. Actually, in this study, for conditions tested, it is shown that the damping rate per wave length of the long waves is even larger than that of short waves. In other words, long waves appear to penetrate further inside the mangrove than short waves, but their attenuation rate per wave length is larger than that of short waves. The results also suggest that the damping rate of the free long waves is largest, larger than that of the mixed bound and free long waves, and bound long waves have the smallest damping rate. Additionally, it is also shown that the higher the waves or the larger the wave period, the faster the wave damping. This means that the attenuation of low frequency waves appears to depend on the wave non-linearity which can be illustrated using the Ursell number.

Studying the relationship between the Ursell number and the rate of wave attenuation shows that if the Ursell number is smaller than 1000, the rate of short and long wave attenuation strongly depends on the wave non-linearity. Furthermore, it is shown that if the Ursell number is smaller than 500, the mangrove density has a strong influence on the wave attenuation. Moreover, for conditions tested, it is shown that bound long waves and mixed bound and free long waves strongly depend on the wave non-linearity, while free long waves are less dependent on this factor. Finally, the results suggest that the larger the Ursell number, the larger the wave height dissipation. This means that the most dominant factor controlling the dissipation rate of the wave height of low frequency waves inside the mangrove forest is the wave non-linearity as expressed by the Ursell number.

References

Agnon, Y. (1993). On a uniformly valid model for surface wave interaction. *Journal of Fluid Mechanics*, 247:589–601.

Augustin, L. N., Irish, J. L., and Lynett, P. (2009). Laboratory and numerical studies of wave damping by emergent and near-emergent wetland vegetation. *Coastal Engineering*, 56(3):332–340.

Baldock, T. and Huntley, D. (2002). Long–wave forcing by the breaking of random gravity waves on a beach. In *Proceedings of the Royal Society of London A: Mathematical, Physical and Engineering Sciences*, volume 458, pages 2177–2201. The Royal Society.

Battjes, J. A., Bakkenes, H. J., Janssen, T. T., and Van Dongeren, A. R. (2004). Shoaling of subharmonic gravity waves. *Journal of Geophysical Research: Oceans*, 109(C2).

Bendat, J. and Piersol, A. (2011). *Random Data: Analysis and Measurement Procedures*. Wiley Series in Probability and Statistics. Wiley.

Brinkman, R. M. (2006). *Wave attenuation in mangrove forests: an investigation through field and theoretical studies*. PhD thesis, James Cook University.

Guza, R., Thornton, E., and Holman, R. (1985). Swash on steep and shallow beaches. In *Coastal Engineering 1984*, pages 708–723.

Hamm, L., Madsen, P. A., and Peregrine, D. H. (1993). Wave transformation in the nearshore zone: a review. *Coastal Engineering*, 21(1-3):5–39.

Janssen, T., Battjes, J., and Van Dongeren, A. (2003). Long waves induced by short-wave groups over a sloping bottom. *Journal of Geophysical Research: Oceans*, 108(C8).

List, J. H. (1991). Wave groupiness variations in the nearshore. *Coastal Engineering*, 15(5-6):475–496.

Longuet-Higgins, M. S. and Stewart, R. (1964). Radiation stresses in water waves; a physical discussion, with applications. In *Deep Sea Research and Oceanographic Abstracts*, volume 11, pages 529–562. Elsevier.

Massel, S. (2006). Experiments on wave motion and suspended sediment concentration at nang hai, can gio mangrove forest, southern vietnam. *Oceanologia*, 48(1).

Mazda, Y., Magi, M., Ikeda, Y., Kurokawa, T., and Asano, T. (2006). Wave reduction in a mangrove forest dominated by sonneratia sp. *Wetlands Ecology and Management*, 14(4):365–378.

Mork, M. (1996). Wave attenuation due to bottom vegetation. In *Waves and nonlinear processes in hydrodynamics*, pages 371–382. Springer.

Phan, L. K., Stive, M. J. F., Zijlema, M., Truong, H. S., and Aarninkhof, S. G. J. (2018). The effects of wave non-linearity on wave attenuuation by vegetation. *Coastal Engineering, under review*.

Phan, L. K., van Thiel de Vries, J. S., and Stive, M. J. F. (2014). Coastal mangrove squeeze in the Mekong Delta. *Journal of coastal Research*, 31(2):233–243.

Quartel, S., Kroon, A., Augustinus, P., Van Santen, P., and Tri, N. (2007). Wave attenuation in coastal mangroves in the red river delta, vietnam. *Journal of Asian Earth Sciences*, 29(4):576–584.

Schäffer, H. A. (1993). Infragravity waves induced by short-wave groups. *Journal of Fluid Mechanics*, 247:551–588.

Symonds, G., Huntley, D. A., and Bowen, A. J. (1982). Two-dimensional surf beat: Long wave generation by a time-varying breakpoint. *Journal of Geophysical Research: Oceans*, 87(C1):492–498.

Truong, S. H., Ye, Q., and Stive, M. J. F. (2017). Estuarine mangrove squeeze in the Mekong Delta, Vietnam. *Journal of Coastal Research*, pages 747–763.

Chapter 5

A Numerical study of coastal mangrove squeeze in the Mekong Delta

Linh PHAN KHANH

All life is an experiment;
The more experiments you make the better.

Ralph Waldo Emerson

In this chapter, the attenuation processes of both low and high frequency waves was numerically investigated regarding different slopes inside and in front of a mangrove forest. Furthermore, the effects of human intervention on this attenuation process was investigated in terms of different mangrove widths associated with different slopes or locations of sea dikes. The results suggest that the variation of the slope inside or in front of a mangrove forest associated with the topography profile of the mangrove forest or the location of sea dikes may significantly influence the wave attenuation processes. On the one hand, the steeper the slope inside the mangrove forest, the larger the wave height propagating toward the mangroves and the faster the normalized wave energy is dissipated per number of wave lengths inside the mangrove forest. On the other hand, the steeper the slopes in front of the mangrove forest, the larger wave heights in front of mangroves and the slower wave height energy absorption inside the mangrove forest.

This chapter is in preparation for submission to Journal of Coastal Research.

5.1 Introduction

Mangroves dominating the inter tidal area between the Mean Sea water Level (MSL) and the Mean High water Level(MHL) are an important tool to absorb the propagating waves and currents (Alongi, 2008; Duke and Schmitt, 2016). In normal conditions, the complex roots, stems and canopies of mangroves can effectively absorb a large amount of energy of incoming waves and flows. Consequently, waves and flows are smaller, increasing thereby the window of opportunity for sediments and nutrients to be exchanged and deposited in and around the vegetation patch. Furthermore, the presence of mangroves is also strengthening the soil (Chapman, 1976; Hong and San, 1993; Kathiresan, 2003). As a result, the stability of the shorelines is significantly increased.

Numerous publications in this field have attempted to clarify the role of vegetation in general, and mangroves in particular, in the protection of shorelines (Adrian and Marusic, 2012; Alongi, 2002; Anthony and Gratiot, 2012; Bao, 2011; Brinkman, 2006; Brinkman et al., 1997; Christensen et al., 2008; Gilman et al., 2007; Nikora Vladimir, 2009).The attenuation of waves through vegetation has been among one of the issues of most concern, as waves are the main hydrodynamic force to which the coastal mangrove forests are primarily exposed (Truong et al., 2017). The studies conducted at the laboratory (Augustin et al., 2009), or in the field (Aucan and Ridd, 2000; Furukawa et al., 1997; Horstman et al., 2014; Mazda et al., 1995; Wolanski et al., 1990), combining various numerical tools (Augustin et al., 2009; Phan et al., 2015; Truong et al., 2017) have confirmed the crucial role of mangroves in damping the waves and protecting the coastal area from erosion.

However, in the Mekong Delta the mangroves are usually squeezed between sea dikes or fish farms and a sea with an increasingly threatening water level rise. Over the last three decades a large part of the mangrove forests in the Mekong area have been destroyed and converted into fish farms (Truong et al., 2017). The river banks and coastal shorelines at the locations where the mangroves were degraded are suffering from a strong erosion of up to 100 $\mathrm{m\,yr^{-1}}$ (Phan et al., 2015). It is found that river banks and coastal areas where the mangroves are healthy and cover a wide area are frequently less erosive than the regions where only a narrow strip of mangroves are left (Phan et al., 2015; Truong et al., 2017). It is observed that most research in the literature focused on the subject of a wide mangrove forest and whether or not and to what extent the defensive role of mangroves can be influenced by changes in boundary conditions, such as a restricted width of the mangrove forest, is unknown.

Furthermore, most published studies have not yet considered the impact of a slope variation inside the forests. In reality, in the condition where there are no sea dikes and no human interventions landward of the mangrove forest, as for example in the Mekong Delta Coast, the width of mangroves can be up to 1500 m and the slope inside the mangroves can range of about 1/500 to about 1/1000 in front of the mangroves strip, and up to a hundred meters a slope is about 1/150 and further offshore, a slope of about 1/1200 was usually observed (Phan et al., 2015). However, in eroded scenarios the slope inside the mangrove forest can be much steeper. For example, the slope inside the mangrove forest in Ganh Hao, Bac Lieu, is about 1/200 (SIWRR, 2010). In this area, only a narrow strip of about 100 m of mangroves was left and the erosion rate is up to 50 $\mathrm{m\,yr^{-1}}$. In this context, the variation in the slope inside a mangrove forest appears to be linked to the

morphological and evolutionary conditions (i.e. the shoreline changes) of mangroves.

Therefore, to understand the changes of the attenuation of both long and short waves through coastal mangroves regarding the variation of mangrove widths associated with the inside and the in front slope of a mangrove forest, the research focused on the “squeeze condition”. The Swash model was validated for the first time with long waves using the experimental data of wave penetration (Phan et al., 2018). The transformation and attenuation of waves in front of and through coastal mangroves at a real scale of the Mekong delta coast was analysed in terms of the “squeeze condition", in which changes of the mangrove width caused by the sea-dike construction were varied in terms of the inside slope.

5.2 Methodology

A schematised model of coastal mangroves in the Mekong Delta was constructed in the SWAN and SWASH model. SWAN is a third-generation spectral wave model that is usually used to calculate wave parameters in coastal regions, estuaries and lake from given wind, bottom and current boundary conditions. Swan is based on the wave action balance equation with sources and sinks. It was developed By Delft University of Technology and was supported by Office of Naval Research (USA) and nowadays partly by Rijkswaterstaat. In the current study, the wave generated by wind, white capping, bottom friction, depth-induced breaking and the dissipation of waves caused by vegetation are the main physics introduced in the Swan model.

Coastal mangroves are considered to dominate the region between the MSL (1.95 m) and MHL (3 m). Three different slopes inside mangroves, which are 1/200, 1/600 and 1/1000, were considered. The corresponding widths of the mangrove forest in these scenarios are 300 m, 900 m and 1500 m.In front of the mangroves, the slope is kept at 1/1200.

It can be noticed that right at the sea edge of the mangroves, long waves have an equal, or an even higher, amount of energy than short waves (Phan et al., 2015). However, as low frequency waves cannot be produced in the SWAN model, a combination of the SWAN and SWASH models is necessary to assess the attenuation of low frequency waves through the mangroves. While the SWAN model is used to provide the wave transformation from offshore to nearshore, the wave energy calculated from SWAN can then be used as an input boundary for the SWASH model to calculate the wave transformation up to the end of the mangrove forest.

In the current study, SWAN will be run in stationary mode. Furthermore, only one cross-section perpendicular to the coastline will be considered. This means that only one dimension (1D) model in SWAN will be studied. It is noticed that due to a very gentle slope of the Mekong Coast (1/1000), the growth of waves induced by wind cannot be neglected. Thus, a constant wind is introduced in SWAN. The direction of the wind is always onshore, and the strength of the wind was estimated based on wave forecasting nomograms. Furthermore, a standard JONSWAP-shape wave spectrum including a peak period and wave height and wave height as a function of the return period is introduced at the offshore wave boundary. This wave spectrum is determined based on the wave data collection at Bach Ho station (Phan et al., 2015). The direction of waves is

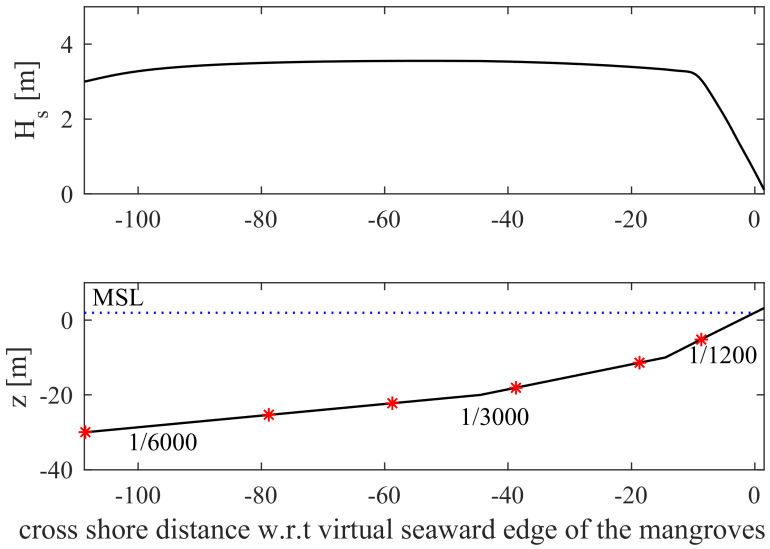

Figure 5.1: SWAN numerical results. Upper panel: Significant wave height transformation from offshore to nearshore in case of no mangroves. Lower panel: Cross shore profile and chosen location to extract wave spectrum (star markers).

onshore directed and is perpendicular to the coastline boundary. Furthermore, the third generation mode for wind input, white capping (linear growth) and triad wave-wave interactions are activated in SWAN. Moreover, a default value of the friction coefficient of 0.038 is used.

The SWAN and SWASH model were validated and shown to be efficient to produce wave transformations from the offshore to the nearshore region (Zijlema et al., 2011).). The capability of the SWASH model in simulating the wave height transformation with and without mangroves was also verified (Phan et al., 2018). However, the ability of the SWASH model in producing both low and high frequency waves was not yet examined. Therefore, before utilizing SWASH to simulate the long and short wave attenuation through the mangrove forest, the capability of this model was examined using the experimental data of Phan et al. (2018). Results of the SWASH validation in this context are presented in Figure 5.2.

Figure 5.1 illustrates the wave height transformation from the offshore to the near shore region calculated by the SWAN model. It is suggested that the wave height first slightly increases to about 3.6 m at 90 km aand then remains almost stable until 40 km offshore. After that, the wave height reduces to about 3 m at 10 km offshore from the shoreline (location $y = 0$ km). Finally, the wave height significantly reduces toward the shoreline. The variance density spectrum is extrapolated at several points along the cross-section and shown in Figure 5.3. It is suggested that the wave energy slightly reduces up to 20 km toward the near shore region. After that the waves start to break and the wave energy is significantly decreased. In this context, the wave energy at location $y = -20$ km was extracted from the SWAN model and introduced into the SWASH model

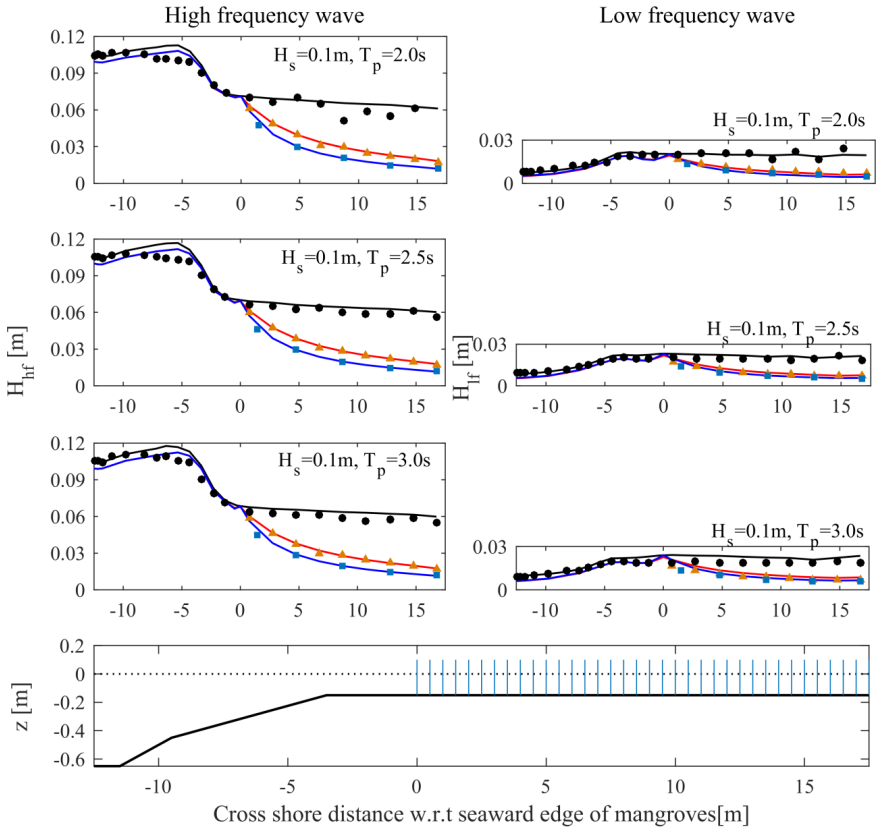

Figure 5.2: Wave height transformation comparisons between physical model: without mangroves (black circles), sparse mangroves (orange triangles), dense mangroves (square blues) and numerical model: without mangroves (black line), sparse mangroves (red line), dense mangroves (blue line) for different wave height conditions. High frequency waves are represented in the left hand side and low frequency waves are represented in the right hand side.

as an input of the seaward boundary condition.

Figure 5.4 illustrates the different sources and sinks of the wave energy determined in SWAN. While the upper panel of the figure shows the evolution of the individual source terms of the wave energy in scenarios without mangroves, the lower panel of the figure shows the corresponding cross-shore profile and chosen locations where the wave spectra were plotted (star markers). It can be clearly seen that the wave energy generated offshore by wind is dissipated due to white capping (location 110 km offshore). From location 110 km to 80 km, there is a decrease in the remaining wave energy as the energy generated by waves remain unchanged and the dissipated wave energy due to white capping increases. This variation in the remaining energy causes a small increase in the variance density (see Figure 5.3).

It is noticed that from location 20 km in front of the edge of the mangroves (the beginning of the surf zone), energy dissipation due to white capping, bottom friction and

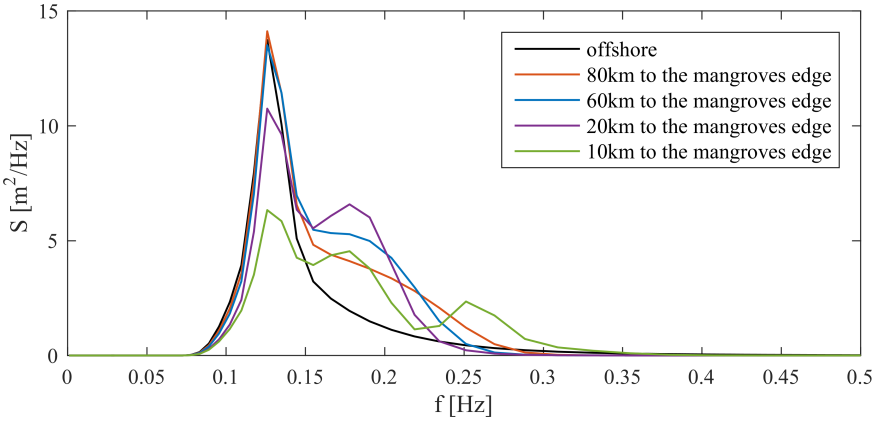

Figure 5.3: Variance density spectrum (S) as a function of frequency at various cross-shore positions.

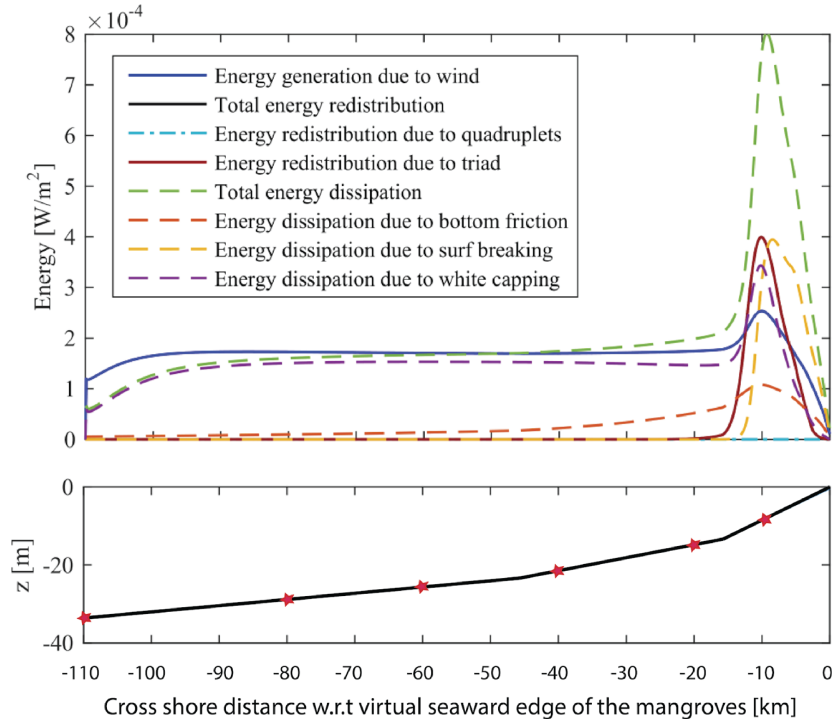

Figure 5.4: Evolution of the individual source terms of the energy balance.

the energy dissipation due to surf breaking increase significantly. As a result, the total energy dissipation exceeds the energy generation due to the wind. Furthermore, at this location (20 km in front of the mangrove edge), the presence of the energy redistribution due to triad interaction causes an energy transfer from low frequency to a higher

frequency. At location 10km in front of the edge of the mangroves (the middle of the surf zone), it can be seen that the total wave energy dissipation is most significant (Figure 5.4) and the variance spectrum is reduced for all ranges of frequencies (see Figure 5.3).

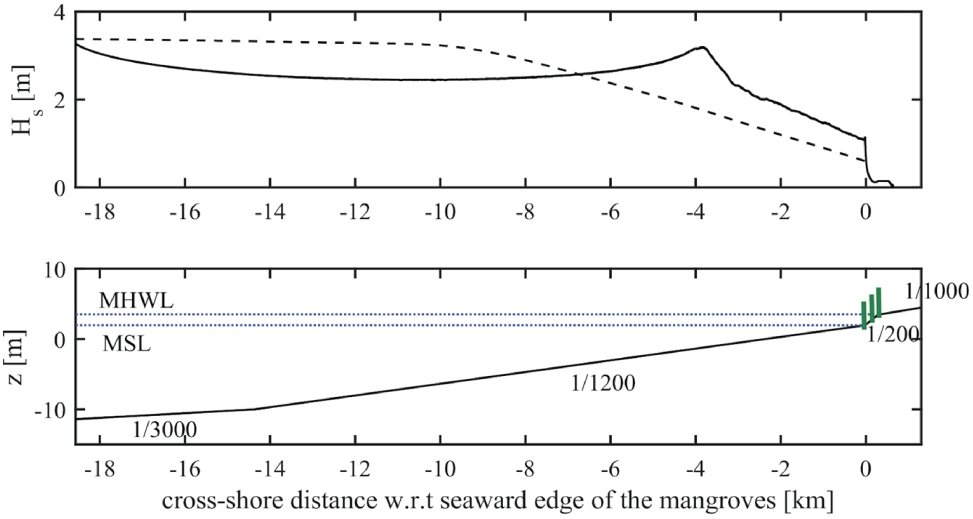

Figure 5.5: SWASH numerical results. Upper panel: Significant wave height transformation near shore from SWAN model (dashed line) and from SWASH model (solid line) in case of mangroves slope is 1/200, average mangroves density. Lower panel: Cross-shore profile.

Figure 5.5 shows the more detailed transformation processes of waves from location $y = -20$ km to $y = 0$ km determined by the SWASH and SWAN model in cases with mangroves and where the slope inside the mangroves is 1/200. It can be clearly seen that there is a large difference in the results of wave height variation between SWAN (dashed line) and SWASH (solid line). While the shoaling and breaking processes can be clearly seen in SWASH, those processes cannot be observed in SWAN, and there is a linear reduction in the wave height in SWAN. For example, it can be seen from the SWASH model that the breaking processes of the waves in this scenario is around $y = -4$ km. Furthermore, the slope of these coastal regions is very gentle. Therefore the shoaling process may occur longer than in coastal regions where the slope is significant. It is noticed that SWAN and SWASH are based on different governing equations. While SWAN is based on the wave action balance equation and is a spectral wave model, SWASH is a non-hydrostatic wave model. Therefore, SWASH is a phase-resolving model and SWAN is a phase-averaged model. In this sense, SWASH calculates a time series of the sea surface, while SWAN calculates the statistics of the sea surface. This means that the performance of SWASH in strongly non-hydrostatic regions such as wave breaking regions is expected to be more reliable than SWAN. Mangroves are assumed to develop in the region from MSL to MHWL, corresponding with the distance from $y = 0$ km to $y = 0.21$ km. The wave height attenuation process through mangroves within this particular area is the main focus of this study.

5.3 Results

5.3.1 Effects of slopes inside mangrove forests on the wave height attenuation

Figure 5.6 illustrates the results of the wave height attenuation through mangroves (upper panel) and the wave set up (middle panel) in scenarios of average density of mangroves with different inside slopes. The results show that changing the slope inside mangroves does not only have an influence on the wave transformation in front of the mangroves (from $x = -0.5$ km to $x = 0$ km), but also on the wave attenuation processes inside the mangroves (from $x = 0$ km to $x = 0.21$ km). It is suggested that the steeper the slope, the higher the wave height at the seaward edge of the mangroves ($x = 0$ km). This is probably due to reflection induced by the presence of mangroves.

Inside the mangrove forest, the wave height is significantly reduced from around 1 m to 0.15 m within the first 200 m of mangroves. After that the wave height appears to remain stable. At the edge of the mangroves and the shoreline (land edge of mangrove forest), where there is no water and the wave cannot propagate further behind this point, the wave heights increase and then strongly reduce toward zero.

Furthermore, in all scenarios it can be clearly seen that the waves set-down due to the mangroves (Figure 5.6B). However, a slight wave set-up can be observed for the steep slope of 1/200 in the first 50 m only. This means that the waves continue to break causing wave set-up. Because of the shallow water depth, the waves start to break again at the end of the forest.

Figure 5.7 illustrates the variation of the totally normalized wave energy attenuation (panel A), the high frequency waves (panel B) and the low frequency waves (panel C) in scenarios of average mangrove density with different mangrove slopes. It is shown that the high frequency waves are damped significantly after only the first 200 m of the mangroves (panel B) of the mangroves (panel B), while low frequency waves can penetrate much further and up to more than 1000 m inside the forest (panel C). Furthermore, these results suggest that for both low frequency and high frequency waves, the steeper the slope, the faster the normalized wave energy is dissipated inside the mangrove forest. This result is in line with that predicted by Phan et al. (2015) based on the XBeach model.

Phan et al. (2018) suggested that the attenuation of waves through mangroves should also be examined in terms of a relative length, *i.e.* the number of the wave length, instead of an absolute length, *i.e.* the length of mangrove forest. Figure 5.8 illustrates the wave attenuation of high and low frequency waves through mangroves regarding the normalized wave energy and the number of wave length. It can be clearly seen that low frequency waves dampen faster than high frequency waves in the first haft wave length.

Furthermore, the result suggests that for all scenarios with three different slopes, while the normalize energy of high frequency waves is strongly reduced to about 1% after the first wave length, the normalized energy of low frequency waves continues to dissipate to 1% after one and a halve wave length. As far as the practice of engineering is concerned, the bathymetry profile inside mangroves appears to associate with the concave, convex and straight configuration (Figure 5.9c). In reality, the concave scenarios seem

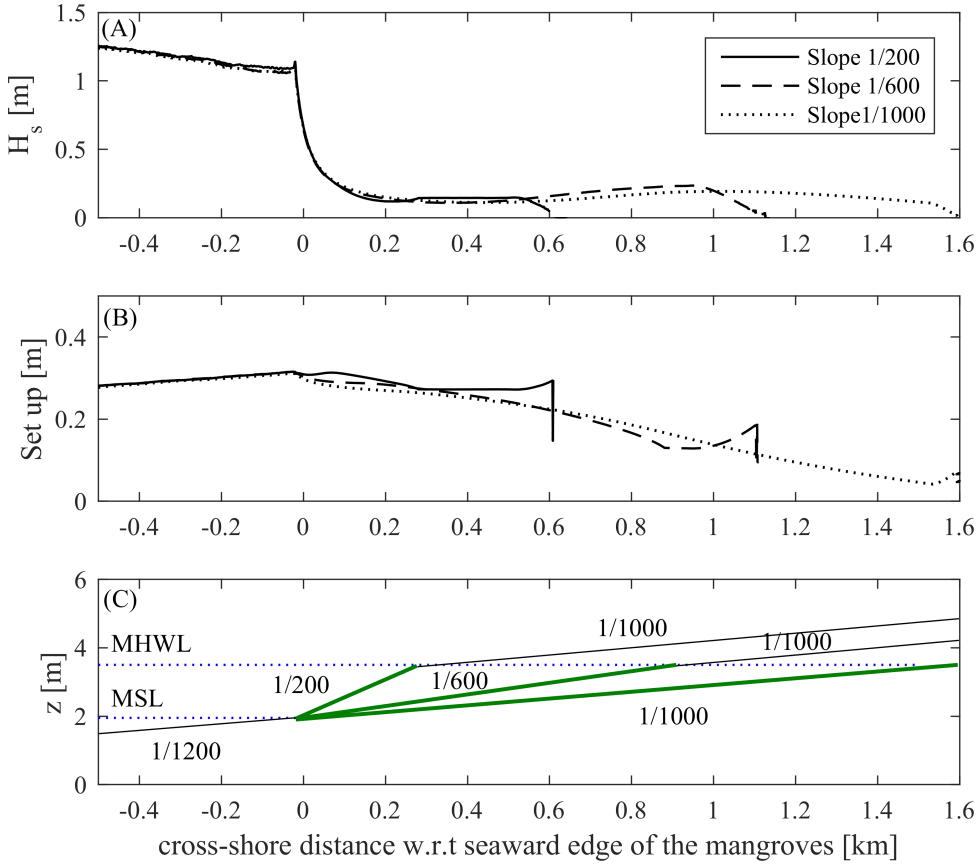

Figure 5.6: Comparisons between significant wave height (panel A) and wave set up (panel B) in case of mangroves slope 1/200 (solid line), mangroves slope 1/600 (dash line), mangroves slope 1/1000 (dot line), average mangroves density. Panel C: Cross-shore profile for each scenarios, mangroves forest is presented by the green line.

to associate with the sedimentation cases and the convex scenarios seem to associate with the most eroded cases. The wave height transformation and attenuation through the mangroves in these different practical situations are illustrated in Figure 5.9a,b, and the corresponding normalized wave energy variations, for both long and short waves, are shown in Figure 5.10a,b. It is found that, although the difference in the wave height attenuation though the mangroves is small, the wave set-up for the concave profile significantly decreases inside the vegetation compared to other scenarios. From a physical perspective, this means that there is a decrease in the local elevation in the mean water level inside mangroves, which is not caused by the reduction in wave height but by the decrease in the water depth induced by the concave profile. A smaller wave set-up means that the local circulation is also smaller. Therefore, for concave profile scenarios more sediments and nutrients may be deposited than for convex profiles, where wave set-up remains unchanged throughout the mangroves (see Figure 5.9).

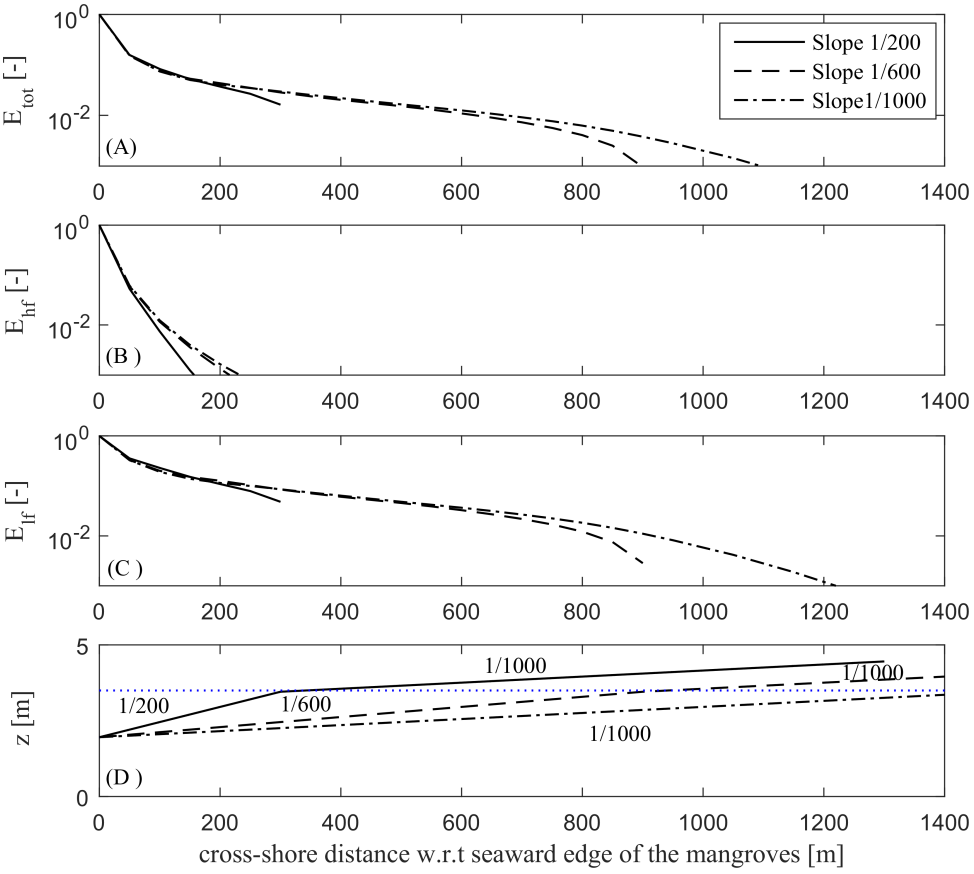

Figure 5.7: Comparison of total (panel A), high frequency (panel B) and low frequency (panel C) normalized wave energy attenuation in case of average mangroves density for different mangroves slopes: slope 1/200 (solid line), slope 1/600 (dash line) and slope 1/1000 (dash-dot line). Cross-shore profile with different mangroves slopes are presented in panel D.

Figure 5.10 shows the total, high and low frequency waves attenuation through mangroves in terms of the wave energy and the length of the mangrove forest. It is found that that for all scenarios, high frequency waves dampen faster than low frequency waves. Furthermore, it is suggested that the wave energy (total waves, high and low frequency waves) reduces fastest for a concave profile scenario and slowest in convex profile scenarios. This demonstrates that a concave profile appears to provide a better natural growing condition regarding energy absorption and sedimentation for a mangrove forest.

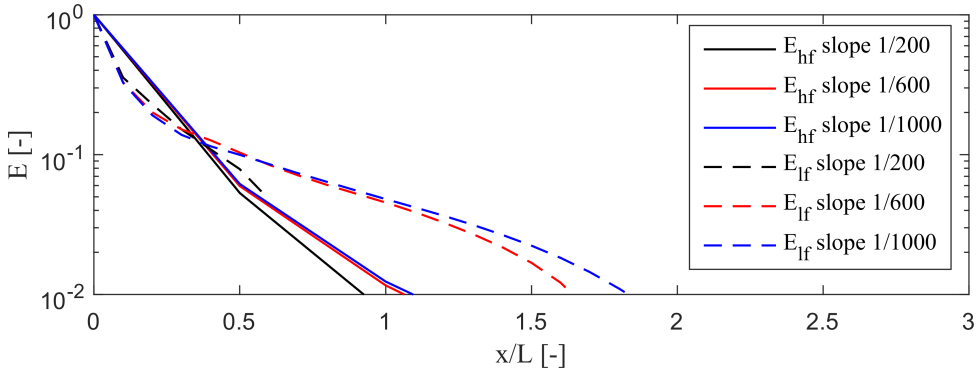

Figure 5.8: Normalized high frequency (solid line) and low frequency (dash line) in case of average mangroves density and different mangroves slope : slope 1/200 (black), slope 1/600 (red) and slope 1/1000 (blue) with respect to the ratio between distance from the seaward edge of the mangroves to the measurement point and the wave length.

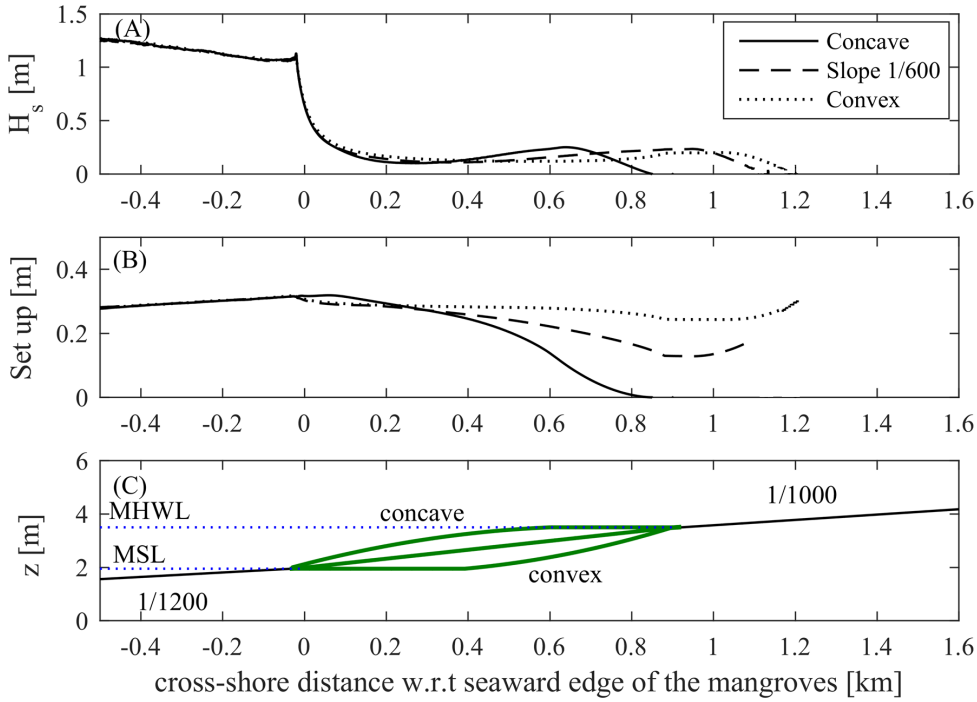

Figure 5.9: Comparisons between significant wave height (panel A) and wave set up (panel B) in case of concave profile, convex profile, and straight profile of the topography inside the mangrove forest. Mangroves forest is presented by the green line.

5.3.2 Effects of slopes in front of mangroves on wave height attenuation due to mangroves

When a mangrove forest has been degraded, the shoreline is usually eroded Phan et al. (2015); Truong et al. (2017). Mangroves at the water edge appear to be eroded first and

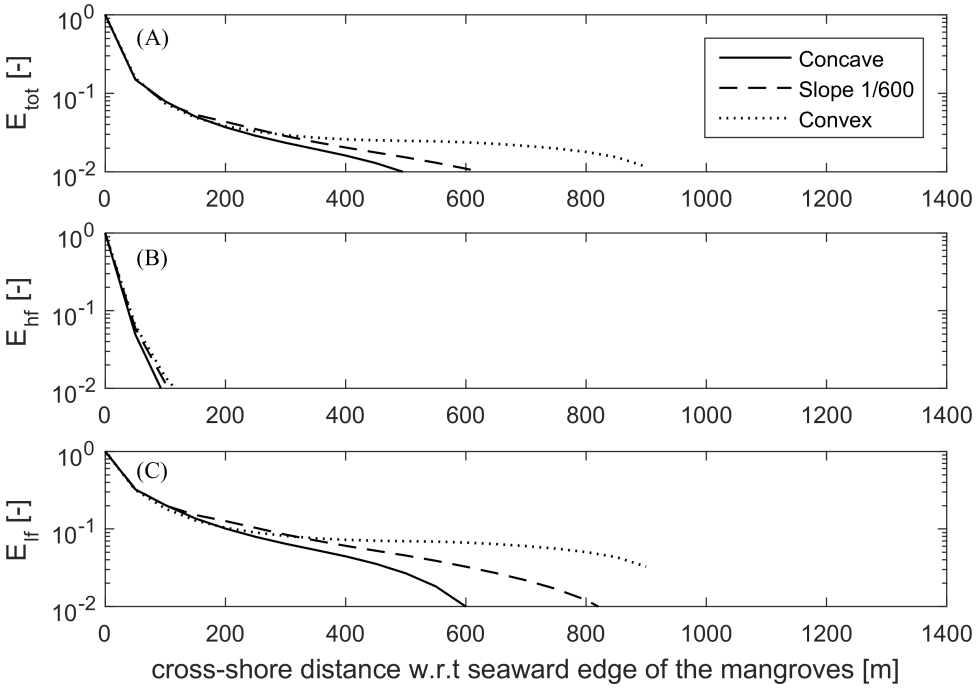

Figure 5.10: Normalize high frequency (solid line) and low frequency (dash line) in case of average mangroves density and different mangroves topography : concave (black), convex (red) and straight (blue) with respect to the ratio between distance from the seaward edge of the mangroves to the measurement point and the wave length.

the slope in front of the mangrove forest may increase significantly. In this chapter, this specific erosion scenario was for the first time considered by changing the slope in front of a degraded mangrove forest from 1/1200 to 1/200. The results of wave height transformation in this condition was shown in Figure 5.11 and Figure 5.12.

The results suggest that the difference of the wave height attenuation inside the mangroves is small in these two conditions. However, it is shown that the presence of a slope of 1/200 in front of mangroves causes a significant change of the incoming wave height, resulting in a larger wave heights in front of the mangrove forest. Additionally, due to the presence of the 1/200 slope there is an increase of wave set-up at around 250 m in front of the mangrove's edge. These conditions appear to be unfavourable for the stability of mangroves at the edge of mangrove-water interface. It is also suggested there is a wave set-down instead of a wave set-up inside the mangrove forest.

Furthermore, it is found that the wave height energy inside the mangrove forest in a normal scenario (slope 1/1200, solid line) dampens much more faster compared to that in eroded scenarios (slope 1/200, dashed line) (see Figure 5.12). This demonstrates that changing the slope in front of the mangrove forest (from 1/1200 to 1/200) can significantly influence the wave height energy absorption (both total, high and low frequency waves) inside the mangrove forest.

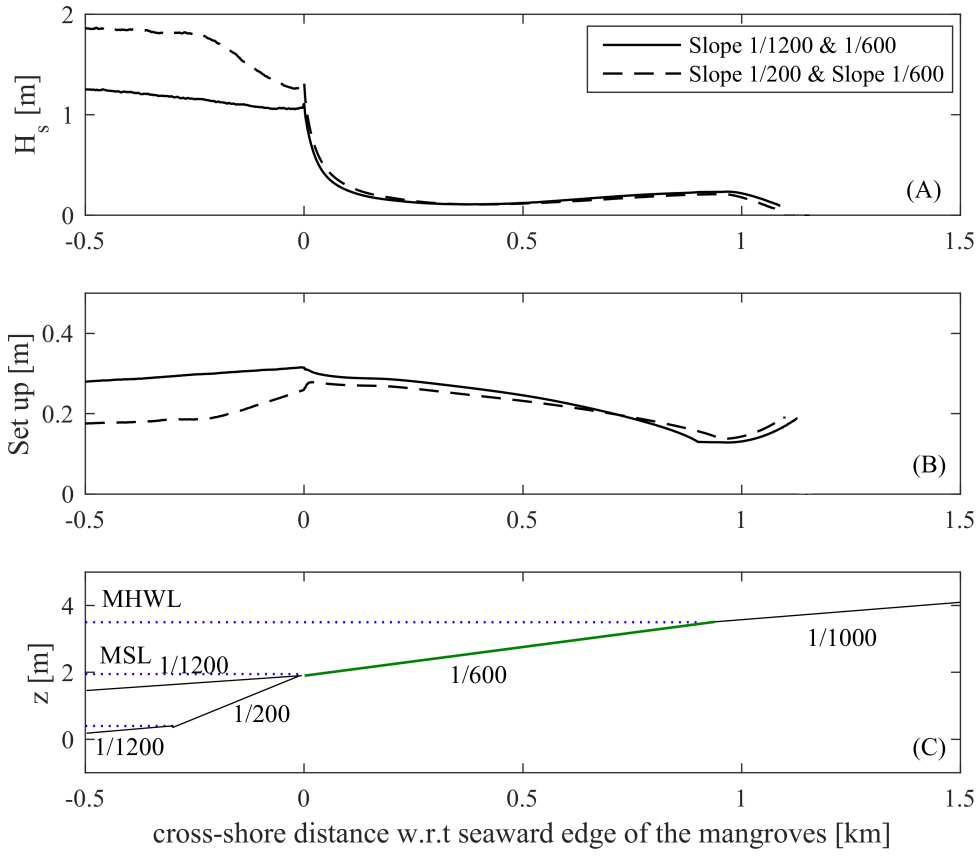

Figure 5.11: Upper panel: Comparisons between significant wave height (panel A) and wave set up (panel B) in case of slope in front of the mangroves is 1/200 (solid line), and slope in front of the mangroves is 1/1200 (dash line), average mangroves density, slope inside mangroves keep at 1/600. Lower panel: Cross-shore profile for each scenarios. Mangroves forest is represented by the green line.

5.3.3 Effects of sea dike locations/mangrove width on the wave height attenuation

Finally, the influence of sea dike locations on the wave conditions in front of and inside the mangrove forest was examined (see Figure 5.13). It is found that although the wave height conditions in front of the mangrove forest remain almost the same when the mangrove width is restricted, the difference in the wave height attenuation is mostly significant after 50 m inside the mangrove forest. This means that, if the sea-dikes were extended, the more vulnerable mangrove species dominating the landward area near the sea-dikes appear to be the ones most influenced by changes in the wave conditions.

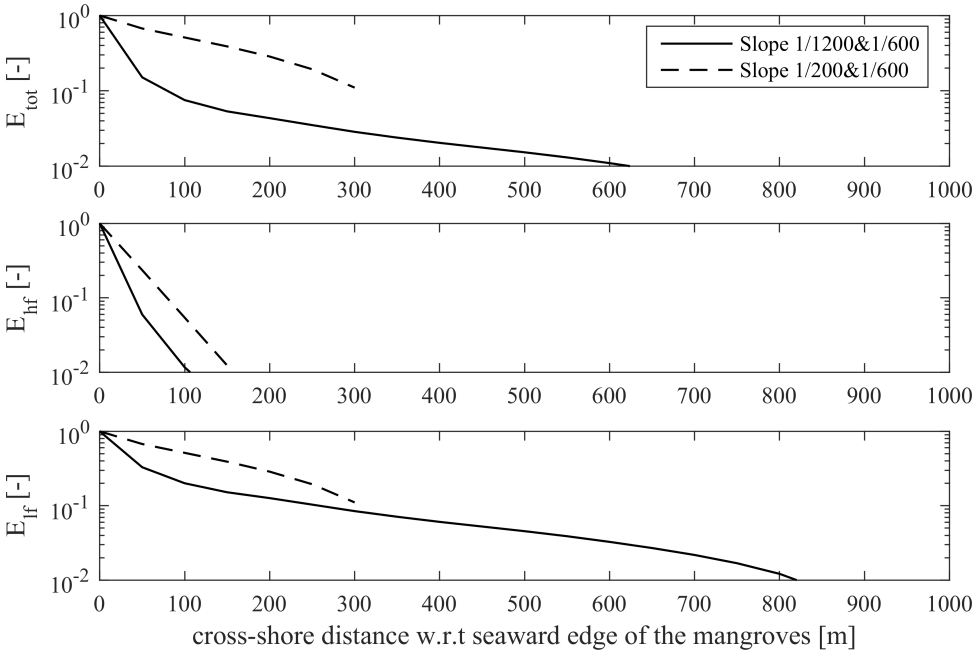

Figure 5.12: Comparison of total (upper panel), high frequency (middle panel) and low frequency (lower panel) normalized wave energy attenuation in case of average mangroves density for different slopes in front of mangroves: slope 1/1200 (solid line) and slope 1/200 (dash line).

5.4 Conclusions

This study numerically investigates the influence of slopes in front of and inside the mangrove forest and the location of a sea dike on the wave attenuation processes. The results suggest that the slope inside mangroves does have certain impacts on the wave characteristics, not only inside the mangroves, but also in front of the mangrove forest. The steeper the slope inside the mangrove forest, the larger the wave height propagating toward the mangrove edge and the faster the normalized wave energy is dissipated inside the mangrove forest. The results show that low frequency waves dampen faster than high frequency waves in the first halve wave length. While the normalized energy of high frequency waves is strongly reduced to about 1% after the first wave length, the normalized energy of low frequency waves continues to dissipate to 1% after one and a halve wave length. An increase of the slopes right in front of the mangrove forest causes larger wave heights in front of the mangrove forest and slower wave height energy absorption (both total, high and low frequency waves) inside the mangrove forest, which may be an unfavourable condition for the stability of mangroves at the edge of mangrove-water interface.

It is found that a concave profile appears to provide a better natural growing condition regarding the energy absorption and sedimentation for a mangrove forest. Although the difference in the wave height attenuation through mangroves is small, the wave set-

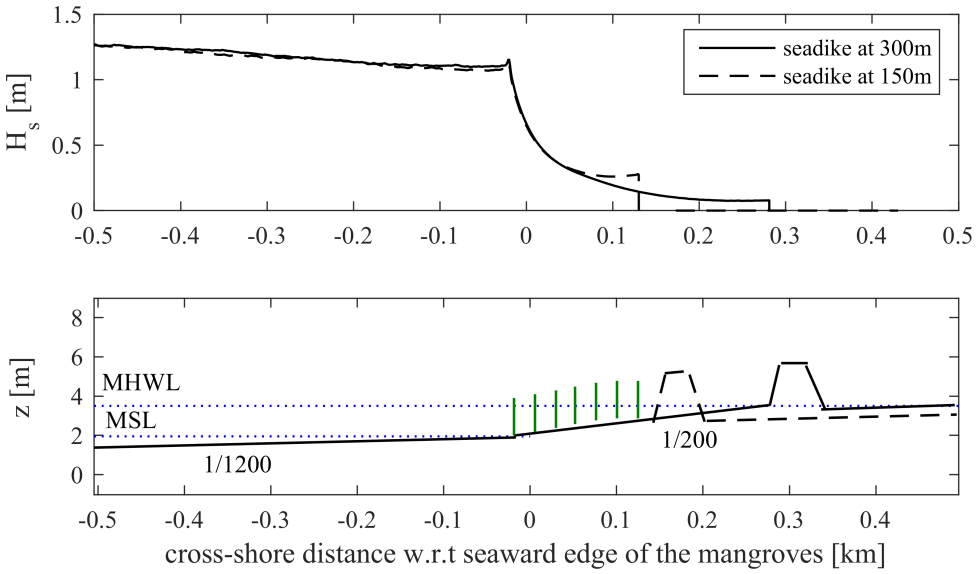

Figure 5.13: Upper panel: Comparisons between significant wave height in case of different sea dike locations: sea dike at 300m (solid line), sea dike at 150m (dash line), average mangroves density, slope inside mangroves keep at 1/200. Lower panel: Cross-shore profile for each scenarios.

up for the concave profile scenario significantly decreases inside the vegetation compared to that in a convex profile scenario. Furthermore the waves energy (total waves, high and low frequency waves) reduces fastest for a concave profile scenarios and slowest in convex profile scenarios. It is also seen that pushing sea-dikes toward the waterside appears to have a significant influence on mangroves at the landside near the structure.

References

Adrian, R. J. and Marusic, I. (2012). Coherent structures in flow over hydraulic engineering surfaces. *Journal of Hydraulic Research*, 50(5):451–464.

Alongi, D. M. (2002). Present state and future of the world's mangrove forests. *Environmental Conservation*, 29(03).

Alongi, D. M. (2008). Mangrove forests: Resilience, protection from tsunamis, and responses to global climate change. *Estuarine, Coastal and Shelf Science*, 76(1):1 – 13.

Anthony, E. J. and Gratiot, N. (2012). Coastal engineering and large-scale mangrove destruction in guyana, south america: Averting an environmental catastrophe in the making. *Ecological Engineering*, 47:268–273.

Aucan, J. and Ridd, P. V. (2000). Tidal asymmetry in creeks surrounded by saltflats and mangroves with small swamp slopes. *Wetlands Ecology and Management*, 8(4):223–232.

Augustin, L. N., Irish, J. L., and Lynett, P. (2009). Laboratory and numerical studies of wave damping by emergent and near-emergent wetland vegetation. *Coastal Engineering*, 56(3):332–340.

Bao, T. Q. (2011). Effect of mangrove forest structures on wave attenuation in coastal vietnam. *Oceanologia*, 53(3):807–818.

Brinkman, R. M. (2006). *Wave attenuation in mangrove forests: an investigation through field and theoretical studies*. PhD thesis, James Cook University.

Brinkman, R. M., Massel, S. R., Ridd, P. V., Furukawa, K., et al. (1997). Surface wave attenuation in mangrove forests. In *Pacific Coasts and Ports' 97: Proceedings of the 13th Australasian Coastal and Ocean Engineering Conference and the 6th Australasian Port and Harbour Conference; Volume 2*, page 909. Centre for Advanced Engineering, University of Canterbury.

Chapman, V. J. (1976). *Mangrove vegetation*.

Christensen, S. M., Tarp, P., and Hjortsø, C. N. (2008). Mangrove forest management planning in coastal buffer and conservation zones, vietnam: A multimethodological approach incorporating multiple stakeholders. *Ocean & Coastal Management*, 51(10):712–726.

Duke, N. C. and Schmitt, K. (2016). Mangroves: Unusual forests at the seas' edge. In *Tropical Forestry Handbook, Second Edition*, volume 2, pages 1693–1724.

Furukawa, K., Wolanski, E., and Muellerc, H. (1997). Currents and Sediment Transport in Mangrove\rForests. *Estuarine, Coastal and Shelf Science*, 44:301–310.

Gilman, E., Ellison, J., and Coleman, R. (2007). Assessment of mangrove response to projected relative sea-level rise and recent historical reconstruction of shoreline position. *Environmental Monitoring and Assessment*, 124(1-3):105–130.

Hong, P. and San, H. (1993). *Mangroves of Vietnam*. IUCN wetlands programme. IUCN.

Horstman, E., Dohmen-Janssen, C. M., Narra, P., Van den Berg, N., Siemerink, M., and Hulscher, S. J. (2014). Wave attenuation in mangroves: A quantitative approach to field observations. *Coastal engineering*, 94:47–62.

Kathiresan, K. (2003). How do mangrove forests induce sedimentation? *Revista de Biologia Tropical*, 51(2):355–359.

Mazda, Y., Kanazawa, N., and Wolanski, E. (1995). Tidal asymmetry in mangrove creeks. *Hydrobiologia*, 295(1-3):51–58.

Nikora Vladimir (2009). Hydrodynamics of aquatic ecosystems. *River research and applications*, 26:367–384.

Phan, L. K., Stive, M. J. F., Zijlema, M., Truong, H. S., and Aarninkhof, S. G. J. (2018). The effects of wave non-linearity on wave attenuuation by vegetation. *Coastal Engineering, under review*.

Phan, L. K., van Thiel de Vries, J. S. M., and Stive, M. J. F. (2015). Coastal Mangrove Squeeze in the Mekong Delta. *Journal of Coastal Research*, 300:233–243.

SIWRR (2010). Tien Estuary Investigation Report [in Vietnamese]. Technical report, Southern Institute of Water Resources Research, Ho Chi Minh, Vietnam: Ministry of Agriculture and Rural Development of Vietnam, 180 p.

Truong, S. H., Ye, Q., and Stive, M. J. F. (2017). Estuarine mangrove squeeze in the mekong delta, vietnam. *Journal of Coastal Research*, 33(4):747–763.

Wolanski, E., Mazda, Y., King, B., and Gay, S. (1990). Dynamics, flushing and trapping in Hinchinbrook channel, a giant mangrove swamp, Australia. *Estuarine, Coastal and Shelf Science*, 31(5):555–579.

Zijlema, M., Stelling, G., and Smit, P. (2011). Simulating nearshore wave transformation with non-hydrostatic wave-flow modelling. In *Conference Proceedings, 12th Int. Workshop on Wave Hindcasting and Forecasting, Hawai'i, USA*.

Chapter 6

Conclusion and recommendations

It always seems impossible,
until it's done.

Nelson Mandela

This is a concluding chapter, where main results of the study are summarised and presented in a logical way. Furthermore, a number of recommendations are presented for further future research.

6.1 Coastal mangrove squeeze

IN the past decades erosion has been observed at various regions along the southern coast of the Mekong Delta, even at locations where sedimentation has been observed. Because the south eastern and the eastern coasts of the MDRS are rich in sediment supply from the Mekong Delta River System, mangrove restoration *i.e.* planting of mangrove forests is considered to be the better solution to mitigate coastal erosion in this region. However, the achievement of this methodology has been limited so far .

At the locations of strong erosion, we observed that only a narrow strip of mangroves of less than 140 m is left. Based on the empirical relationship of mangrove forest width and coastline evolution from 1989 to 2002, it is suggested that the south eastern and the eastern coasts of the MDRS appeared to be stable with a mangrove width ranging from approximately 30 m to 259 m and 140 m on average. From a physical perspective, it is noted that the complex roots, stems and canopies of mangroves can significantly reduce wave energy and trap sediment and, thereby, enhance sedimentation within and around the mangrove forest. In this context, the narrower the mangrove forest, the less sedimentation would be attained.

Therefore, the hypothesis is that there should be a critical minimum width of the mangrove forest in order for the mangrove forest to grow sustainably. If the human interventions, such as fish-farms or sea-dikes, are too close to the mangroves (mangrove width < critical minimum width), then the amount of wave height energy required to be absorbed by the system is not enough. Consequently, mangroves, in this so called "squeeze" condition, cannot grow sustainably.

In order to investigate the physical reason of this squeeze phenomenon, a schematized model mimicking the wave attenuation processes in the Soc Trang province was constructed in the XBeach model. Results from the XBeach model for the Soc Trang case study illustrate the effectiveness of short-wave attenuation in a mangrove forest. On the one hand, it is found that the short-wave height (high frequency wave height) is significantly reduced to virtually zero after passing through less than 100 m of mangrove width. On the other hand, long waves (low frequency wave height) need further distance for their attenuation and thereby are able to penetrate much deeper inside the mangroves. The simulation results show that for the case of dense mangroves, long waves can penetrate in the order of 1000 m into the mangrove forest. However, after 300 to 400 m the long-wave energy is about 10% of the wave height at the seaward edge of the mangroves. This means, that the health of a mangrove forest appears to be related to the attenuation processes of long waves, and that short waves seem to play a less important role. In other words, within the mangrove forest, long waves play an more important role in creating a favourable environment for seedlings and sedimentation than short waves.

6.2 Wave non-linearity effects

PReviously, it is shown that long waves require a further distance to attenuate inside mangrove forests than short waves. This means that the attenuation of wave height inside mangroves appears to depend on the wave characteristic i.e. wave height, wave length and wave period. Furthermore, it is noted that although many studies have been

published on this topic, understanding the influence of wave characteristics on the wave height attenuation inside a mangrove forest is still unclear. For example, how and to what extent the wave's non-linearity affects the rate of wave height attenuation is unknown. Consequently, the attenuation of wave height inside vegetation is always presented and examined as a function of an arbitrary, absolute length scale *i.e.* per 100 m, or according to the length of the mangrove forest. As a result, the attenuation rate reported in the literature is usually inconsistent.

Therefore, in order to obtain more insight, a laboratory study of wave attenuation through mangroves was performed with different scenarios covering a large range of wave characteristics, including different wave heights and periods, including regular, irregular, broken, and non-broken waves as well. The experimental results demonstrate the role of vegetation in absorbing the wave energy, and thereby reducing wave height. Additionally, it is observed that a wave set-down instead of wave set-up occurred inside the vegetation. Furthermore, the effects of the wave non-linearity on the wave height damping processes were investigated. It is suggested that the wave height reduction should be evaluated according to a relative length, i.e the number of wave lengths and, thereby, an effective wave transmission coefficient is proposed.

Moreover, the Ursell number was used to assessed the wave characteristics. The results illustrate that, as the Ursell number increases from 0 to 250, the wave attenuation processes are significantly affected. This means that the stronger the wave non-linearity, the stronger the wave height attenuation. However, it is found that for an Ursell number larger than 250, the wave attenuation processes appear to be independent of the wave characteristics. In this context, once the characteristics of wave height represented by Ursell and the vegetation, represented by its density, and drag coefficient are known, it is possible to predict the attenuation rate of the waves.

Additionally, a numerical model was constructed in SWASH and validated using the experimental data. It is found that the model with only default values can well capture the transformation processes of the wave heights observed and measured in the experiment. For all experiments, a drag coefficient of 1.5 is adopted accounting for the turbulent energy dissipation processes that cannot be resolved in the simulations. Moreover, the attenuation distance of the mangroves in the physical model was broadened using the numerical model, so that the wave attenuation rate of over up to ten wave lengths could be determined. Finally, the wave attenuation rate for a specific mangrove density was presented as a function of the number of wave lengths and the Ursell number, using experimental data and extended numerical results.

6.3 Long wave attenuation

So far, the wave height attenuation processes through the mangrove forest were examined by means of the number of wave lengths and the effects of wave non-linearity on these damping processes were evaluated through the Ursell number. In this new context, a unique laboratory experiment, including the attenuation of three main types of infra-gravity waves through mangrove forests, was performed. These experimental data sets were used to examine the wave height attenuation processes regarding the cross-correlation functions, the wave energy dissipation per number of wave lengths and

the Ursell number. While the mechanisms, in which different types of long waves are created, propagated and penetrated into the mangrove forest, can be studied through the cross-correlation function, the dependence of the low frequency wave attenuation through mangroves on the length of a wave can be evaluated through the attenuation rate of wave height according to the number of wave lengths. Finally, the influence of wave non-linearity on the damping processes of low frequency waves can be shown through the Ursell number.

The generation of low-frequency waves in the experiment was demonstrated and clarified by a cross-correlation function. Furthermore, by adding additional low frequency wave energy together with the short wave group at the wave paddle, free long waves can be generated. Meanwhile, bound long waves can be created by the development of the long waves with the short wave group. Moreover, forcing part of bound long waves to break allows to reproduce the mixed bound and free long waves.

The effect of mangroves on the absorption of the low frequency wave energy was shown by comparing the auto-correlation function of long waves, short waves and the cross-correlation function between them in cases with and without vegetation. It is found that the reflection of low frequency waves, clearly observed in cases without mangroves, cannot be observed in cases with dense mangroves. This demonstrates that most of the reflected long waves were absorbed by the mangroves.

Furthermore, introducing the low frequency wave energy dissipation according to the number of wave lengths allows to demonstrate that both high and low frequency waves dampen significantly over the first wave length. It is found that the long waves can penetrate further into the mangrove forest than short waves. This means that the attenuation rate of the wave depends on its length and, thereby, the wave height attenuation should be interpreted and determined according to a relative length scale, *i.e.* the number of wave lengths. In other words, longer waves require a further distance, depending on their corresponding lengths to dampen, to the same attenuation rate achieved by short waves. However, the experimental results suggested that the damping rate per number of wave lengths of the long waves is even larger than that of short waves for conditions tested. This means that although long waves appear to penetrate further inside the mangrove than shortwaves, their attenuation rate per wave length seems to be larger than that of short waves.

It is also found that the attenuation rate of bound long waves is smallest, smaller than that of the mixed bound and free long waves, and free long waves have the largest attenuation rate. Moreover, it is suggested that the larger the waves or the longer the wave period, the faster the wave damping. In this sense, the attenuation of low frequency waves appears to depend on the wave non-linearity and can be examined using the Ursell number.

Therefore, the relationship between the Ursell number and the rate of wave attenuation was studied, showing that the rate of short and long wave attenuation significantly depends on the wave non-linearity: if the Ursell number is smaller than 1000, the mangrove density has a strong influence on the wave attenuation if the Ursell number is smaller than 500. For conditions tested, it is also found that while free long waves are less dependent on the wave non-linearity, bound long waves and mixed bound and free long waves strongly depend on the wave characteristics. Finally, It is shown that the

larger the Ursell number, the larger the wave height dissipation. This means that the wave non-linearity expressed by the Ursell number is the major factor controlling the dissipation rate of the wave height of low frequency waves inside the mangrove forest.

6.4 Synthesis

Last but not least, in order to evaluate the philosophies learned at a small scale laboratory and by numerical studies, a larger, real scale schematised numerical model was again constructed, but considering a different topography in and around the mangrove forest. The results show that the topography within mangroves (slope inside mangroves) does have an impact on the wave characteristics in front and inside of the mangrove forest. It is found that the steeper the slope inside the mangrove forest, the larger the wave height propagating the edge of mangroves and the faster the normalized wave energy is dissipated inside the mangrove forest. It is also suggested that high frequency waves dampen more slowly than low frequency waves in the first half wave length, after the normalized energy of the high frequency and the low frequency waves is reduced to about 1% after one wave length and one and a half wave length, respectively. The larger the slopes in front of the mangrove forest, the larger the wave heights in front of the mangrove forest and the slower the wave height energy absorption (both total, high and low frequency waves) inside the mangrove forest.

As far as practical engineering is concerned, a concave profile appears to provide the best natural growing condition in regard to the energy absorption and sedimentation for a mangrove forest. The results show that for the concave profile scenario, the wave setup significantly decreases inside the vegetation compared to the wave set up in a convex profile scenario. Furthermore, the wave energy, including total waves and high and low frequency waves, reduces slowest in convex profile scenarios, and fastest for a concave profile scenarios. It is also suggested that the smaller the mangrove width, the larger the significant wave height inside the mangroves and the slower the attenuation processes.

6.5 Recommendations

At the end of this dissertation, certain knowledge gaps still exist; among which a real scale validation and simulation regarding bed and suspended sediment are the most challenging, but essential to better understand the squeeze phenomenon. Therefore, the following suggestions are proposed:

- A field measurement data set in the context of the squeeze phenomenon would allow to collect a complete, exclusive and comprehensive data set of (1) topography in and around a mangrove forest with different scenarios including eroded, accreted and normal cases; (2) wave propagation in front of mangroves; (3) wave height attenuation inside mangroves. This data set is important to evaluate the wave height propagation and attenuation processes under different conditions in real situations. Based on the results, a practical engineering solution can be proposed to restore the mangrove degradation and to reduce the erosion.

- A detailed 2D and 3D numerical model, validated with field measurements including the wave height conditions, but also the bed and suspended sediment in and around the mangrove forest should be taken into account.

Acknowledgements

As I look back at my PhD journey, a period full of memorable moments, I am thankful for all the fantastic people that stayed by my side and have supported me along the way.

First of all, I want to express my thanks to Professor Marcel Stive, who, not only as my promoter, but also as my daily supervisor has inspired me throughout this work with his unique thinking. He never criticised me when I felt that I asked silly questions, but who with his profound knowledge was always able to translate these questions into a new and different approach and, most importantly, stimulated me with his unstoppable questions in finding the "true mechanism" In this way, he gave me not only freedom of thought, but also challenged and encouraged me to find the answer myself and taught me to be more confident, proactive and independent. How can I ever thank you for everything you have taught me!

I also want to express my gratitude to Dr. Jaap van Thiel de Vries, who has been involved from the beginning of my research. His knowledge of modelling, Matlab and Xbeach has guided me throughout this study. Together we published my very first international journal paper successfully! Thank you so much for your patience and your kindness.

I also would like to thank to "King of Modelling", Dr. Marcel Zijlema. Despite your busy schedule, I could always drop by your office and you were able to solve all kinds of modelling issues within minutes. I want to thank Dr. Marion Tissier, who has enthusiastically taught me a lot about wave theory: I learned a lot from your detailed feedback on my work. I want to thank Prof. Thieu Quang Tuan who supported my experimental work in Vietnam. I really appreciate your help with the set up of my physical model. I also want to thank Mr. Arnold van Rooijen who enthusiastically supported my modelling work.

I also want to express my gratitude to Mr. Sander de Vree and his colleagues at the water lab for their incredible support with my experimental work. Their hard work has made me feel so much more comfortable at the water lab. I really appreciate all the efforts you have made to support me.

I am also extremely grateful to four special ladies who took great care of me during the time of my stay in the Netherlands. Thanks, Mariette for being so gentle and thoughtful. Thanks, Veronique and Marjan for your understanding and kindness. And, thanks to Diana for your incredible support. Many "thank you's" to all my good friends in Delft, the Netherlands. Last but not least, I give my heartfelt appreciation to my family: my husband Son, my son, Sumo and my daughter, Sumi!

Delft, 10 May 2018

Curriculum Vitæ

Linh KHANH PHAN

18-10-1986	Born in Ha Noi, Viet Nam.

Education

2004–2009	Bachelor of Hydraulic structure in Civil Engineering. B.Sc. cum laude. Thuy Loi University, Vietnam
2010–2012	Master in Coastal and Marine Engineering and Management. M.Sc. Eramus mundus. University of Science and Technology (NTNU), University of Southampton (Soton), Delft University of Technology (Tu Delft).
2013-2018	PhD. in coastal engineering *Thesis:* Wave attenuation in coastal mangroves; Mangrove squeeze in the Mekong Delta. *Promotor:* Prof. dr. M. J. F Stive Prof. dr. S. G. L Aarninkhof dr. M. Zijlema

Awards

2008	Consolation prizes in National Mechanics Olympic in soil mechanics.
2008	Third prize in "Innovation Technology in Vietnam" (VIFOTEC).
2009	ADB world bank research fellowships.
2010	Erasmus Mundus Scholarship, EU.
2013	Nuffic Scholarship.

List of Publications

1. **Phan, K. L.**, Stive, M. J. F., Truong, H. S., Zijlema, M., The effects of wave non-linearity on wave attenuation by vegetation, *Coastal Engineering*, Accepted, 2019.

2. **Phan, K. L.**, Van Thiel de Vries, J. S. M., Stive, M. J. F., Coastal mangrove squeeze in the Mekong Delta, Vietnam., *Journal of Coastal Research*, 31(23), pp.243-253, 2015.

3. **Phan, K. L.**, Stive, M. J. F., Tissier, M. F. S., Truong, H. S., Aarninkhof, S. G. J., A laboratory study of infragravity wave attenuation by vegetation, *Coastal Engineering*, in preparation for submission, 2019.

4. **Phan, K. L.**, Stive, M. J. F., Truong, H. S., Aarninkhof, S. G. J., A Numerical study of coastal mangrove squeeze in the Mekong Delta, *Journal of Coastal Research*, in preparation for submission, 2019.

5. **Phan, K. L.**, Van Thiel de Vries, J. S. M., Stive, M. J. F., Coastal mangrove squeeze in the Mekong Delta, Vietnam, *IAHR*, 2016.

6. **Phan, K. L.**, Truong, H. S., Stive, M. J. F., A Laboratory study of wave attenuation through mangrove forest, *International Conference, Coastal Lab*, 2018.

7. Hu, Z., Zijlema, M., Suzuki, T., **Phan, K. L.**, Kumada, K., Non-hydrostatic modeling of drag, inertia and porous effects in wave propagation over dense vegetation fields, *Coastal Engineering*, under review, 2019.

8. Truong, H. S., **Phan, K. L.**, Stive, M. J. F., Uijttewaal, W. S. J., A Laboratory study of the shallow flow field in a vegetated compound channel, *International Conference on Estuaries and Coasts (ICEC)*, 2018.

9. Du, T.D., **Phan, K. L.**, Truong, H. S., Khoa, D. V., The application of hydraulic automatic gate in caisson sluice to prevent salt intrusion in Mekong delta Vietnam, *Proceedings of the 4th International Conference on Estuaries and Coasts*, Vietnam, volume 2, pp.260-264, 2013.